Doctoral thesis

Repurposing Ciclopirox as a pharmacological chaperone active against Congenital Erythropoietic Porphyria

Presented by

Pedro David Urquiza Ortiz

Supervised by

Dr. Óscar Millet Aguilar-Galindo

Dr. Juan Manuel Falcón Pérez

Faculty of Science and Technology
Department of Biochemistry and Molecular Biology
Doctoral Programme in Molecular Biology and Biomedicine

Leioa, 2018

“Las lágrimas me subían a los ojos, y no eran lágrimas de pesar ni de alegría, eran de plenitud de vida silenciosa y oculta por estar en Granada”.

— **Miguel de Unamuno**.

“Por el agua de Granada, sólo reman los suspiros”.

— Federico García Lorca.

En memoria de mi tío Gabriel,

AGRADECIMIENTOS/ACKNOWLEDGMENTS

Cuando te enfrentas a algo de tal magnitud como es escribir todo el trabajo que has llevado a cabo durante cuatro largos años, sinceramente, no sabes por dónde empezar. Ha sido todo un reto y una forma de aprendizaje el tener que escribir además en inglés. Pero ya hemos llegado muy lejos, no vale asustarse ahora y echarse para atrás, sigamos avanzando, todo irá bien.

Quisiera mostrar mi agradecimiento en primera instancia al centro de investigación donde ha tenido lugar este trabajo, **CIC bioGUNE**, en especial al director del centro José María Mato y al director científico Jesús Jiménez-Barbero. Gracias por vuestra gestión, apoyo y soporte proporcionados. Así como, de forma oficial me gustaría agradecer el trabajo de administración por parte de Mada, Ainara, Loli, Begoña y José por las llamadas, los cientos de mails y las visitas con mil dudas que me han soportado.

Gracias a Óscar, por confiar en mí todos estos años, por el aprendizaje tanto personal como profesional, por enseñarme que los "ná de ná" se convierten en un "tó de tó" llegando incluso a superar las expectativas, todo esfuerzo tiene su recompensa. Gracias por tus insistencias, por no tirar nunca la toalla y empujarnos a ir más lejos, por tus impulsos y motivación, por no perder nunca la esperanza en nosotros y confiar en nuestros resultados, por hacernos pensar y buscar soluciones. Sé que siempre piensas en que estemos en continuo aprendizaje, que usemos bien el método científico y que saquemos lo mejor de nosotros, y como más de una vez me has dicho cual padre, que seamos felices. Gracias por haberme dado esta oportunidad.

Gracias a JuanMa, por lo que comenzó como una pequeña colaboración y ha terminado con un gran y bonito proyecto conjunto. Gracias por acogerme en tu laboratorio, por haber aceptado ser también director de mi tesis, por tus consejos, por todo el tiempo explicándome y ayudándome cuando me sentía perdido, por entrar al despacho pensando que había terminado el experimento y salir con mil ideas nuevas ampliando horizontes (así como multiplicando el trabajo) pero siempre motivado y con ganas de aprender y mejorar. Gracias por tus palabras de ánimo, por tu paciencia, por tu amabilidad, por las charlas en inglés, los lab meetings que tanto miedo me daban. Gracias por haber confiado en mí.

A mi grupo de RMN, a Arantza por ser mi amatxu del labo, por todo el cariño y las millones de conversaciones científicas y no tan científicas, por los abrazos, por la comprensión, por todo lo que he aprendido a tu lado, por todo lo que aportas, sobre todo por tu profesionalidad y calidad como persona, gracias. A Ana, por su magnífica gestión del laboratorio, porque nunca nos falta de nada, porque lucha día a día con los mil pedidos, por soportarnos cuando estamos insoportables, por ayudarme siempre con las cuentas matemáticas y por tu forma tan eficiente y buena de trabajar. Gracias a ambas por vuestro magnífico trabajo, por el screening *in vitro*, por las PCR, los ensayos enzimáticos y por todo el duro trabajo que habéis hecho y ha contribuido a este proyecto. A Iratxe, sé que no ha sido nada fácil y tuviste que adaptarte al cambio, pero lo has hecho genial, has avanzado muchísimo, eres una excelente compañera, he sido muy feliz trabajando contigo a tu lado, compartiendo mil momentos, aprendiendo a usar nuestro queridísimo HPLC y sus mil errores de origen desconocido que, finalmente conseguimos dominar. Gracias por la compañía mutua en cultivos, gracias por escucharme y apoyarme, por darme energía y contagiarme de

optimismo, por aprender y madurar juntos en el ámbito científico, por complementarnos diseñando experimentos, aunque a veces la frustración se apoderara de nosotros y levantaras mesas, jejeje. Nunca olvides que, frente a una situación incómoda, tose, tose muy fuerte. A Itxaso, por ser muy buena alumna, por escucharme y querer aprender en todo momento, por las infinitas horas compartidas en cultivos, por las millones de líneas celulares que llevábamos a la vez y por haber estado dispuesta al trabajo siempre, mucho ánimo, puedes con todo, a por ello! y gracias. A Laura, porque, aunque tal vez nos hayamos conocido un poco a destiempo, siempre tienes palabras de ánimo y apoyo, por estar siempre, por valorarme, por todas las charlas infinitas, los paseos, por una amistad que espero nunca termine, mucho ánimo y suerte, ya sabes que puedes con todo y te deseo lo mejor. A Nieves por los abrazos, por escucharme y comprenderme, por las palabras de ánimo, por las conversaciones, las risas, y por las palabras tan bonitas que siempre me has dedicado, que me calaron hondo y nunca olvidaré. A los chicos del labo, Ganeko, Siva, Gabo y Luca, gracias por estar en todo momento y ser más que compañeros, grandes amigos. En especial, gracias a Ganeko por los análisis de RMN, los dockings y todo lo que ha tenido que ver con la bioinformática, gracias por ser un apoyo y nunca olvidaré aquel día en el que tu Yatekomo estaba roto e Iratxe te ofreció un cuscurro de pan duro. A Siva, por ser el “indio gurú” con la mejor filosofía de vida del grupo, por tu optimismo y ganas de comerte el mundo, ¡por las copas de vino pasadas y por las futuras! A Luca, por ser un gran alumno de cultivos, por las charlas, por confiar en mí y porque todo salga de lujo en el futuro. A Gabo por ayudarme tanto cuando aterricé en Bilbao, por los papeleos y los consejos, sobre todo el de tener mucha paciencia.

A Espe, por soportarme al principio cuando no encontraba nada, pero eso cambió con el tiempo y ahora te doy las gracias por todas las discusiones científicas, por todo lo que he aprendido a tu lado, gracias por tus consejos, por escucharme, por compartir grandes momentos, por todos los westerns analizados, por ser tan gran y maravillosa persona y por hacerme sentir que no siempre el vaso está tan vacío como creo ver. A Félix, por su paciencia conmigo también, por todo lo que me has aportado durante estos años, por transmitirme tranquilidad para las charlas y gracias por tus palabras de ánimo siempre.

To Julie, thank you so much for all support, you were my little salvation in the laboratory being my official translator and you become a great friend forever. I will never forget the white and green vegetable in “Le petit Mignon”, and of course "la fourmi cro-onde". Thanks to the laboratory of Emmanuel for welcoming me and treating me so well from the first day, it was a wonderful scientific stay. Merci beaucoup!

En general, quisiera agradecer a todo el equipo de trabajo por acogerme y quererme, sin vosotros este proyecto no habría sido posible, ni tampoco mi estancia en Bilbao habría sido igual. Gracias a todas las personas del BioGUNE que he conocido, a todos los amigos que después del trabajo estaban dispuestos a tomar un “zurito”, a Miguel, Amaia, Ilaria, Helena y todo el grupo de predocs cuya lista es numerosa y ruego me disculpen si no nombro a todos, pero os agradezco a cada uno el haber hecho especial mi vida aquí. Me llevo un pedacito de cada uno y aunque aún no sé por dónde me llevará la vida, espero mantener siempre el contacto. Por ahora, os espero en Granada, allí siempre tendréis una casa.

Sin mis amigos este trabajo tampoco hubiera sido posible, por eso tengo que agradecer todo el apoyo que me han proporcionado desde la distancia, llamadas infinitas, millones de mensajes, así como millones de audios.

Mi especial agradecimiento a mi querida Anabel, gracias porque desde el primer momento en el que nos conocimos tu luz invadió mi vida para quedarse, gracias por las conversaciones infinitas, por los cafés al atardecer donde sólo la voz y la intuición de nuestras siluetas son protagonistas, gracias por ser tan maravillosa, por cuidarme, por comprenderme, por ser como eres, porque nunca te rindes y cuando estoy contigo el tiempo parece pararse y un día a tu lado son como minutos, nunca es suficiente. Gracias por tanto amor y tanto apoyo. Siempre entre la aorta y la pulmonar, nos vemos en Málaga.

A Fati, a Aranza por llevar juntos toda una vida, por conocerme tan bien, porque sin decir nada ya saben lo que pienso, por su cariño y comprensión, por su apoyo incondicional, por escucharme, por sus consejos, por las risas, por el vino y las cenas de reconciliación con gambas, por todo los que nos queda por vivir, por recuperar el tiempo perdido en la distancia y por un futuro prometedor.

A Eli, por todas las experiencias vividas, por ayudarme tantísimo en todo, por la tarde intentando arreglar el ordenador, por recuperar todo el trabajo, por todo el apoyo durante la escritura, por acompañarme en la biblio, por las excursiones, por las noches en vela hablando, por los pequeños grandes detalles, las canciones, las dedicatorias, por intentar convencerme de que los gatos son buena gente, por ser una persona sincera, honesta, humilde, trabajadora y estupenda. Te voy a echar mucho de menos, pero siempre nos quedará Graná y los audios de más de 10 min.

A Cris y a toda la gente que ha hecho que Bilbao sea mi segundo hogar, gracias por el apoyo incondicional, por las locuras, por entrar al Guggem en chándal y con barro porque era gratis, por los cafés, por las innumerables historias, los viajes y por una amistad eterna.

A Adrián, por ser un amigo ejemplar, por tus palabras sinceras, tu humor, tu valentía, tu apoyo en todo momento, por preocuparte cuando he estado mal, gracias por aguantarme durante este periodo, ahora se empieza a ver la luz y esta vez espero que haya luz de verdad y menos distancia, eres muy grande y ¡vales muchísimo!

A mis compañeros de piso, mi pequeña familia en Bilbao, la tranquilidad y el bienestar de un hogar. Gracias por todo, no tengo palabras para describir todo lo que siento, sois más que compañeros, más que amigos, para mi sois mi familia aquí. Tuvo que llegar el día en el que la vida nos lleva por rumbos diferentes, siento ser el primero en romper la armonía, pero nunca podré olvidaros, gracias por cada detalle, gracias por escucharme siempre y guiarme, gracias por soportarme cuando ni yo lo hacía, gracias por animarme, por darme buenos consejos, por los momentos de películas y series en el salón (ese que digamos, es poco masculino), por confiar en mí, por estar siempre ahí, gracias Cristina, gracias Tomás. Va a ser difícil, voy a echar de menos las largas cenas, los ¿qué tal el día?, las risas y al fin y al cabo la complicidad en el piso. Cris, gracias a ti y María por salvarme, nunca olvidaré Henao, sin duda, ha sido la mejor decisión de mi vida, os deseo todo lo mejor y espero que podemos seguir compartiendo momentos, aunque exista un poco de distancia. Gracias por conocerme tan bien, tus consejos, tu ayuda, no cambies nunca, estoy seguro de que todo irá bien. Chicos, colegas, Friends (¿dónde veraneáis?), muchas gracias por vuestro apoyo

durante esta época dura, no me imagino una mejor compañía, mucha suerte en vuestros caminos, os deseo de todo corazón que todo vaya de lujo, sois muy grandes y unas personas maravillosas, gracias.

Por último, gracias a mi familia, mis padres, mi abuela, mis hermanos y a la futura miembro de la familia, mi pequeña sobrina Vera, gracias por todo el apoyo, por confiar en mi en todo momento, por haberme brindado esta oportunidad de poder continuar con mi formación, porque a pesar de las adversidades, nos mantenemos unidos y salimos adelante. Gracias por enseñarme el valor de la familia, por las lecciones de humildad y por no dejar que me rinda nunca, por darme ánimo y valor y sobre todo por todo el esfuerzo de mis padres para que, tanto mis hermanos como yo, lleguemos lejos. Gracias a mi tito Gabi, te marchaste tan fugazmente, no pude despedirme de ti, nunca podré olvidar todas las lecciones de vida, todo el cariño y todo el amor que nos dabas, gracias por transmitirme esa pasión por la biología, no había mejor maestro, siempre recuerda; alcance y contenido, joven. Te echo mucho de menos, ojalá estuvieras aquí, siempre me animabas en todo, la mejor de las mejores personas que se pueden conocer, gracias tito por todo, siempre vivo en mi recuerdo. Dedico especialmente mi trabajo en tu memoria.

Sin más dilación, espero que sea del agrado del lector, escrito con esfuerzo y dedicación, esta tesis doctoral muestra un gran trabajo que no habría sido posible sin cooperación y trabajo en equipo. Gracias a todas las personas y compañeros que han participado, así como los servicios de RMN, animalario e histología que se han requerido para el desarrollo de la presente tesis.

RESUMEN/SUMMARY

“Nothing in life is to be feared, it is only to be understood.
Now is the time to understand more, so that we may fear less”.

— Marie Curie

RESUMEN

La porfiria eritropoyética congénita (CEP) es una enfermedad rara, autosómica recesiva producida por la deficiencia en la actividad de la proteína uroporfirinógeno III sintasa (UROIIIS), la cuarta enzima de la vía biosintética del grupo hemo. Se considera una enfermedad multisistémica mutilante debido a la amplitud de signos y síntomas que sufren los pacientes, incluidas patologías hematológicas, cutáneas, oculares y esqueléticas, llegando a ser potencialmente mortal y para la cual, actualmente no existen tratamientos curativos disponibles. Bioquímicamente, en general, las mutaciones hereditarias reducen la estabilidad de la enzima, alterando su homeostasis y, en última instancia, disminuyendo la producción de hemo intracelular. Esto da como resultado la acumulación de subproductos de uroporfirina en el cuerpo, lo que agrava la patología con síntomas como fotosensibilidad de la piel y lesiones cutáneas fototóxicas desfigurantes.

En la última década, los estudios sobre chaperonas farmacológicas que ayuden a la estabilidad de proteínas en enfermedades relacionadas con mal plegamiento de proteínas, han aumentado considerablemente debido su alto potencial terapéutico con bajos costes y alta eficiencia. Sin embargo, el uso de chaperones farmacológicas químicas presenta ciertas limitaciones relacionadas con la inespecificidad de la proteína diana, lo que puede conllevar a conflictos con el centro activo y una alta demanda de dosis para conseguir un efecto beneficioso. En este contexto, las chaperonas farmacológicas alostéricas emergen como una alternativa terapéutica más eficaz en la restauración de la proteostasis, sin afectar al centro activo y, en principio, con un radio de actuación a dosis bajas. En este trabajo, nos hemos enfocado en el desarrollo de una terapia basaba en chaperonas farmacológicas alostéricas para CEP, abordando la enfermedad desde el punto de vista mecanístico de la patología. Para ello, se ha llevado a cabo el desarrollo de una estrategia integral de detección de fármacos que integra enfoques computacionales y estructurales, en combinación con experimentos funcionales *in cellula* e *in vivo*. El éxito de esta estrategia se traduce en la detección demostrada de diferentes compuestos que potencialmente pueden actuar como chaperonas farmacológicas por unión a la proteína deficiente uroporfirinógeno III sintasa.

En el presente trabajo, demostramos que uno de estos fármacos encontrados por la plataforma, el antifúngico sintético comercial ciclopirox (CPX), es capaz de asociarse a la enzima y estabilizarla. Cumpliendo el propósito de búsqueda, CPX se une a la enzima en un sitio *alostérico* distante del centro activo, por lo que no afecta a su función catalítica, *actuando como chaperona farmacológica alostérica*. Se ha comprobado que el fármaco es capaz de restablecer la actividad *in vitro*, *in cellula* e *in vivo*, además de aliviar la mayoría de los signos clínicos en un modelo murino (*bona fide*) de la enfermedad a concentraciones sub-tóxicas, estableciendo, en definitiva, una *nueva línea de intervención terapéutica contra CEP*, aplicable a la mayoría de las mutaciones sin sentido (nonsense) perjudiciales que causan esta enfermedad devastadora.

SUMMARY

Congenital erythropoietic porphyria (CEP) is a rare autosomal recessive disease produced by a deficient activity in uroporphyrinogen III synthase (UROIIIS), the fourth enzyme of the heme biosynthetic pathway. It is considered a mutilating multi-system disease due to the wide range of signs and symptoms that patients suffer, impacting in many organs, being potentially devastating. The disease could be life-threatening and currently there are no curative treatments available. Biochemically, inherited mutations most frequently reduce enzyme's stability, altering its homeostasis and ultimately blunting intracellular heme production. This results in uroporphyrin by-product accumulation in the body, aggravating the pathology with symptoms like skin photosensitivity and disfiguring phototoxic cutaneous lesions.

In the last decade, studies on pharmacological chaperones to assist protein stability in misfolding diseases, have increased considerably due to the high therapeutic potential in terms of efficiency and low costs. Nevertheless, the use of chemical pharmacological chaperones presents certain limitations related to the non-specificity of the target protein, which can lead to conflicts with the active site and often require a high demand of doses to achieve a beneficial effect. In this context, allosteric pharmacological chaperones emerge as a more effective therapeutic alternative in the restoration of proteostasis, since it does not affect the catalytic site and, in principle, with a proper action at low doses. In this work, we are focused on the search and development of allosteric pharmacological chaperones for CEP, addressing the underlying pathology of the disease from the mechanistic point of view. For that purpose, the development of a comprehensive drug detection strategy that integrates computational and structural approaches, in combination with functional experiments *in cellula* and *in vivo* has been carried out. The success of this strategy results in the proven detection of different drugs that can potentially act as pharmacological chaperones by binding to the deficient protein uroporphyrinogen III synthase.

In here, we demonstrate that the synthetic marketed antifungal ciclopirox (CPX) associates to the enzyme and stabilizes it. Fulfilling the purpose of search, CPX targets the enzyme in an *allosteric site* distant from the active centre, not affecting the enzyme's catalytic, *acting as allosteric pharmacological chaperone*. We prove that the drug restores the activity *in vitro*, *in cellula* and *in vivo*, and is able to alleviate most of the clinical signs in a *bona fide* mouse model of the disease at sub-toxic concentrations, *establishing a novel therapeutic intervention line against CEP*, applicable to the majority of the deleterious missense mutations causing this devastating disease.

CHAPTER I

INTRODUCTION

“There are, in effect, two things, to know and to believe one knows;
to know is science; to believe one knows is ignorance.”

— Hippocrates

I. INTRODUCTION

I.1. Congenital erythropoietic porphyria (CEP).

Heme group acts as a prosthetic addition to many enzymes, transporters, and receptors including hemoglobin, myoglobin, catalases, peroxidases, cytochromes P450 (CYP), and in sensor proteins for diatomic gases such as O_2 or NO[1]. In eukaryotes and prokaryotes except archaea and some eubacteria, heme synthesis belongs to the well-established and conserved biosynthetic pathway[2]. Malfunction of this pathway will unequivocally result in the onset of pathologies, termed porphyrias. The porphyrias are defined as a clinically and genetically heterogeneous group of metabolic diseases which result from an either inherited or acquired dysfunction of the enzymes crucial for heme biosynthesis. In mammals, heme synthesis is accomplished by the sequential action of eight enzymes (mainly expressed in liver and in erythroid cells), each type of porphyria depends on the affected enzyme, suffering an accumulation of heme precursors denominated porphyrins, which causes acute neurovisceral symptoms and/or skin lesions[3]. Hence, porphyrias may be classified by different ways; according to the location of the deficient enzyme: erythropoietic (bone marrow) or hepatic (liver); based on the clinical manifestation; cutaneous or noncutaneous types or classified as either photosensitive or neurologic, but some porphyrias cause both symptoms; or alternatively, they can be classified either acute or non-acute porphyria, depending on whether the patient presents with an acute life-threatening attack[4] (Figure 1).

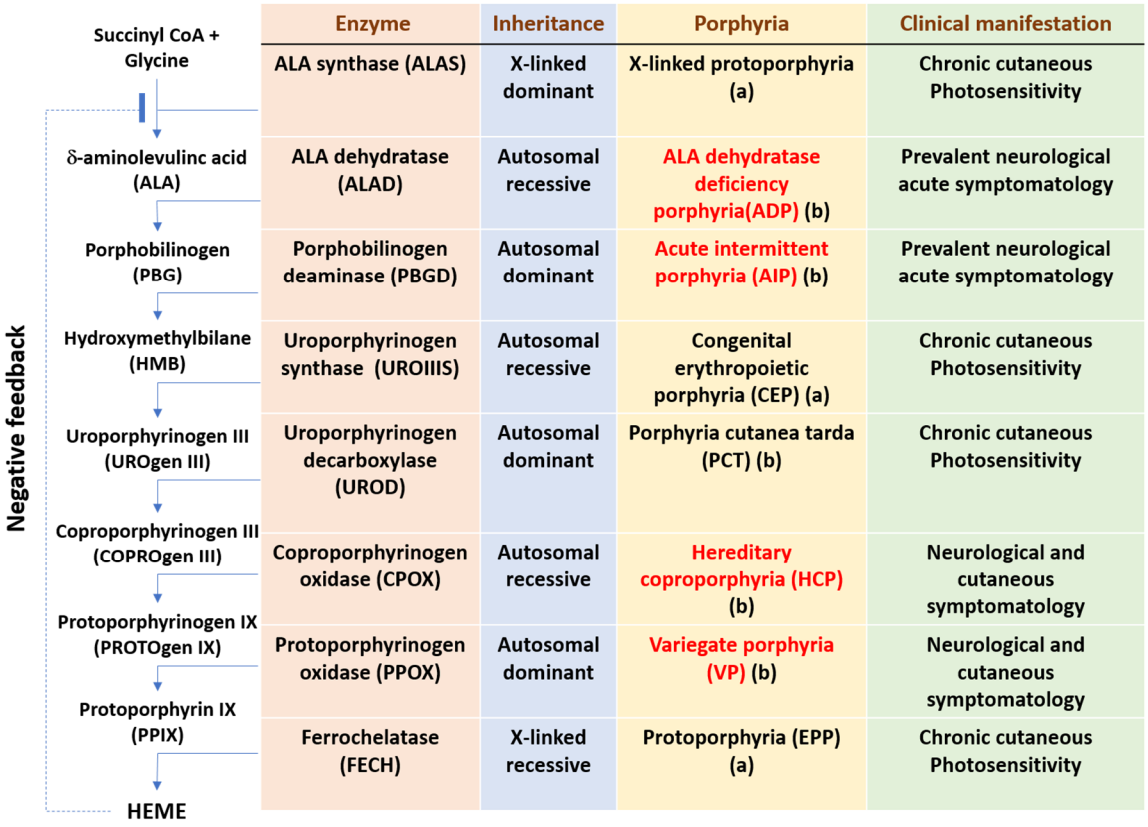

Enzyme	Inheritance	Porphyria	Clinical manifestation
ALA synthase (ALAS)	X-linked dominant	X-linked protoporphyria (a)	Chronic cutaneous Photosensitivity
ALA dehydratase (ALAD)	Autosomal recessive	ALA dehydratase deficiency porphyria(ADP) (b)	Prevalent neurological acute symptomatology
Porphobilinogen deaminase (PBGD)	Autosomal dominant	Acute intermittent porphyria (AIP) (b)	Prevalent neurological acute symptomatology
Uroporphyrinogen synthase (UROIIIS)	Autosomal recessive	Congenital erythropoietic porphyria (CEP) (a)	Chronic cutaneous Photosensitivity
Uroporphyrinogen decarboxylase (UROD)	Autosomal dominant	Porphyria cutanea tarda (PCT) (b)	Chronic cutaneous Photosensitivity
Coproporphyrinogen oxidase (CPOX)	Autosomal recessive	Hereditary coproporphyria (HCP) (b)	Neurological and cutaneous symptomatology
Protoporphyrinogen oxidase (PPOX)	Autosomal dominant	Variegate porphyria (VP) (b)	Neurological and cutaneous symptomatology
Ferrochelatase (FECH)	X-linked recessive	Protoporphyria (EPP) (a)	Chronic cutaneous Photosensitivity

Figure 1. Classification of porphyrias. Heme biosynthetic pathway (left) and porphyria classification according to deficient enzyme, tissue location and the most clinical manifestation. The porphyrias highlighted in red correspond to acute porphyrias. (a) Erythropoietic porphyrias; (b) Hepatic porphyrias.

In the present work, within all types of porphyria, we focus our investigation on congenital erythropoietic porphyria (CEP; ICD-10 #E80.0; MIM #263700) or Gunther's disease, which is related to a deficient function of the fourth enzyme in the pathway. Historically, the name of the disease has evolved until finally agreed to the name CEP. The first case was described in 1874 by J.H. Schultz who reported clinical features from a patient with skin photosensitivity, anemia, splenomegaly and red urine since childhood but was treated as a special form of leprosy, "pemphigus leprosus"[5]. The studies of the patient urine allowed identifying different pigments which considered as "hematoporhyrin" (dicarboxyl porphyrin derived in the laboratory from hemoglobin), suggesting that they were originated from an error of biosynthesis of hemoglobin[6,7]. In 1912, the physician Hans Gunther reported the case of Mathias Petry, a 19-year-old male who presented skin lesions and red urine, the disease was named as "congenital hematoporphyria"[8]. Subsequently, Gunther proposed to classify the pathologies of porphyrin metabolism in four types: *hematoporphyria acuta*, *hepatoporphyria acuta toxica*, *hematoporphyria chronica*, and *hematoporphyria congenita* [9]. In 1923, Gunther was recognized as the first to define this rare condition as an inborn error of metabolism[10] and, accordingly, CEP was also named after him as Gunther disease [11]. Studies of Hans Fisher demonstrated that the pigments were different from hematoporphyrin and contributed stronger to the knowledge of the chemistry of porphyrins, abandoning the prefix "hemato" for porphyrins[12]. In 1955, Schmid and co-workers underlined the erythroid nature of this disease suggesting '*porphyria erythropoietica*' as a more appropriate name[13]. Finally, this form began to be called '*congenital erythropoietic porphyria'* to reflect an early onset of this clinical status compared with the other erythropoietic forms[14].

Nowadays, CEP is defined as an autosomal recessive genetic disease caused by a remarkable deficient activity of uroporphyringen III synthase (UROIIIS; EC 4.2.1.75), enzyme involved in the biosynthetic heme pathway[15,16], although not completely absent activity (<1 to ~10% of normal). It is one of the less common porphyrias; considered a rare disease, whose prevalence has been estimated at 1 or less in 1 000 000, with approximately 280 cases reported in the world[14]. Pathologically, the loss of enzyme activity causes the overproduction and accumulation of the non-physiological porphyrin at toxic levels, especially porphyrin isomers I [uroporphyrin I (URO I) and coproporphyrin I (COPRO I)] which are not metabolized inducing the hemolysis and release them into the plasma, distributed and deposits in the tissues[17] causing the most characteristic features; skin photosensitivity and hemolytic anemia, among other symptomatology.

The severity of CEP is normally classified according to the clinical features. Mild patients show cutaneous symptoms and can often live a normal live in adulthood; moderate patients have mild anemia and/or weak splenomegaly with skin lesions; and severe patients which are transfusion-dependent and sometimes show reduced life expectancy[18,19].

I.2. Clinical features of CEP.

CEP is always characterized by skin photosensitivity and hemolytic anemia. In addition, it is considered a mutilating multi-system disease due to the wide range of signs and symptoms that patients suffer, including hematological, cutaneous, ocular and skeletal pathologies. The severity of the clinical manifestations varies considerably among CEP patients and it is likely interdependent of the amount of porphyrin accumulated in the tissues, ultimately correlated with the levels of residual UROIIIS activity in the cells dependent on the different mutations of the enzyme[20].

I.2.1. Hematological manifestations.

The main hematological pathology found in CEP is hemolytic anemia. In the bone marrow, it was observed that developing erythropoietic cells contained large amounts of porphyrins. Under fluorescent microscope most normoblasts have persistent red fluorescence localized to their nuclei, with heme-containing inclusion bodies being detected into the nuclei as well as in peripheral blood (Figure 2). The overproduction of porphyrin isomers I, mainly accumulated in these erythroid cells, causes variable hemolytic anemia associated with dyserythropoiesis, a defective development of blood red cells (RBC), producing defects such as abnormal nuclear division and disintegration of the nuclear envelope. This condition favors hemolysis that releases high content of porphyrins to circulating plasma. In addition, poikilocytosis, nucleated red cells, and basophilic stippling are common sings, and the marrow present erythroid hyperplasia [21,22] .

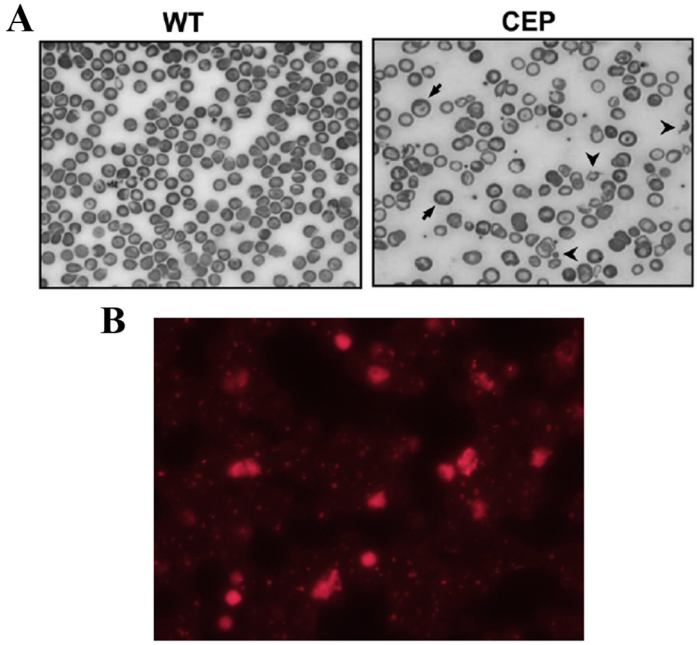

Figure 2. Hematological CEP manifestations. A) Hemolytic anemia. Red blood cell smears. Anisocytosis and poikilocytosis are shown by arrow heads and hypochromic red cells by arrows[23]. B) Fluorescent blood red cells smear from CEP patient. Fluorescence due to intracellular accumulation of porphyrins, mainly URO I and COPRO I [21] .

Hemolytic anemia of varying severity is found in nearly all reported cases, from mild to severe depending on the balance between bone marrow erythroid hyperplasia and the rate of erythrocyte destruction, which often fluctuates considerably during the lifetime of a patient or from one patient to another. Eventually, in counted cases anemia is not present[21]. When severe hemolysis occurs, patients become transfusion dependent. Very severe hemolytic anemia may even cause hydrops fetalis[22] .

Generally, anemia is accompanied by secondary splenomegaly developed as a response to hemolysis and the need for the organism to eliminate the damaged RBCs, which are removed and destroyed in the spleen. The high turnover required induces for this organ to gradually become bigger, being the magnitude of splenic closely related to the severity of hemolysis, which may worsen the anemia inducing leucopenia and symptomatic thrombocytopenia[24].

At the level of regulation of the pathway, there is an attempt to compensate the anemia and the heme deficiency by increasing the enzymatic activity of δ-aminolevulinate synthase 2 (ALAS2) and porphobilinogen deaminase (PBGD), as observed in hemolysates of CEP patients[25]. Therefore, erythropoiesis is being stimulated in response to anemia (Figure 3). This compensatory up-regulation increases UROIIIS upstream deficient bone marrow, which in turn increases the overproduction and accumulation of porphyrins worsening the symptomatology. On the other hand, approximately 20% of patients with mild phenotype of CEP are not showing anemia, which suggests that this compensation for increased erythropoiesis may be sufficient to compensate for the hemolysis[26].

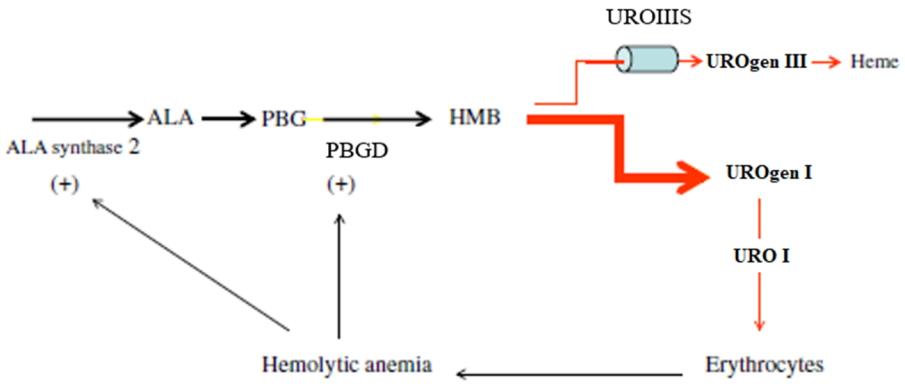

Figure 3. Stimulation of erythropoiesis in response of hemolytic anemia. The compensatory upregulation of ALAS2 in heme biosynthesis pathway. Adapted from[21].

I.2.2. Photosensitivity; cutaneous damage and others manifestations.

Skin photosensitivity is the result of the chemical qualities of porphyrins, whose photochemical properties can explain porphyrin phototoxicity. The electronic configuration of an aromatic porphyrin molecule provides unusual photoexcitation characteristics. Porphyrins have a largely conjugated double bond structure and the electrons are excited by wavelength light between 500 nm and 650 nm with main absorption peak at 408 nm (Soret band, in the visible spectrum). When multi-wavelength

photon radiation excites the porphyrins, the photochemically induced excited state returns to the ground state by releasing energy in form of the characteristic red fluorescence, phosphorescence or by heat dissipation. Yet, the fraction of light around the 408 nm promote porphyrins to a longer-lived excited state which, in turn, transfer the energy surplus to neighbouring molecules, ultimately leading to the phototoxicity responsible for the clinical features of the cutaneous damages manifested as skin photosensitivity after sun-exposition. These photodynamic reactions stimulate the production of reactive oxygen species (ROS) that damage tissues directly, and also indirectly by stimulating proinflammatory mediators, complement activation, mast cell degranulation and matrix metalloproteinase activity[21,22,27] (Figure 4).

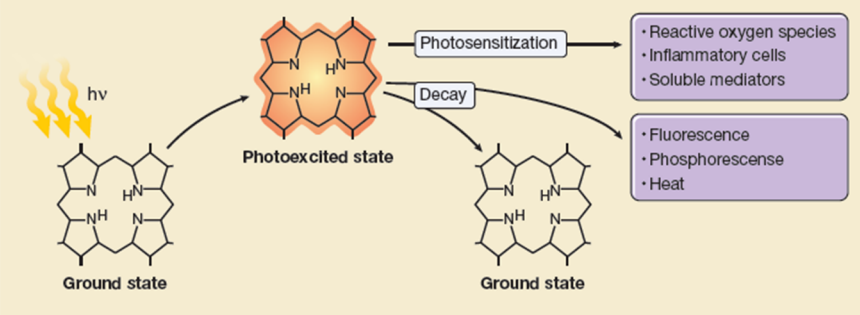

Figure 4. Photodynamic reactions of porphyrins. Radiant energy (hν) stimulates the transition to photoexcited states. The photoexcited porphyrins generate reactive oxygen species, which damage cells and tissues[27].

Generally, the phototoxic cells damage includes lipid peroxidation and alteration of the membranes, which contributes to the release of enzymes and mediators from cells such as mast cells and polymorphonuclear cells, increasing serum histamine levels and causing an inflammatory response. As well as the interaction between activated mast cells and fibroblasts may contribute to fibrosis and sclerodermoid skin changes[27].

At the symptomatology level, CEP photosensitivity is manifested early in life as a series of cutaneous damages such as vesicular or bullous eruptions in the skin exposed to light. The fragility in the skin is associated with secondary infections with erosions that heal slowly, leaving scars with hyperpigmentation. Ultimately, this type of cutaneous damage can lead to severe mutilation of fingers, hands, ears, lips and nose (Figure 5).

Figure 5. CEP cutaneous damage. Progressive scarring and mutilations of severe CEP patients. 8-year-old girl (left)[21]. Severe case of CEP in an adult (right) [28].

As progress of the disease, depending on the severity of the disease, have been described other types of manifestations derived from the photosensitivity and the accumulation of porphyrins, such as ocular involvement (chronic conjunctivitis, leukoma, cataracts, corneal ulcers, iritis or Scleromalacia perforans), erythrodontia (deposition of porphyrins in the enamel by binding to dental calcium phosphate during teeth development) and skeletal abnormalities (Deposits of porphyrins in bones that result in osteodystrophy characterized by osteolysis and turnover type of osteoporosis) (Figure 6).

Figure 6. Other clinical CEP manifestations. Scleromalacia perforans in the external interpalpebral region of a woman adult CEP patient (left). Erythrodontia of a CEP boy patient (right)[21].

I.3. Diagnosis.

The diagnosis of CEP usually is suspected in infancy from the early onset of severe cutaneous photosensitivity accompanied by pink to dark-brown fluorescent urine and erythrodontia. Urine porphyrins, primarily URO I, fluoresce with a brilliant pink color when exanimated under Wood's light (long-wave ultraviolet (UV) light lamp)[29,30] (Figure 7).

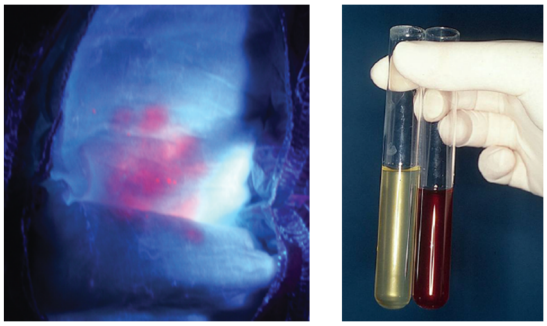

Figure 7. Observation of urine porphyrins (primarily URO I). The diaper from a child with CEP, porphyrins fluoresce with a brilliant pink color when illuminated with a Wood's light (left)[28]. Comparison between normal urine and red-to-brown urine of CEP patient (right) [21].

In addition to physical and careful familiar medical history, the definitive diagnosis requires biochemical analysis of porphyrins from biological samples as urine, stool, plasma, or RBCs. Fractionation and separation of isomers I and III is the main basis in this type of analysis, preferentially by high-performance liquid chromatography (HPLC) with a fluorescence detector[31]. Due to the pathological state and the regulation of the organism trying to eliminate the accumulated amount of porphyrins, the biological samples have a characteristic pattern with abnormal high peaks of porphyrins (URO I and COPRO I) detected by HPLC (Table 1; Figure 8).

Laboratory diagnosis of CEP.

Urine	Stool	Plasma	RBC
Uro I ↑ Copro I ↑	Copro I ↑	Uro I ↑ Copro I ↑	Uro I ↑ Copro I ↑
Hepta III (n)	Coprol/III ratio↑	Emission peak[a]	UROIIIS activity ↓
PBG/ALA (n)		615–618 nm	

Table 1. CEP diagnostic tests. Porphyrins increment from biological samples. n = normal concentration. [a] Fluorescence emission spectrum shows a peak at 615–618 nm when the plasma is excited at a wavelength of 405 nm, which is indicative of a positive result[21].

Determination of the residual activity of UROIIIS reinforces CEP diagnosis. The analysis is normally performed from erythrocytes or lymphocytes, and the enzymatic assay is performed after the incubation of hemolyzed cells with porphobilinogen (PBG), which leads to the formation of hydroxymethylbilane (HMB), substrate of UROIIIS. The isomer I and III formation are analyzed by HPLC and the profiles allow the identification of patients CEP and carriers[32].

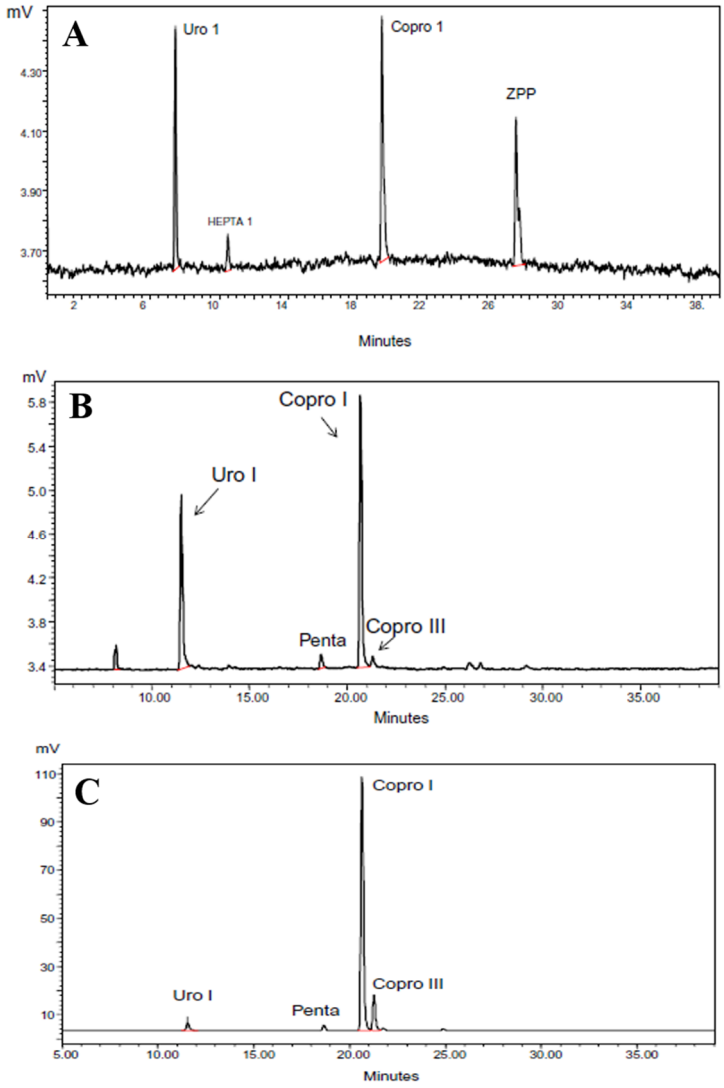

Figure 8. Characteristic HPLC profiles of hemolysate (A), urine (B) and stool (C) of a patient with CEP showing the predominance of isomers porphyrins I resulting from the oxidation of the respective porphyrinogens [21]. Uro I: uroporphyrin I; Hepta I: Heptaporphyrin I; Penta: pentaporphyrin; Copro III/I: coproporphyrin III/I; ZPP: zinc-protoporphyrin. Adapted from[21].

The ultimate confirmation diagnostic test consists in the identification of mutations encoded in the *UROS* gene, by amplification of the latter after blood DNA extraction. The sequencing should allow the detection of mutations and confirms the biochemical diagnosis[18] (Figure 9).

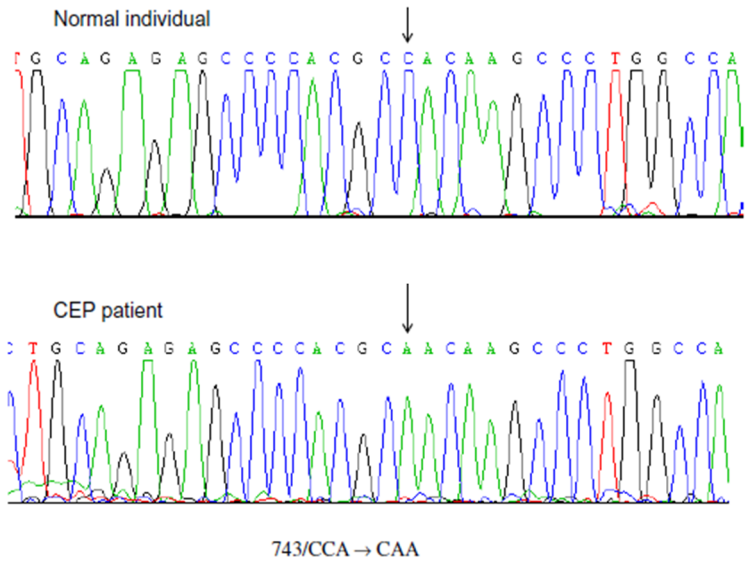

Figure 9. DNA sequencing of CEP patient. Electropherogram of UROIIIS exon 10 from CEP patient compared to a normal individual. P248Q mutation results in a proline-glutamine substitution in the protein[21].

These analyses are important for the diagnosis since they allow to differentiate CEP patients from other types of congenital photodermatoses. Cutaneous defects in patients with xeroderma pigmentosum, epidermolysis bullosa, hydroa vacciniforme, and bullous pemphigoid may resemble those found in patients with CEP, yet porphyrins analysis is determinant to distinguish them.

Finally, a rapid and reliable diagnosis (including prenatal diagnosis) of CEP is essential. This should allow non-delayed clinical decisions and the instaurations of early preventive measures in infants.

I.4. Treatment.

Currently, different preventive strategies are devised to decrease the amount of accumulated porphyrins: suppression of erythropoiesis, short or long-term blood transfusions, splenectomy in severe cases, use of agents that help excrete porphyrins such as cholestyramine and charcoal, among other palliative therapies. In general, these treatments vary from one patient to another, being ineffective or mostly, producing secondary effects and various complications especially emphasizing iron overload, thrombocytopenia or risk of infections among others[26,28,33].

Another strategy is the photoprotection, for example, the oral administration of beta carotene increases sun tolerance of the skin but it alone does not become effective[34] and sunlight avoidance is fundamental. Thus, it is strongly recommended for CEP patients the use of sun protective clothing, hats, opaque sunscreens with pigmentary grade titanium dioxide or zinc oxide, possibly with added iron oxide can be effective. Unfortunately, these physical barriers could lead to vitamin D deficiency, so additional supplementation can be necessary[35].

The current curative treatments that are applied are bone marrow or hematopoietic stem cell transplantation (HSCT) and genetic therapy. HSCT is currently the most effective to cure CEP, however involves many operative risks and there are cases of patients who have died[36,37] as well as post-operative complications such as transplant rejection or infections[35,38]. In any case, not all transplanted patients have been reported and their follow-up is currently deficient. Concerning gene therapy, the use of viral vectors containing non-deficient human UROIIIS cDNA has corrected *in vitro* the enzymatic defect in CEP cells [39]. This supports a future use of this approach for the cure of CEP in humans. However, the use of gene-transfer techniques in the clinical setting should avoid the risk of genotoxicity. The alternative use of induced pluripotent stem cells (iPSCs) for gene therapy may be a safer alternative [40].

Consistently, there are currently no approved treatments for CEP, highlighting the need of identifying novel therapeutic strategies that addresses the underlying pathology to impact significantly in the quality of life of these patients.

I.5. Molecular basis of CEP pathogenesis.

The molecular basis of CEP pathologies is closely related to the alteration of the biosynthesis of heme group. In particular, as defined above, the deficient enzyme is UROIIIS. Therefore, we will make an in-depth review of the structure, thermodynamic as well as mechanistical studies of the involved enzyme, for which the mutations detected generate instability leading ultimately to the pathology of the disease by accelerating protein misfolding.

I.5.1. Heme group biosynthesis.

The heme group plays important roles in oxidation-reduction reactions and oxygen transport, which is necessary for a variety of hemoproteins, such as hemoglobin, myoglobin, respiratory cytochromes, and cytochrome P450 (CYP) enzymes. In humans, although the heme group is produced in all cells, approximately 85 % daily is mainly synthesized by erythrocytes in the bone marrow and most of the rest takes place in hepatocytes cells[41], for obtaining CYP, which are especially abundant in the liver endoplasmic reticulum (ER). At least in humans, under normal conditions, physiological concentrations of porphyrins stay low because of the high efficiency of heme synthesis, which seems to indicate that the enzymes work at the maximum possible speed.

On the contrary, abnormal regulation of heme synthesis may result from defects in enzymes of the synthetic pathway, and this may occur as the result of inherited and/or environmental factors leading to the accumulation in the body of one or more heme pathway intermediates, such as the porphyrins or their precursors, as occurs in the case of CEP, produced ultimately by the fourth enzyme deficiency of the route (UROIIIS).

Heme biosynthesis is a chemically sophisticated process, constituted by a series of sequential reactions carried out by eight different intracellular enzymes localized between the mitochondria and the cytosol (Figure 10). The first enzyme, δ-aminolevulinate synthase (ALAS; EC 2.3.1.37), as well as the last three enzymes, coproporphyrinogen oxidase (CPOX; EC 1.3.3.3), protoporphyrinogen oxidase (PPOX; EC 1.3.3.4) and ferrochelatase (FECH; EC 4.99.1.1) are mitochondrial, whereas the remaining enzymes including δ-aminolevulinic acid dehydratase (ALAD; EC 4.2.1.24,), porphobilinogen deaminase (PBGD; EC 4.3.1.8), uroporphyrinogen III synthase (UROIIIS), and uroporphyrinogen decarboxylase (UROD; EC 4.1.1.37) are localized in the cytosol. The synthesis of heme group is the result of several chemical processes including the formation of the pyrrole moiety, the condensation of pyrroles to render a linear tetrapyrrole and the subsequent cyclization with inversion of configuration. This metabolite is the scaffold for further modifications of the tetrapyrrole side chains and a final oxidation of protoporphyrinogen IX (PROTOgen IX) to protoporphyrin IX (PPIX) followed by insertion of iron.

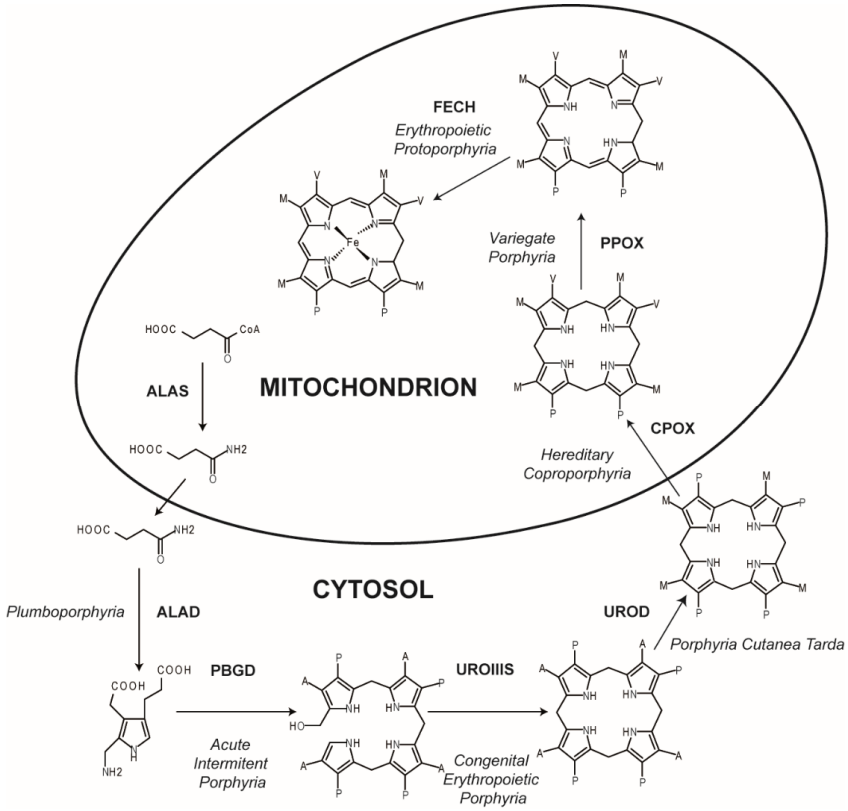

Figure 10. General scheme of heme group biosynthetic pathway, which occurs between the mitochondrion and the cytosol. Acronyms for the enzymes: δ-aminolevulinate synthase (ALAS), δ-aminolevulinate deaminase (ALAD), porphobilinogen deaminase (PBGD), uroporphyrinogen III synthase (UROIIIS), uroporphyrinogen decarboxylase (UROD), coproporphyrin oxidase (CPOX), protoporphyrin oxidase (PPOX) and ferrochelatase (FECH). Each specific porphyria is linked to a deficient activity in each enzyme of the pathway. Adapted from[16].

The synthesis begins with the formation of δ-aminolevulinic acid (ALA) as a natural precursor of the route in the mitochondrial matrix, being the first and rate-limiting reaction in the pathway. Two different ways of ALA production have been described; Shemin and the "C5-pathway"[2,42] (Figure 11). The first one, discovered by Shemin, involves the condensation of glycine and succinyl-CoA by ALAS and occurs in mammals, fungi, and α-proteobacteria. The "C5-pathway" is found in plants, archaea and most bacteria. In this alternative biosynthetic path, ALA is produced from tRNA-bound glutamate in two steps: an initial reduction of glutamyl-tRNA to glutamate-1-semialdehyde by the glutamyl-tRNA reductase (GluTR; EC 1.2.1.70) and the subsequent transformation into ALA by glutamate-1-semialdehyde-2,1-aminomutase (GSAM; EC 5.4.3.8)[43].

Whereas there is usually only one isoform of bacterial ALAS proteins, mammals carry two different ALAS isoforms; ALAS1 and ALAS2. ALAS1 is ubiquitously expressed in all tissues providing the basic needs of heme in the non-erythropoietic cells. ALAS2 is expressed exclusively in the erythropoietic cells sustaining high levels of heme biosynthesis and playing an important role during the late stages of erythropoietic differentiation, becoming essential for the maturation of the blood cells[44]. Regardless of the isoform, ALAS always uses pyridoxal 5'-phosphate (PLP) as an essential cofactor[45].

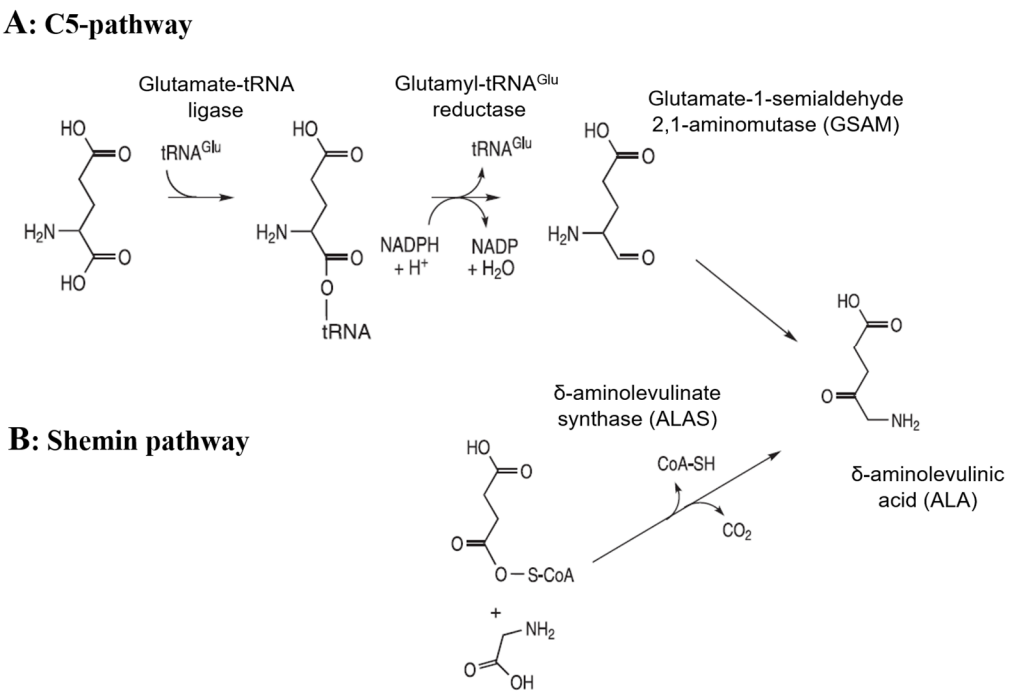

Figure 11. C5 and Shemin pathways for ALA biosynthesis. Adapted from[42].

ALA is exported to the cytosol. The mechanism of ALA transport is not fully understood, but a role for solute carrier family 25 member 38 (SLC25A38) and ATP-binding cassette subfamily B member (ABCB)10 has been suggested[41,46,47]. Once on the cytosol, two molecules are condensed to yield the pyrrole ring porphobilinogen (PBG), in an enzymatic reaction catalyzed by ALAD. The assembly of tetrapyrrole occurs when four molecules of PBG are condensed by PBGD to render the highly unstable linear tetrapyrrole hydroxymethylbilane (HMB)[48], substrate of UROIIIS (Figure 12).

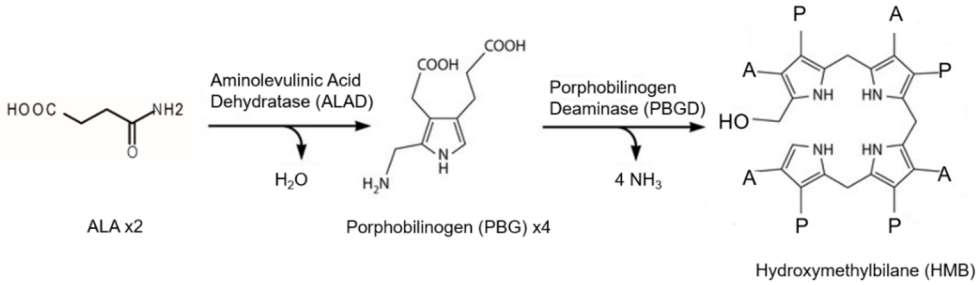

Figure 12. Biosynthesis of the linear tetrapyrrole HMB from ALA. A= Acetate; P= Propionate.

Particularly, under the biochemically point of view PBGD is an interesting enzyme because of it catalysis four distinct reactions: it forms a linear tetrapyrrole from four units of PBG using a single active site, with a distinct and yet chemically equivalent bond being form each time. The existence of four distinct complexes of the enzyme, each containing a separate reaction intermediate was proven before[49], but the complexes were never characterized at the structural level. Our laboratory for the first time has been able to capture, separate and monitor stable reaction intermediates of PBGD. The results prove the dynamic character of the enzyme and results in the first diffraction of PBGD crystal with an intermediate bound.

Following the pathway, UROIIIS catalyzes the rapid cyclization of the linear tetrapyrrol HMB, inverting the configuration in one of the aromatic rings to form the first cyclic intermediate of tetrapyrrole uroporphyrinogen III (UROgen III). Since this enzyme is the source of mutations that produce CEP, a detailed mechanistic and structural description of UROIIIS is reported in section I.5.2. In the absence of the UROIIIS enzyme (or when ill-functioning), HMB spontaneously degrades to the by-product uroporphyrinogen I (UROgen I). This process occurs by non-enzymatic reaction and the by-products cannot lead to the heme group and accumulates in the body, producing some of the symptoms observed in CEP patients. The subsequent steps of the route enable the modifications of tetrapyrrole side chains required to produce heme. UROD catalyzes the stepwise decarboxylation of the four acetic acid chains of UROgen III (and UROgen I) to yield the corresponding methyl groups of coproporphyrinogen III (COPROgen III) or COPROgen I (Figure 13). Remarkably, such decarboxylation is produced step-wise with all the intermediates (Hepta-, Hexa- and Penta- porphyrinogen III/I, Figure 13) being natural substrates of UROD.

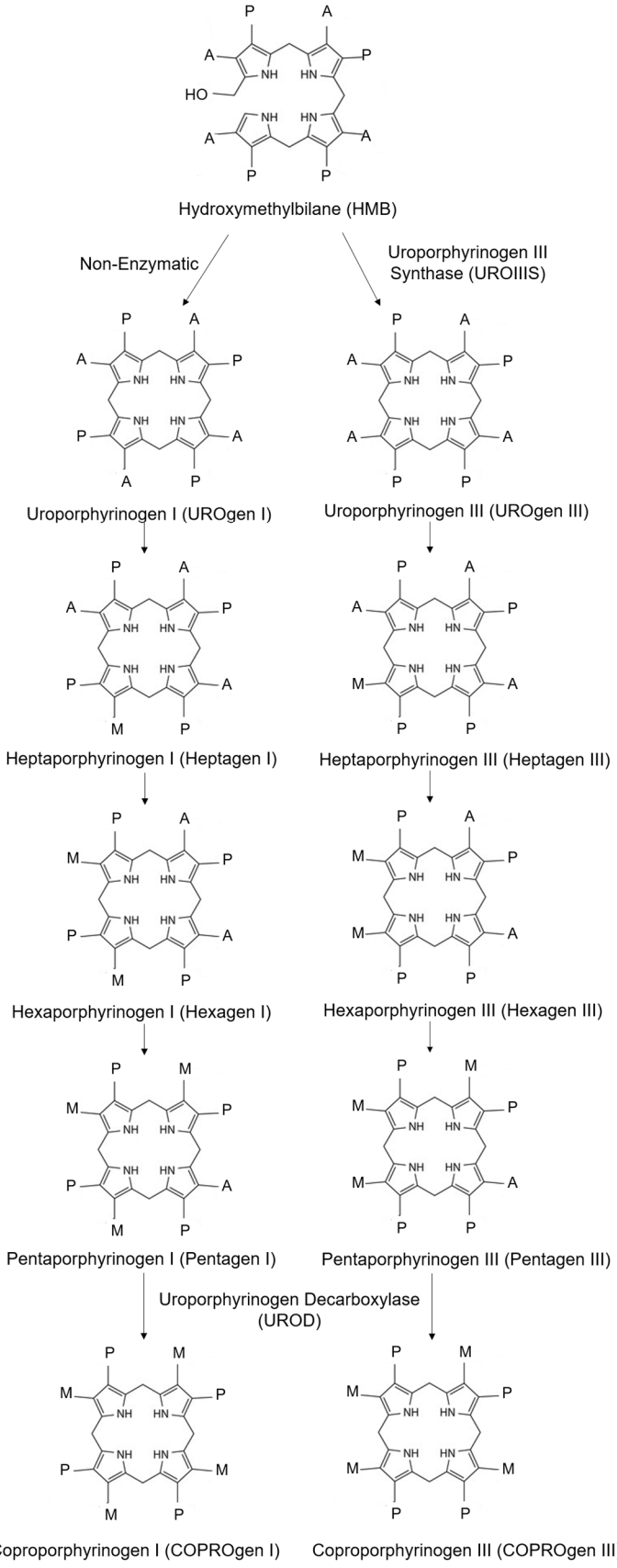

Figure 13. Biosynthesis of the macrocycle tetrapyrrole COPROgen III from HMB. Part of HMB is also condensed non-enzymatically to form the biologically inactive UROgen I. Decarboxylation of UROgen III/I to form COPROgen III/I catalyzed by UROD. Intermediates are represented; Heptaporphyrinogen III/I, Hexaporphyrinogen III/I and Pentaporphyrinogen III/I. A= Acetate; P= Propionate; M= methyl.

Analyzing further down in the metabolic pathway, COPROgen III is imported into the mitochondrial intermembrane space by the membrane transporter ABCB6[50], and it is then transformed into PROTOgen IX by the action of the oxygen-dependent CPOX. PROTOgen IX is further oxidized to PPIX by PPOX. Finally, ferrous iron is incorporated into PPIX to form heme in the mitochondrial matrix, a reaction catalyzed by FECH (Figure 14). FECH is another rate-limiting enzyme of the heme biosynthetic pathway.

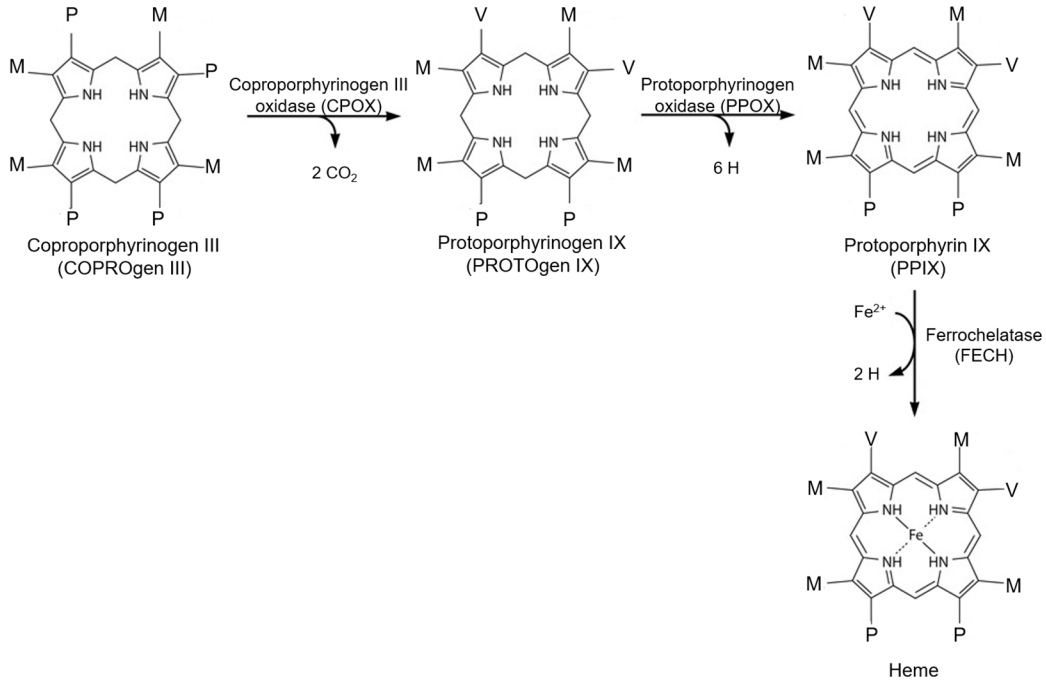

Figure 14. Final part of the biosynthesis of heme group from COPROgen III. A= Acetate; P= Propionate; M= methyl; V= vinyl group.

In non-erythrocytes cells, the regulation of the pathway depends on the pool of free heme levels, where ALAS1 is regulated by negative feedback of the free heme pool produced. Instead, in the erythrocytes, the heme group activates its own synthesis due to the high requirements of heme during differentiation and maturation of the erythropoietic cells. In this case, heme biosynthesis is closely related to the amount of iron regulating the expression of ALAS2 and FECH enzymes. Such regulation is produced at the RNA level thanks to a special structural element in the promoter region (erythroid promoter region, PE), which selectively recognizes the iron ion.

I.5.2. Human Uroporphyrinogen III synthase (UROIIIS); Structure and Function.

UROIIIS is the fourth enzyme of the heme biosynthesis pathway localized in the cytosol, whose importance lies in the formation of the first cycled tetrapyrrole UROgen III, without becoming a limiting step in the route. Its structure was crystallized for the first time by Mathews, M. *et al*.[51] at a resolution of 1.85 Å determining that the protein folds into two alpha/beta domains connected by a beta-ladder, with the active site between the domains (Figure 15).

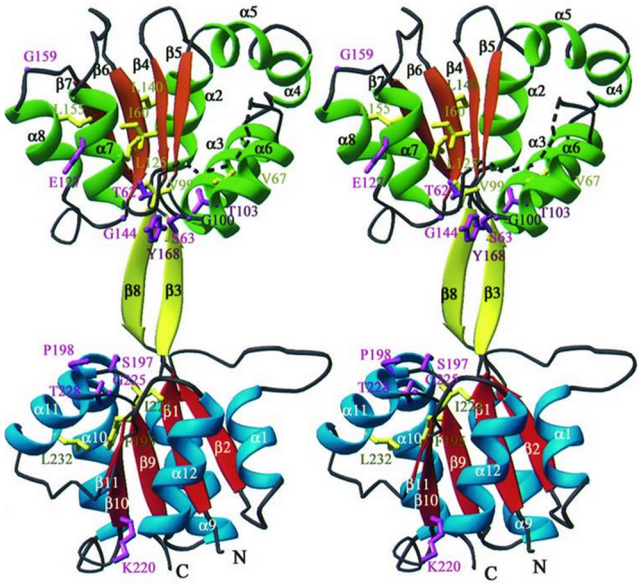

Figure 15. UROIIIS structure in stereo. Helices and strands of domain 1 are blue and red, helices and strands of domain 2 are green and orange. Strands connecting the two domains are yellow. Secondary structure elements and chain termini are labeled. The dotted line represents the disordered loop (residues 114-118)[51].

It has been described that UROIIIS is a remarkably thermolabile and highly efficient enzyme[32] with a catalytic activity of 2.5×10^8 sec^{-1} M^{-1}, being more active than other cytosolic enzymes in the pathway[52]. Consequently, UROIIIS does not catalyze a rate-limiting step in heme biosynthesis, this may explain why in some mild CEP patients do not present hematological abnormalities. The high catalytic efficiency of UROIIIS combined with the relative low PBGD activity in RBC precursors favoring the conversion of HMB substrate into the physiologically active form UROgen III, and only a minor part yields the non-physiological product UROgen I [53]. Such UROgen I product constitute a minimal amount and the oxidized form of this metabolite, uroporporphyrin I (URO I) will be eliminated by the urine[31]. In most CEP patients, the residual UROIIIS activity in erythrocytes ranges from 5 to 35 % of the normal values[21].

As mentioned above in the description of heme biosynthesis, UROIIIS catalyzes the formation of UROgen III from the linear tetrapyrrole HMB. In order to clarify the mechanism of action and based on the structural data available, it has been proposed a scheme of the catalytic mechanism for UROIIIS, in which rearrangement of the A ring results in the loss of the C20 hydroxyl group to create a carbocation at C20 that performs an electrophilic attack on C16 to form a spirocyclic pyrrolenine intermediate (Figure 16). This intermediate can resolve in the same direction thus restoring the substrate or in the opposite direction to generate an azafulvene. Intriguingly, UROIIIS forces a conformation in the tetrapyrrol that separates C19 from C20 to avoid the electrophilic attack that would lead to the formation of the I isomer. The high degree of flexibility conferred to the D ring may be required for the flip that this ring has to undergo prior to the formation of the III isomer product[16,51].

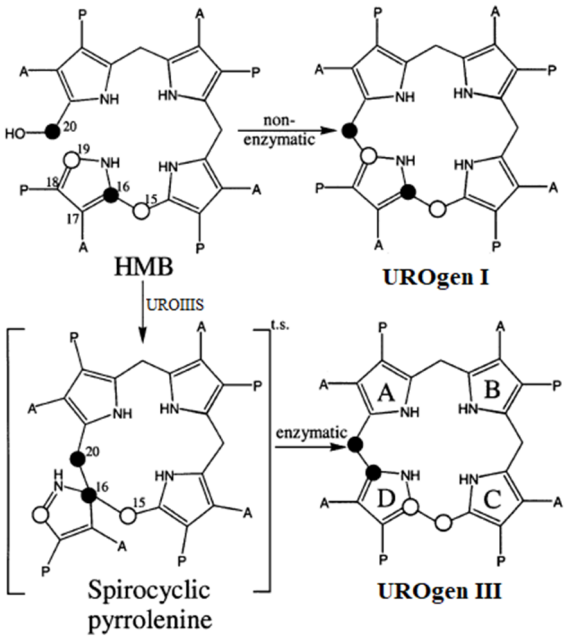

Figure 16. Conversion of HMB to UROgen I (non-enzymatic) and UROgen III (enzymatic). A, acetate; P, propionate. The linear tetrapyrrole is cyclized by UROIIIS with inversion of ring D to form the asymmetric product UROgen III (pyrrole rings labeled A–D). Adapted from[51].

I.5.3. Missense mutations on UROIIIS causing CEP.

The UROIIIS human protein is composed of 265 amino acids (aa) encoded by the *UROS* gene, located on chromosome 10q25.2-q26.3 (Figure 17), whose total length is about 34 kb and consists of 10 exons and 10 introns. Alternative promoters with tissue-specific regulatory elements for housekeeping for constitutive expression in all cells or erythroid-specific expression increased during hemin-induced erythroid differentiation[54] (Figure 17). The protein is active as a monomer with an apparent molecular mass of 29.5 kDa[32].

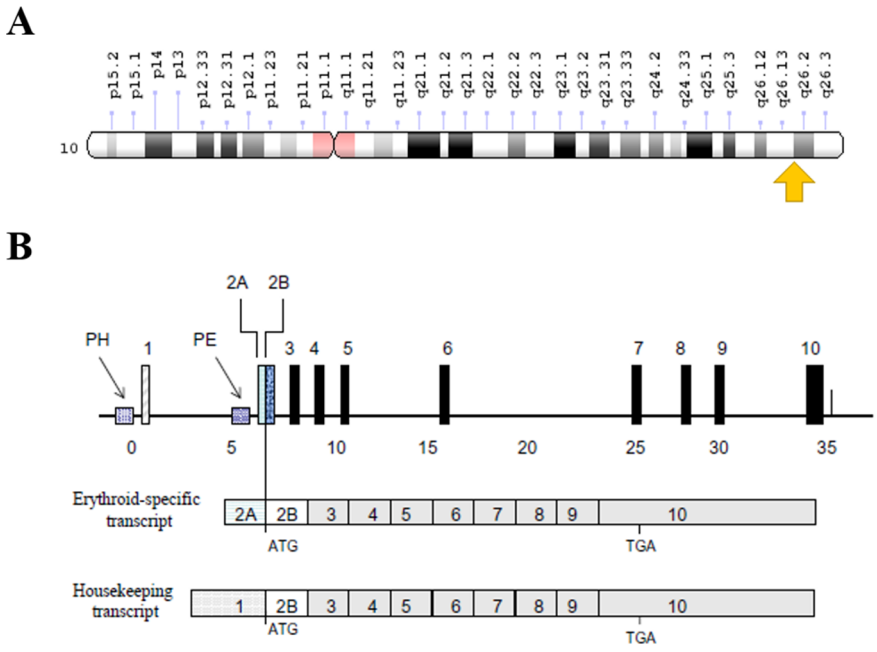

Figure 17. *UROS* gene location and regulation. A) *UROS* gene location on chromosome 10q25.2-q26.3. Image from Genome Decoration Page/NCBI (https://ghr.nlm.nih.gov/gene/UROS).B) Schematic architecture of the *UROS* gene and the different housekeeping and erythroid mRNA transcripts. AT and TG indicate the translation start and stop sites. Arrows and letter P indicate the housekeeping (PH) and erythroid promoter (PE) regions. The housekeeping promoter region is upstream of the non-coding exon 1, while the erythropoietic promoter region is within intron 1 upstream of the non-coding exon 2A, which is immediately upstream of the coding exon 2B. The translation start site for both transcripts is 26 bp downstream of the exon 2A/B junction. Hence, single gene yields two alternative RNA transcripts, a housekeeping transcript containing the 5' untranslated exon 1 joined to exons 2B through 10 and an erythroid-specific transcript with the 5'untranslated exon 2A joined to coding exons 2B through 10. This arrangement yields different transcripts in erythroid and non-erythroid cells, although both initiate translation at the same initiation codon and thus yield identical URO synthase proteins. Adapted from[21,54].

To date, over 49 URO-synthase disease-causing mutations are listed in the Human Gene Mutation Database (www.hgmd.org), divided in missense mutations (29/49), splicing defects (4/49), insertions/deletions (10/49) and mutations in the erythroid promoter or transacting erythroid-specific transcription factors (6/49). That said, patients with CEP genotype also have been diagnosed without mutations identified in any of the alleles[35] and produced by enzyme activating mutations in the *ALAS2* gene. Nevertheless, missense mutations in the coding region are the most common source of CEP pathogenesis, where according to the cases reported, by far, the most frequent mutations in CEP are C73R (exon 4) and P248Q (exon 10) whose allelic frequency is established in 35% and 10% respectively (Table 2). On the other hand, due to the diversity of mutations for the *UROS* gene and the recessive characteristic of transmission, both progenitors must carry a mutation for the enzyme showing different severity of the disease.

Nucleotide change	Amino acid change	mutant design	Frequency of the allele /%[a]
		WT	-
c.7G>T	p.Val3Phe	V3F	4
c.10C>T	p.Leu4Phe	L4F	4
c.56A>G	p.Tyr19Cys	Y19C	4
c.139T>C	p.Ser47Pro	S47P	8
c.158C>T	p.Pro53Leu	P53L	3
c.172G>A	p.Gly58Arg	G58R	1
c.184A>G	p.Thr62Ala	T62A	1
c.197C>T	p.Ala66Val	A66V	1
c.205G>A	p.Ala69Thr	A69T	5
c.217T>C	p.Cys73Arg	C73R	35
c.243A>T	p.Glu81Asp	E81D	1
c.244G>T	p.Val82Phe	V82F	1
c.296T>C	p.Val99Ala	V99A	4
c.311C>T	p.Ala104Val	A104V	1
c.338A>T	p.Asp113Val	D113V	1
c.386T>C	p.Ile129Thr	I129T	2
c416T>G	p.Leu139Pro	L139P	2
c.517C>T	p.His173Tyr	H173Y	2
c.560A>C	p.Asn187Pro	Q187P	1
c.562G>A	p.Gly188Arg	G188R	2
c.562G>T	p.Gly188Trp	G188W	1
c.634T>C	p.Ser212Pro	S212P	3
c.656T>G	p.Ile219Ser	I219S	2
c.673G>A	p.Gly225Ser	G225S	5
c.683C>T	p.Thr228Met	T228M	3
c.707G>T	p.Gly236Val	G236V	1
c.710T>C	p.Leu237Pro	L237P	3
c.743C>A	p.Pro248Gln	P248Q	10
c.764T>C	p.Ile255Thr	I255T	1

Table 2. Missense mutations of *UROS* gene. Human Gene Mutation Database (www.hgmd.org).
[a]Accounting for all the cases reported in the scientific literature to date. Adapted from[55].

It is clear then that there is a relationship between the genotype/phenotype according to the classification established by Warner, C. *et al*.[18]; Fontanellas, A. *et al*.[19] and briefly stated in section I.1, the severity is divided in mild patients with cutaneous symptoms and can often live a normal live in adulthood; moderate patients have mild anemia and/or weak splenomegaly with skin lesions; and severe patients which are transfusion-dependent and sometimes show reduced life expectancy. Since it is clear that the disease onset is related to the specific genotype inherited, Figure 18 now shows the genotype/phenotype relationship according to this classification.

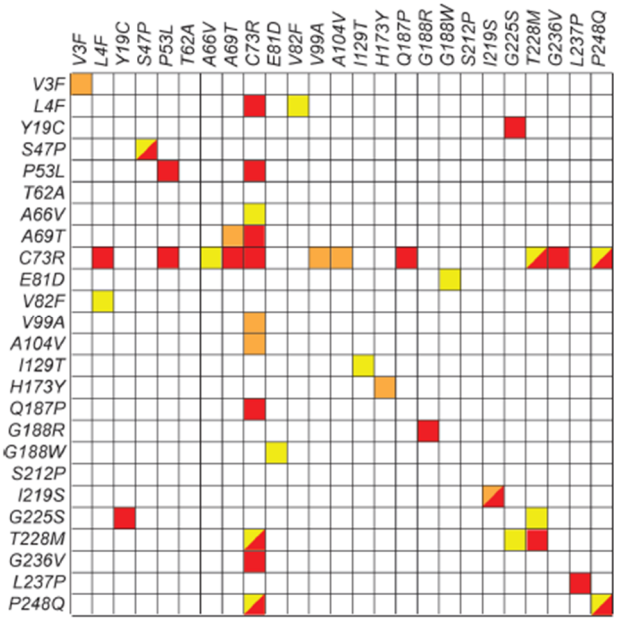

Figure 18. Genotype/phenotype analysis of the studied cases of congenital erythropoietic porphyria. Mild, moderate, and severe phenotypes are colored in yellow, orange, and red, respectively. Patients with different phenotypes but sharing genotype are represented by triangles[16].

It has been observed that the majority of reported patients inherit the same mutation, which could be explained from a local spread of the mutation within demographic groups. C73R is the most aggressive and frequent mutation, responsible for more than one-third of all reported known cases of CEP. Therefore, from the clinical point of view, C73R is the most relevant mutation in CEP[56], it has received special attention in the literature and it also constitutes and important scientific goal to be addressed in the present work.

I.5.4. Stability and catalytic activity of UROIIIS variants associated to CEP.

UROIIIS is a thermolabile protein undergoing irreversible denaturation, being an unstable enzyme that evolves into an unfolded and aggregated final form over time. However, at physiological temperature and *in vitro*, UROIIIS has a half-life time of 61.1 h, a sufficiently long time for the enzyme to exert its function in the cell[57]. This dynamic energy landscape for the UROIIIS protein has been characterized using a simple three-state model, which is suitable to describe the so-called kinetically stable proteins[58]:

$$\mathrm{N} \underset{k_{UN}}{\overset{k_{NU}}{\rightleftharpoons}} \mathrm{U} \xrightarrow{k_{UF}} \mathrm{F}$$

where k_{NU}, k_{UN}, and k_{UF} are the kinetic rates of the process, N is the native state and U the unfolded state that spontaneously converts into the more stable (often inactive) final state F. Nuclear magnetic resonance (NMR) studies determined that the unfolding rate (k_{UN}) for UROIIIS at physiological temperature is $1.6\pm0.2\text{x}10^{-6}\text{s}^{-1}$ [16]. In this model, F is thermodynamically more stable than N whose behavior is explained in Figure 19.

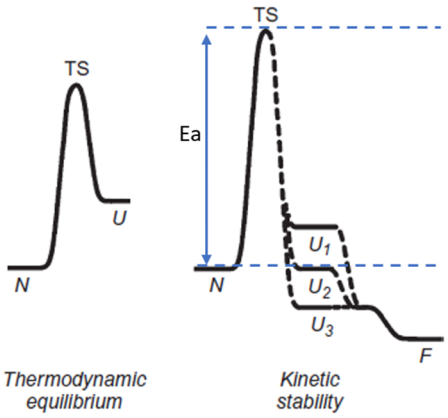

Figure 19. Thermodynamic versus kinetic stability. In the thermodynamic equilibrium, the native state (N) is always more stable that the unfolded one (U). When the kinetic stability regime applies, the folded state is always less stable than another conformation of the protein (generically called F). The N state only exists for a certain time and due to the large energy barrier (E_a) that separates it from the transition state (TS). Under these conditions, the U state can have less, the same or more stability than the N form of the protein U_1, U_2 or U_3 represent the possible unfolded states of the system, which eventually evolves to a final, aggregated state (F). Adapted from[16].

On the other hand, the activation energy is obtained by the temperature dependence of the unfolding rate constant, applying the Arrhenius model:

$$k_{NU} = A \cdot e^{-E_a/RT}$$

where R is the universal gas constant and A is the frequency factor that includes the entropic contribution. The activation energy for wild-type UROIIIS, derived from the slope of the linear plot of $\ln(k_{UN})$ versus 1/T is 101.5 kcal mol^{-1}. The energy barrier (E_a) explains the energetic difference between the active folded conformation (N state) and the highest energy conformation in the unfolding process. For WT (Wild Type) UROIIIS the E_a value is large falling in the normal range of proteins kinetically stable[59].

It is educational to compare the *in vitro* determined kinetic stability from WT and CEP-causing mutants of UROIIIS and frame this data in the context of their catalytic activity, as determined by enzymatic assays[60]. Most of mutations that produce CEP are associated with the loss of the stability of the UROIIIS bioactive conformation due to misfolding, reducing their kinetic stability, while maintaining much of the catalytic activity (Table 3). This situation is pretty general among the deleterious mutants and introduces the *stability defect*[16]. Remarkably, C73R becomes the most unstable of all the mutant variants of UROIIIS, being >400 times more prone to denaturation than wildtype UROIIIS, the unfolding half-life dropped from 61.1 h (WT) to less than 10 minutes (C73R) at physiological temperature (37ºC)[57], providing an explanation for the severity of the phenotype observed inpatients carrying this mutation.

Sequence variant	Kinetic Stability[a]	Eukariotic Expression[b]	E.a.(Mut/WT) /%[c]
WT	100,0	46,8	100,0
V3F	21,9	3,5	19,3
L4F	20,3	4,1	20,2
Y19C	8,3	3,2	13,0
S47P	40,0	2,3	100,0
P53L	81,4	2,8	80,0
G58R	50,5	3,9	n.a.
T62A	91,7	40,7	1,2
A66V	61,2	18,9	95,6
A69T	10,3	2,5	24,4
C73R	3,2	2,5	14,5
E81D	87,0	15,8	100
V82F	81,6	15,8	93,8
V99A	91,2	24,2	88,2
A104V	84,7	24,3	60,6
D113V	n.a.	12,0	n.a.
I129T	13,6	3,9	20,0
L139R	29,7	4,5	n.a.
H173Y	24,0	5,5	72,6
Q187P	10,7	4,9	15,0
G188R	32,7	4,1	41,4
G188W	24,9	2,4	31,6
S212P	6,8	2,7	20,0
I219S	34,0	5,8	85,0
G225S	89,7	29,4	32,4
T228M	72,2	11,1	97,5
G236V	15,0	4,0	34,0
L237P	27,0	3,6	57,9
P248Q	25,2	2,9	29,2
I255T	63,7	4,6	n.a.

Table 3. Stability properties of the reported CEP pathogenic mutants. [a]Determined from the stability of the secondary structure, monitored by circular dichroism. [b]Percentage of EGFP in K562 cells expressing UROIIIS-EPFG. [c]Referred to WT UROIIIS specific activity (E.a).

I.5.5. Activity rescue of deficient UROIIIS protein.

It has been demonstrated that the mutations that speeded up the process of protein denaturation, cluster in a specific region of the protein: the third helix of the C-domain which is not involved in the catalytic center[21]. This fact has received special attention in stability studies in order to rescue the enzymatic activity. Structurally, the combination of *in silico* and *in vitro* studies have attempted to modify the charge configuration of helix C-domain that contains the C73R mutation. This C-domain with C73 is highly amphiphilic, while the alpha helix of the protein prone to produce electrostatic repulsions. The computationally designed rescue mutants L43D/C73R and A69E/C73R improves the electrostatic field of this affected region, retaining up to 75% of the catalytic activity. Assays in mammalian cells with these double mutants are not effective, but docking studies demonstrated that the interaction network surrounding R73 hotspot conforms to a solvent accessible pocket which may be exploited in further therapeutic interventions[61].

On the other side, the sequence of UROIIIS protein carrying C73R mutation has been cloned and expressed in different mammalian cell lines, where in contrast to the WT, the C73R variant does not accumulate in the cytoplasm at detectable levels, indicating that the mutant protein is processed rapidly by the cellular degradation pathways[62]. In this context, it has been demonstrated by inhibition of the main cellular degradation pathways that the levels of the mutant protein are recovered under the presence of MG132, an inhibitor of the proteasomal system (Figure 20). Alternatively, in the presence of lysosome inhibitors such as ammonium chloride (NH_4Cl) or chloroquine, no rescue is observed, indicating that the proteasome is the natural pathway degradation for UROIIIS (Figure 20). The mutant protein accumulated in the cells by inhibition of the proteasome shows a partial recovery of the catalytic activity, the mutant retains 50 % activity with respect to UROIIIS WT[62].

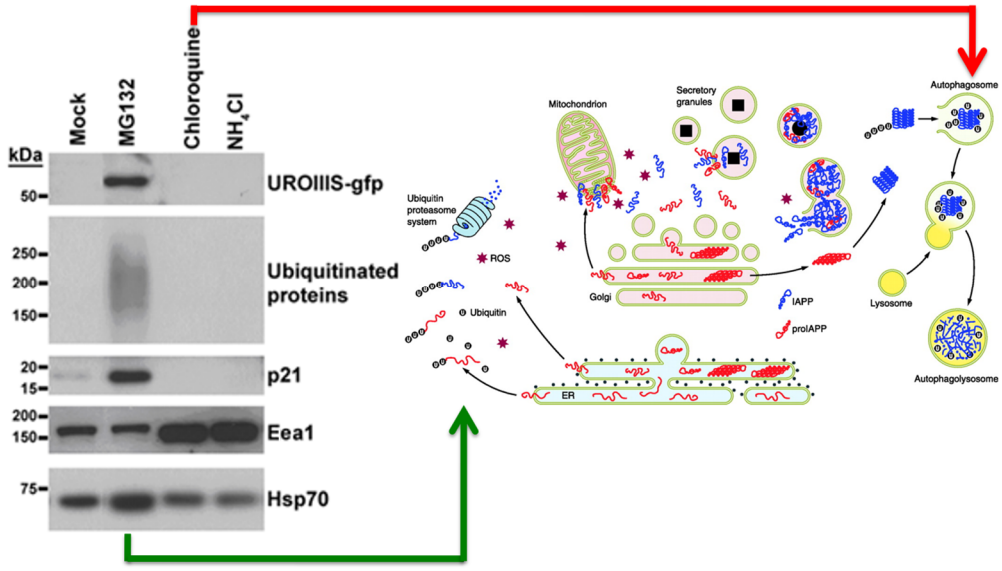

Figure 20. Inhibition of main intracellular degradation pathway of UROIIIS. Western blot of MLP29 cells stably expressing C73R UROIIIS-GFP protein cultured in the presence of dimethyl sulfoxide (mock), or inhibitors of degradative pathways, proteasome (MG132), and lysosome (chloroquine and NH_4Cl), were analyzed by Western blotting. The C73R UROIIIS-GFP protein was detected by using an antibody against the GFP (green fluorescent protein) moiety. Hsp70 serves as a protein loading control, and the accumulation of early endosomal antigen 1 (Eea1), p21, and ubiquitinated proteins confirms that the inhibitors were working properly. Green arrow indicates the proteasome degradation pathway in the right diagram and the red arrow indicates the lysosomal pathway. Adapted from[62].

I.5.6. Accumulations of porphyrins.

The pathology in porphyrias is largely associated with the accumulation in excess of some of the intermediary products (porphyrins). Specifically, CEP is altered at the level of the fourth enzyme, producing the accumulation of porphyrins of the isomers I series as a consequence of the UROIIIS defect. As we have seen previously, UROIIIS misfolding decreases the catalytic activity in cells favoring the non-enzymatic conversion of HMB to UROgen I. UROD enzyme recognizes this isomer and decarboxylates it to the COPROgen I form. However, the specificity of CPOX enzyme for the COPROgen III isomer, prevents

COPROgen I to be metabolized nor used to form heme[21]. The overproduction of UROgen I combined with the non-metabolized of COPROgen I by CPOX lead to decrease of heme biosynthesis with the accumulation of isomer I intermediates undergo autooxidation, mainly URO I and COPRO I. Thus, these non-physiological porphyrins I are accumulated in cells and tissues (skin, bone marrow and other organs) constituting the pathogenic basis of the disease.

The main source of porphyrin production in CEP is located in bone marrow due to its function as a hemoglobin producing organ. Also found high amounts of porphyrins in spleen and liver[24], organs associated with the metabolism of heme or erythropoiesis. Definitively, the accumulation of porphyrins in bone marrow occurs in the erythrocyte precursors (normoblasts), where part of these porphyrins will be released into the plasma. This pattern also occurs in the circulating erythrocytes of the blood stream, the accumulation of porphyrins induces hemolysis and release of porphyrins into the plasma that subsequently are deposited in the tissues and bones.

As a natural physiological disposal pathway, part of the porphyrin overproduction is eliminated by excretion. In urine the amount of porphyrins can be increased about 1000 times over the upper normal value[26], providing a characteristic dark-reddish color usually observed from the childhood of the patient. A relationship between the amount of porphyrins in urine and the severity of the disease has been established in the literature[63]. In general, the water-soluble URO I is the main porphyrin found in urine, although concentration of COPRO I is also elevated. Fecal excretion of porphyrins, which is mainly dependent of biliary excretion and subsequent transformation by intestinal bacteria, is also increased in CEP patients, where the major porphyrin found in stool is COPRO I [64]. The decarboxylation of uroporphyrinogen to coproporphyrinogen, and thence to protoporphyrinogen, decreases water solubility, so that uroporphyrinogen is only excreted via the kidneys whereas hydrophobic protoporphyrinogen and protoporphyrin are exclusively excreted into the bile. Coproporphyrinogen is excreted by both routes. Physiological concentrations of porphyrins stay low because of the high efficiency of heme synthesis.

I.6. Misfolding or conformational diseases.

It is clear from previous results from our laboratory and other's that most of the mutations alter the protein stability *in vitro*. The stability defect (as found in CEP mutations) is ultimately related to a deficient protein homeostasis. In this section this concept is further explored making emphasis on the deleterious effect of a proteostatic imbalance and the possible strategies to correct it.

I.6.1. Protein homeostasis (Proteostasis).

In biology, the term homeostasis is defined as: set of self-regulation phenomena, leading to the maintenance of a relative constancy in the composition and properties of the internal environment of an organism. Under this concept, proteostasis is coined to define the protein homeostasis within the cell than spans from the study of individual protein from its biosynthesis, localization and function, up to their half-life and degradation. Proteins are surrounded by a dynamic cellular environment, constantly receive insults of stress, but the

integrity of the proteome is designed to remain intact, owing to a system that maintains protein homeostasis. This system was described by Balch, W. *et al.*[65] called proteostasis network (PN) that control the biogenesis, folding, trafficking and degradation of proteins.
For a protein to become biologically functional it must attain their correct three-dimensional conformation (tertiary structure), which is achieved after a series of conformational transitions required to acquire the native conformation[66]. In principle, the DNA sequence of proteins contains all the information for the protein to fold without intermediaries. Yet, proteins newly formed in the eukaryotic cells are synthesized on ribosomes as linear chains of up to several thousand amino acids. These chains are versatile allowing proteins to adopt a high number of conformations during folding ($>10^{30}$ for a 100-aa protein)[67], being the reactions highly complex and heterogeneous, relying on the cooperation of many weak, non-covalent interactions[68]. In this context, protein folding becomes an error-prone process, requiring a balance between function and risk of aggregation in crowded biological microenvironments where total protein concentrations can range from 100–400 mg/mL[69,70] with a biosynthesis between 10.000 and 20.000 different proteins in mammalian cells[71].

In terms of the conformational landscape, the native conformation of a protein occurs because this state is thermodynamically the most stable in the intracellular environment[72] achieving the lowest energy state possible. Thus, from the physicochemical point of view of a protein, the amino acids pack in such a way that the free energy of the molecule reaches its minimum value[73]. To explain the folding pathway and its rate, a theoretical model is proposed based on the compromise between thermodynamic stability and the conformational flexibility protein required for function, known as the protein's folding energy landscape (Figure 21). In the current model, polypeptide chains are thought to explore funnel-shaped potential energy surfaces as they progress, along several downhill routes, which means that the molecules must cross substantial kinetic barriers during folding towards the native structure[70]. Certain intermolecular interactions may promote chain collapse and lead to states of misfolding or aggregation (amorphous aggregates, β-sheet-rich oligomers, and amyloid fibrils) which are potentially toxic. To prevent or regulate protein aggregation the PN is available, comprising molecular chaperones and other factors forming a cell quality control to ensure proper protein folding and to eliminate misfolded proteins when folding repair mechanisms are unsuccessful[71]. Signaling pathways that regulate PN include the unfolded protein response (UPR), the heat shock response (HSR), the ubiquitin proteasome system (UPS), the endoplasmic-reticulum-associated protein degradation (ERAD) and epigenetic programs[74]. In this context, the endoplasmic reticulum (ER) plays important role as responsible for secretory proteostasis, involving the quality control of ~1/3 of the proteome[75]. Some of this quality control mechanisms in the ER rely on molecular chaperones and folding factors, such as BiP, calnexin, calreticulin, thiol-disulfide oxidoreductases, and protein disulfide isomerase[76].

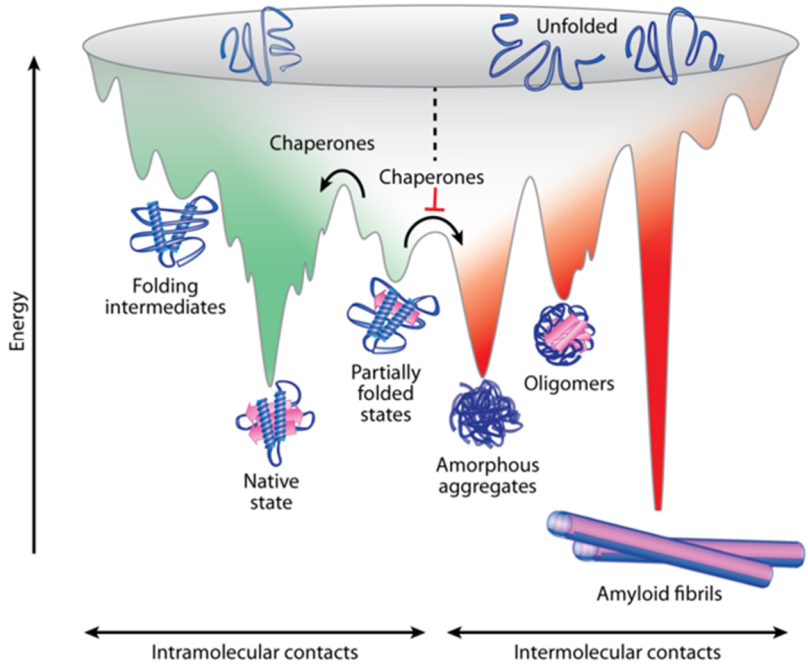

Figure 21. Energy diagram of protein folding. The diagram represents the proteins fold by sampling various conformations in a folding energy landscape. Energetically favorable intramolecular interactions (green) are stabilized as the protein progresses on a downhill path through the landscape toward their correct minimal-energy conformation, the functional native state. Energetically favorable but nonnative conformations result in populations of kinetically trapped states that occupy low-energy wells (partially folded or misfolded states). These states are prone to form amorphous aggregates or oligomers that can join together generating non-functional protein aggregates (amyloid fibrils). Molecular chaperones assist misfolding proteins in overcoming free energy barriers and prevent intermolecular interactions (red) leading to aggregation[68].

I.6.1.1. (Im) balanced proteostasis; sources of alterations.

In general, cellular proteostasis is highly controlled and can be considered as a balance of the protein folding load that maintain a healthy cellular state (Figure 22). When the system is balanced, it means that the PN function properly; cells maximize production of properly folded, functional proteins. Whereas, quality control mechanisms ensure that the production of misfolded and aggregated proteins is minimized. Deregulations of the PN result in an imbalance of the cellular proteostasis (Figure 22). PN deregulations can be caused: (i) by many genetic mutations that destabilize or prevent the folding of a protein; (ii) by dysregulated ER (unresolved by the UPR); (iii) by environmental stressors (adverse physiological conditions; oxidative stress) or (iv) by an apparent loss of age-dependent proteastasis capacity[75,77,78]. All these sources of PN alteration leads to diverse protein misfolding and aggregation-related diseases.

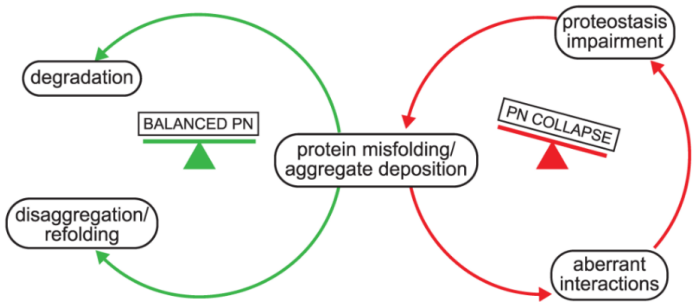

Figure 22. Proteostasis (im)balance in health and disease. The cellular proteostasis is a balance of the folding load (green circle), quality control mechanisms ensure that the production of misfolded and aggregated proteins is minimized. Perturbance of proteostasis, e.g., aberrant interactions or proteostasis impairment, lead to a collapse of the PN result in an imbalance of the celular proteostasis (red circle) favoring the deposit of misfolding or aggregate proteins. These sources of PN alteration leads to diverse protein misfolding and aggregation-related diseases[67].

Specifically, deficiencies in proteostasis has been linked to an expanding list of pathologies lead to metabolic, oncological, cardiovascular and neurodegenerative disorders. These diseases must be classified in: loss-of-function and toxic gain-of-function diseases[71] (Figure 23). The first group is characterized by dysfunction of protein due to mutations (single-nucleotide polymorphisms) that may render proteins metastable and prone to degradation, causing the lack or accumulation of metabolites in the organism, as in the case of cystic fibrosis and a wide range of metabolic defects. The second group is related to accumulation of metastable proteins which undergo aggregation in a process associated with cellular toxicity as occurs with neurodegenerative diseases [Alzheimer disease (AD) and Parkinson disease (PD)], Creufeld-Jackob disease, type II diabetes and certain forms of heart disease and cancer. However, protein aggregation may also be caused by inherited mutations, as in early onset AD and PD or Huntington disease (HD)[79–81]. Understanding the molecular basis of these reactions would guide future efforts to define the PN as a target for pharmacological intervention in protein misfolding diseases.

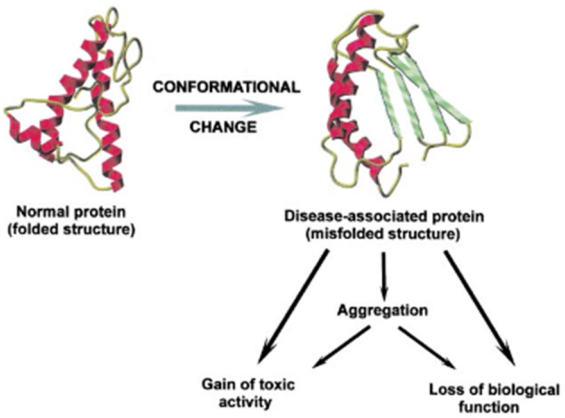

Figure 23. Protein misfolding and disease. The diseases associated with misfolding can be grouped into two different types: loss of biological protein function or gain of toxic activity. Aggregation of the misfolded protein may also contribute to the disease pathogenesis[82].

I.6.2. Molecular chaperones.

Molecular chaperones are families of multi domain specialized proteins that play a fundamental role in the regulation of intracellular proteostasis. In particular, under physiological conditions, they assist newly protein biosynthesis from the ribosome and ensure protein folding, protein trafficking and assembly of macromolecules at the same time that they prevent protein misfolding and re-direct non-native intermediates to the native state[70] or for clearance mediated by the UPS or the autophagy system[83] (Figure 24). They are present in all organisms, both prokaryotic and eukaryotic. In addition, chaperones intervene in maintenance processes under stress conditions such as oxidative stress or thermal shock. In general, chaperones are defined as assistant proteins that help other proteins to reach their native conformation under any circumstance in order to maintain the proteome system balanced.

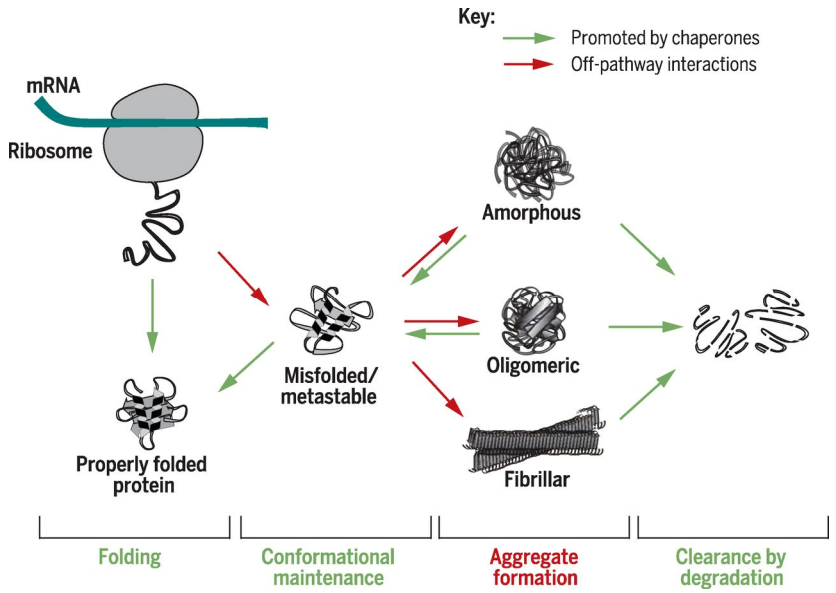

Figure 24. Molecular chaperones are key players in the cellular PN and maintain a balanced proteome. They assist the newly biosynthesis proteins helping to achieve functional native conformation. Also prevent potentially toxic off-pathway protein aggregation by cooperation with other components of PN such as proteasome system and autophagy removing misfolded and aggregated proteins[67].

Although the family of chaperones is broad, they share a certain degree of homology. They can be grouped based on their sequence of homology, being most of them stress proteins or heat shock proteins (Hsps). This diverse family of the striking Hsps is divided according to their molecular weight (in kDa): Hsp40s, Hsp60s, Hsp70s, Hsp90s, Hsp100s and the small heat shock proteins (sHsps). As a generic mechanism of action, chaperones bind to the hydrophobic surface of the unfolded or partially folded proteins in order to avoid aberrant folding and confer further stability to promote the native state of protein. In this context, chaperones are composed of highly coordinated moving parts (displacements and rotations) which most of them depend on energy input such as ATP binding and hydrolysis for their function and, although they tend not to have a broad spectrum of substrates, their specificity is large enough to ensure the integrity of the PN as part of quality control[84] (Figure 25). On the other hand, the mechanisms which chaperones distinguish native from non-native conformations and assist in folding of proteins are yet unknown.

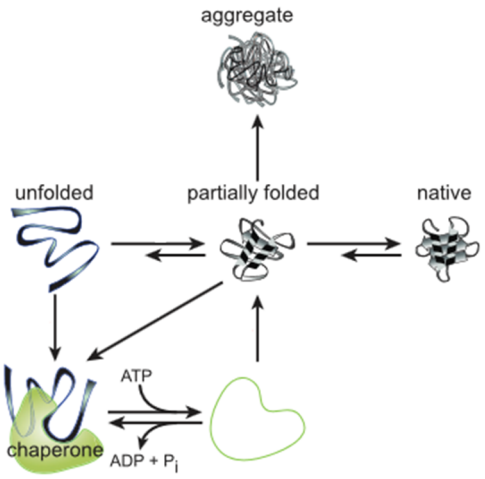

Figure 25. Molecular chaperones promote protein folding by a generic mechanism of nonnative states. ATP binding and hydrolysis are necessary for the performance of most chaperones. They prevent the hydrophobic surface of the unfolded or partially folded proteins from reaching aberrant conformations or aggregates and promote the native state. Adapted from[67].

Deficiencies in protein homeostasis caused by mutations alter the free energy of the folded conformation and leads to reduce folding efficiency. In such cases, the compensatory or regulatory mechanisms of cell quality control, such as the molecular chaperones, are not able to solve. In principle it is possible to propose chaperone-based therapeutic approaches taking advantage of the described assistance properties of chaperones and employing small-molecule ligands that bind to these mutant proteins and stabilize their native state and/or destabilize the transition state to compensate for the influence of the mutation[85]. Natural, chemical or pharmacological chaperones have been shown to be promising as therapeutic agents of many protein-misfolding diseases, including cystic fibrosis, AD, PD and HD, as well as several forms of prion diseases[86].

I.6.3. Types of therapeutic chaperones

Two types of potentially therapeutic chaperones can be distinguished:

Chemical chaperones: chemical molecules with low molecular weight that are capable to correct the folding protein defects helping to achieve the native conformation and to stabilize proteins against thermal and chemical denaturation[86,87]. Typical examples of chemical chaperones are the intracellular osmolytes glycerol, trehalose or deuterated water, which bind and stabilize the unfolded protein. Specifically, glycerol increases the *in vitro* folding ratio and also improves the protein assembly ratio since it is able to decrease the solvent-accessible area of protein, improving its stability[86,88,89]. Meanwhile, others molecules have been classified as hydrophobic chemical chaperones, including sodium 4-phenylbutyrate (PBA) and bile acids, which interact with hydrophobic regions of the unfolded protein exposing certain hydrophobic segments, this interaction suggests that protects the protein from aggregation[90]. Currently, chemical chaperones have not been tested in humans, but the data in mouse cells have been satisfactory. In this context, intracellular positive effects have been described and suggest an improvement in the

stability of various misfolded proteins such as α-antitrypsin[91], vasopressin V2 receptor[92], aquaporin-2[93], p53 and P-glycoprotein[94], cystic fibrosis transmembrane regulator (CFTR)[95], as well as prion protein PrP[96]. Although in theory, chemical chaperones can be considered as potentially therapeutic from the medical point of view, they present mainly some disadvantages; their inespecifity, the fact that the protein binding site of interest is not known. Additionally, they may stabilize most of the proteins in a cell drastically altering the homeostatic balance. Finally, the concentration required to achieve stability may be millimolar or even molar, which is impractical for use in treatment since the doses may be too toxic *in vivo*[97].

Pharmacological chaperones: are considered as a special subtype of chemical chaperones, but the main advantage is their specificity to bind to their target protein and, acts on, at most, only a small number of protein targets, ideally, stabilizing only that macromolecule (Figure 26). Pharmacological chaperones can be, for example, ligands for a receptor promoting its proper folding, or, more specifically, a molecule or drug designed especially to bind the native conformation of the target protein, stabilizing its conformation and pushing the balance toward the native state[76,98].

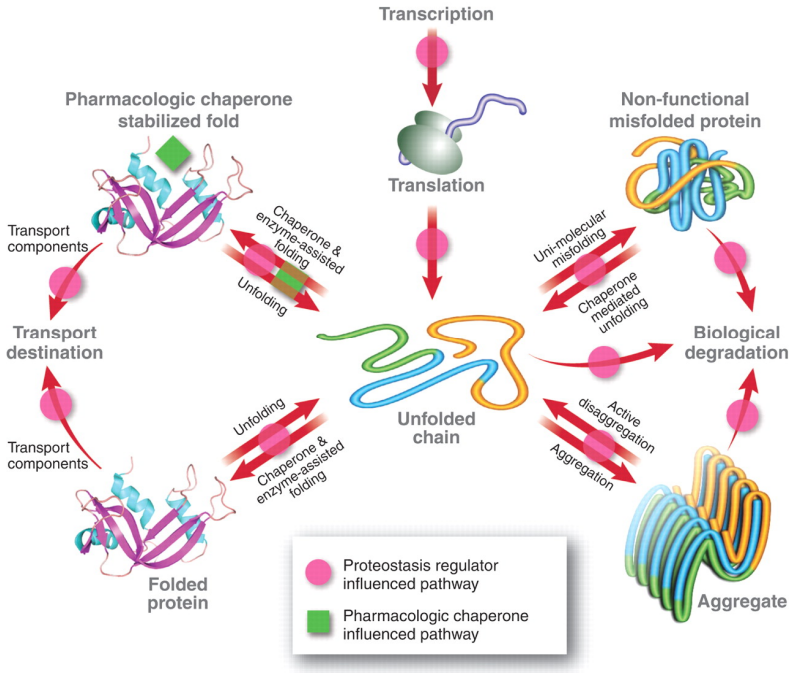

Figure 26. General representation of the proteostasis regulation. Proteostasis regulatory pathways are represented (red arrows) as well as proteostasis regulators (magenta circles). Imbalances in proteostasis lead to disease, regulators can restore protein homeostasis and ameliorate both loss- and gain-of-function diseases. Pharmacological chaperones (green squares) enhance folding and trafficking of a specific protein target through a mechanism distinct from the innate biological pathways influenced by proteostasis regulators[65].

In the literature we can find examples of pharmacological chaperones that show partial or complete restoration of normal function for the targeted mutant proteins including G protein-coupled receptors (GPCRs), ion channels, ATP-binding cassette (ABC) or solute carrier (SLC) transporters, and enzymes such as galactosidases or oxidoreductases[99]. The activity of most pharmacological chaperones has been proved *in vitro* as well as in animal models and humans. Specifically, there is a pharmacological chaperone for the treatment of Fabry disease which is in phase III of clinical trials: migalastat is a drug that has been demonstrated to be safe and effective in improving disease parameters[100]. In addition, the low concentrations required for its function are physiologically acceptable, would overcome the limitations due to high doses of chemical chaperones. Definitely, the properties of pharmacological chaperones offer a novel therapeutic strategy to treat misfolding diseases, which main advantage is their higher specificity where only the folding of the selectively targeted protein will be influenced.

Our laboratory group is involved in the investigation of a new therapeutic line based on pharmacological chaperones for the deficient enzyme UROIIIS against CEP, in order to improve the proteostasis of the protein, re-establishing its stability that ultimately will enhance the symptomatology of the disease. This is the work developed in the present thesis.

I.6.4. Other molecular interventions: modulation of the proteostasis network.

The interest in therapeutic interventions focused on the pharmacological modulation of proteostasis has grown significantly during the last decade. From the point of view of protein stability, these therapies can take the form of drugs that increase the rate of clearance of misfolded/aggregated proteins, and drugs that increase the native-state stability or increase the kinetic barrier to misfolding aggregation[85]. However, therapeutic interventions can also occur at the levels of protein biosynthesis protein or even at the level of the regulation of the homeostatic pathway where the protein of interest belongs to. The modulation of proteostasis opens up a broad field of investigation in which the mechanisms that promote or inhibit its activity can be manipulated and offer new opportunities to treat the wide range of diseases associated with declining proteostasis. In this context, the therapeutic possibilities include drugs that reduce the biosynthesis of a certain protein, up or downregulate chaperones factors, up or downregulation of degradation pathways (UPS or lysosomal degradation) or partially inhibition of previous substrate of the misfolding protein, among others. Of note, both strategies are not mutually exclusive and combined therapies could be more effective when improving the symptomatology and increasing the life expectancy of the patients.

Generally, the modifications in the proteostasis are oriented to the improvement in its regulatory capacity or, by contrary, to its inhibition. In principle, the intracellular proteostatic capacity can be enhanced in several ways (Figure 27): (i) by inhibition of protein biosynthesis to reduce the production of misfolded proteins by compounds which inhibit DNA replication, RNA synthesis (mRNA, tRNA or rRNA), translation, amino acid metabolism, ATP synthesis, cofactor synthesis, etc[101]; (ii) by up-regulating chaperone levels to improve folding and conformational repair; and (iii) by enhancing the clearance

of misfolded proteins and aggregates or by promoting the formation of inclusions that are nontoxic[67]. Conversely, attenuating the proteostasis capacity by inhibiting specific chaperone or degradation pathways is effective in cancer treatment, because oncogenic proteins are often metastable and thus highly chaperone dependent[67,80,102,103]. The inhibition of chaperone Hsp90 prevents the activation of proteins that promote tumor growth factors and are directly degraded[102].

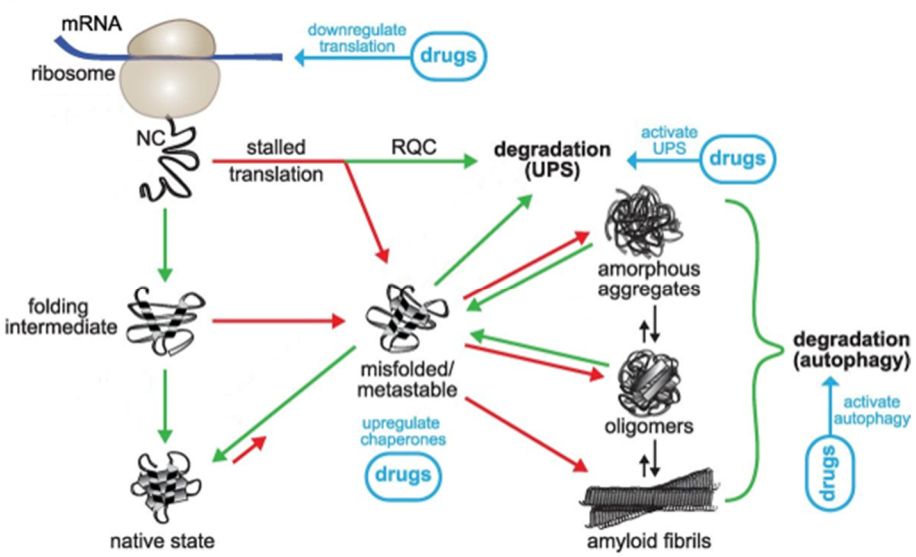

Figure 27. Alternative therapies of proteostasis modulation; drugs targets. Pathways promoted by chaperones are shown with green arrows, off-pathway reactions with red arrows. Options to modulate the proteostasis pharmacologically are indicated. RQC, ribosome quality control machinery. UPS, ubiquitin proteasome system Adapted from[67].

Misfolding diseases that are related to metabolic defects, known as inborns errors of metabolism disorders result from defects in the biochemical pathways of the organism due to the deficiency or the abnormality of an enzyme, its cofactor or a transporter resulting in the accumulation of one or several metabolites normally accompanied by the deficiency of the metabolic product(s)[104]. Biochemically, the modulation of the biosynthetic pathway as therapeutic intervention has been much less studied. Our laboratory has investigated another potential therapeutic line in CEP based on the partial inhibition of the enzyme prior to the affected enzyme, to ultimately decrease the production of some by-products. At the right concentration, this chemical modulation of the route should decrease the accumulation of metabolites due to the frustration of the route since the amount of substrate would decrease, compensating with the functional deficiency of the enzyme. In this sense, the combined use of pharmacological chaperones that retain or stabilize the misfolded enzyme with inhibitors of the previous enzyme of the route may constitute a new therapeutic modality for furthers studies with promising applications in rare diseases of metabolism.

CHAPTER II

OBJETIVOS / OBJETIVES

“We build too many walls and not enough bridges”

— Isaac Newton

II. OBJETIVOS

Los objetivos del presente trabajo están basados en la hipótesis inicial, planteada por nuestro laboratorio, del reestablecimiento de la estabilidad del enzima UROIIIS afectado por mutaciones que causan su mal plegamiento (principalmente C73R), impidiendo que alcance su conformación nativa funcional. El reestablecimiento de esta estabilidad, rescataría la actividad catalítica del enzima, llevando a cabo su función en la ruta de biosíntesis del grupo hemo y, por tanto, mejorando las manifestaciones clínicas de CEP.

Hasta la fecha, estudios previos en nuestro laboratorio han demostrado *in silico* que la incorporación de residuos propensos a interactuar con la mutación C73R en CEP, podría modular la estabilidad cinética, siendo capaces de restaurar la actividad catalítica del enzima[61]. Por otra parte, estudios *in vitro* en células han demostrado que es posible la restauración de los niveles de proteína intracellular por inhibición del proteosoma, vía principal de degradación del enzima, rescatando parcialmente la actividad catalítica[62]. Sin embargo, el uso de inhibidores del proteosoma en modelos *in vivo* tiene efectos beneficiarios a corto plazo, la inespecificidad del tratamiendo hace que sea especialmente tóxico a largo plazo con efectos adversos graves, por lo que no constituye una terapia segura para CEP[105]. Bajo estas pruebas de concepto, el objetivo principal ha estado enfocado en la propuesta de una nueva vía terapéutica más segura para CEP, basada en la **detección de chaperonas farmacológicas que actúen sobre la proteostasis del enzima defectuoso *in vivo***. Para ello, se han llevado a cabo los siguientes objetivos:

1. Desarrollo de una plataforma para el descubrimiento de chaperones farmacológicas, incluyendo:

    1.1. Identificación *in silico* de posibles sitios de unión alostéricos terapéuticos de pequeñas moléculas químicas o fármacos a la proteína UROIIIS.

    1.2. Caracterización *in vitro* del complejo de unión de la proteína UROIIIS y las moléculas de librerías comerciales mediante ensayos de termoestabilidad.

    1.3. Puesta a punto de un sistema celular *in vitro* (*in cellula*) que permita la monitorización de la proteína mutante UROIIIS intracelular.

2. Aplicación de la plataforma para el caso específico de CEP.

3. Caracterización y validación de ciclopirox (CPX).

II. OBJETIVES

The objectives of this study are based on the initial hypothesis proposed by our laboratory to re-establish the stability of the enzyme UROIIIS affected by mutations that cause misfolding (mainly C73R) and prevent to achieve its functional native conformation. The restoration of enzymatic stability would rescue the catalytic activity carrying out its function in the heme biosynthesis pathway and therefore improving the clinical manifestations of CEP.

To date, previous *in silico* studies in our laboratory have shown that the incorporation of residues prone to interact with the C73R mutation in CEP, could modulate the kinetic stability, being capable to restore the catalytic activity of the enzyme[61]. On the other hand, *in vitro* cells studies have shown that is possible to restore intracellular protein levels by inhibition of proteasome, the main route of degradation of the enzyme, partially rescues its catalytic activity[62]. However, the *in vivo* use of proteosome inhibitor in CEP mouse model, has short-term beneficial effects since the treatment is especially toxic in the long term with serious adverse effects, not constituting a safe and long-term therapy for CEP[105]. Under these proofs of concept, the main objective has been focused on a novel therapeutic approach for CEP, based on the **discovery of pharmacological chaperones targeting the defective enzyme and designed to enhance the proteostasis *in vivo***. Based on this hypothesis our main goals are:

1. To develop a platform for the discovery of pharmacological chaperones, including:

    1.1. Identification *in silico* of putative therapeutic allosteric binding sites of small chemical molecules or drugs to the UROIIIS protein.

    1.2. Characterization *in vitro* by thermostability assay of UROIIIS protein bind with small organic molecules from a commercial library.

    1.3. Set up of a cellular *in vitro* system (*in cellula*) to monitoring of the intracellular mutant protein UROIIIS.

2. Application of the platform to the specific case of CEP.

3. Characterization and validation of ciclopirox (CPX).

CHAPTER III

MATERIALS & METHODS

“Make things as simple as possible, but no simpler.”

— Albert Einstein

III. MATERIALS & METHODS

In the present thesis we are interested in finding pharmacological chaperones for deficient UROIIIS, therefore our efforts have been focused on the use of methods that allow us a broad and efficient search. This methodology is closely related to the field of drug discovery based on those techniques that involve a wide range of scientific disciplines, including structure-based approaches and, most recently, computational methods which constitute the first key step in the lengthy process of developing new drugs. In this section we will see a plethora of materials and methods used for this work involving *in silico*, *in vitro* and *in vivo* analyses.

III.1. NMR and computational analyses

The structure-based experiments of NMR and molecular docking have been carried out in collaboration with the technological platform Chassys^{TM} approach from the company Atlas Molecular Pharma S.L. (Basque Country, Spain).

III.1.1. Virtual and commercial chemical libraries

This work is based on different screening assays of chemistry libraries: a virtual library as well as two commercial chemical libraries.

III.1.1.1. Virtual library

For virtual screenings were used a ligand library of 25000 small “drug-like “compounds retrieved in Simplified Molecular Input Line Entry Specification (SMILES) format from the website ZINC (zinc.docking.org), a free online drugbank database of commercially-available compounds. To date, the database contains over 230 million commercially available molecules in biologically relevant representations that may be downloaded in popular ready-to-dock formats, SMILES or 3D formats and subsets. These provided structures improve the potency as well as the selectivity in the process of drug discovery which allow to predict and detect the formation of ligand-receptor interactions. ZINC is provided by the Irwin and Shoichet Laboratories in the Department of Pharmaceutical Chemistry at the University of California, San Francisco[106].

III.1.1.2. Commercial chemical libraries

Library L1: a commercially available chemical library, the Maybridge Rule of three (Ro3) Fragment Library® (Maybridge, Fisher Scientific Int., NH, USA) or so-called in this work as library L1 was used to searching potential pharmacological chaperones for UROIIIS. The Maybridge fragment library contains 2500 selected small compounds (MW <300) ensuring diversity and pharmacophoric content (Table 4). Ro3 compliance delivers superior ADME (Absorption, Distribution, Metabolism and Excretion) attributes, optimizing the development of new orally accepted drugs for human consumption[107,108]. Pre-dissolved in dimethyl sulfoxide (DMSO) at 200 mM solutions.

Ro3 fragments value							
Code	MW	cLogP	NROT Flexibility	HBA	HBD	PSA	Purity
L1.1.A2	206,12	0,28	0	1	3	32,5	≥95%
L1.4.C8	221,20	2,2	2	1	2	43,09	≥95%
L1.6.E5	192,26	1,31	1	1	3	24,5	≥95%
L1.7.G7	125,16	1,42	2	1	2	25,17	≥95%
L1.8.H7	195,57	2,64	0	0	1	12,89	≥95%
L1.9.E6	205,13	1,7	2	0	3	39,19	≥95%
L1.14.D4	137,18	1,32	1	2	1	32,86	≥95%
L1.15.G2	267,19	1,83	2	2	3	49,49	≥95%
L1.17.A5	138,19	0,92	2	0	2	36,68	≥95%
L1.19.F4	178,25	1,73	1	1	2	24,92	≥95%
L1.21.C6	134,17	1,71	0	1	1	20,23	≥95%
L1.23.C11	197,66	1,36	0	0	2	29,96	≥95%
L1.26.A2	166,22	1,7	2	2	3	55,12	≥95%
L1.27.B8	141,19	0,03	1	1	2	43,09	≥95%
L1.30.A5	151,16	0,83	1	2	3	49,33	≥95%
L1.31.B11	95,10	0,11	0	3	1	51,8	≥95%

Table 4. Extract of Maybridge Ro3 Fragment library L1.

Library L2: a second library of 1800 compounds (FDA approved-drug library®, Selleck Chemicals) or so-called in this work as library L2 was used in the drug repurposing studies. The drugs have passed exhaustive tests of control for human consumption by the agency from Unites States responsible for protecting the public health so-called FDA (Food and Drug Administration) department (Table 5). Pre-dissolved DMSO at 10 mM solutions.

FDA Approved Drug Library			
Name	MW	Indication	Target
Atracurium	386,47	Cancer	VEGFR, PDGFR, c-Kit
Afatinib (BIBW2992)	485,94	Cancer	EGFR, HER2
Bortezomib (Velcade)	384,24	Cancer	Proteasome
Bosutinib (SKI-606)	530,45	Cancer	Src,Abl
Dasatinib (BMS-354825)	488,01	Cancer	Src, Bcr-Abl, c-Kit
Erlotinib HCl	429,9	Cancer	EGFR
Gefitinib (Iressa)	446,9	Cancer	EGFR
Imatinib Mesylate	589,71	Cancer	PDGFR, c-Kit, Bcr-Abl
Lapatinib Ditosylate (Tykerb)	925,46	Cancer	EGFR, HER2
Lenalidomide	259,26	Cardiovascular Disease	TNF-alpha
Nilotinib (AMN-107)	529,52	Cancer	Bcr-Abl
Pazopanib HCl	473,98	Cancer	VEGFR, PDGFR, c-Kit
Rapamycin (Sirolimus)	914,18	Immunology	mTOR
Sorafenib (Nexavar)	637,03	Cancer	VEGFR, PDGFR, Raf
Sunitinib Malate (Sutent)	532,56	Cancer	VEGFR, PDGFR, c-Kit, Flt
Temsirolimus (Torisel)	1030,29	Cancer	mTOR

Table 5. Extract of FDA library repurposing drugs (library L2).

III.1.2. NMR spectroscopy

In the field of drug discovery, protein-ligand interactions constitute the heart of the research. Hence, NMR spectroscopy is an excellent and powerful tool to identify and validate these interactions because of its high-structural resolution. In addition, it is the only technique that allows exploring the dynamic behaviour of biological systems in solution. Importantly, another advantage of NMR-based strategies is its high sensitivity to identify weak-binding compounds as well as provide quickly information about ligand binding properties and aid their development into potent, drug-like for use as lead compounds in drug discovery[109].

In this work, to observe the protein we used mainly the experiments of two-dimensional ^{1}H-^{15}N SOFAST-HMQC (sensitive fast-pulsing spectroscopy experiments)[110] and TROSY (Transverse relaxation optimized spectroscopy) version of the ^{1}H-^{15}N-HSQC (Heteronuclear Single-Quantum Correlation experiments) spectra. The spectrum obtained is two-dimensional with one axis for proton (^{1}H) and the other for a heteronucleus (an atomic nucleus other than a proton), in this case ^{15}N (stable isotope of nitrogen) and correlates the chemical shift (δ) of the proton with that of a heteronucleus. Thus, the resulting spectrum contains a signal for each proton attached to the heteronucleus. Hence, if you know the chemical shift of each proton, the chemical shift of the heteronucleus can be determined. In this context, NMR is sensitive to minimal changes in the chemical environment, being possible measure the chemical shift perturbation (CSP) by monitoring spectrum, useful method to determinate the interactions protein-ligand, calculated according to the following expression:

$$CSP = \sqrt{0.1 * \delta_N^2 + \delta_H^2)}$$

where δ_H and δ_N are the ligand induced perturbations of the ^{1}H and ^{15}N chemical shifts respectively.

The NMR experiments have been carried out using samples of ^{15}N-labeled UROIIIS at 50 μM according to previous studies in our laboratory performed by Fortian A., *et al.*[57], recorded at 298 K on Bruker AVANCE III 800 MHz spectrometer with cryoprobe. NMR measurements were made in 20 mM potassium phosphate pH 7.0, 150 mM KCl with 5% deuterated water (D_2O) added. The NMR data were processed using TopSpin 3.5 and analyzed using CCPNMR (Collaborative Computing Project for the NMR community)[111]. When indicated, binding of selected ligands from the chemical libraries were tested by preparing a sample in a 1:10 protein:ligand ratio. For some of the compounds CSP were observed which were used to determine the ligand binding pocket and the key residues involved in the binding phenomena.

III.1.3. Computational analyses; *in silico* or molecular docking

Analyses *in silico* predict the interactions of protein-ligand by simulations constituting an increasingly used tool in drug discovery. With docking strategies, the druggability of the compounds and their specificity against a particular target can be calculated for further lead optimization processes. Specifically, molecular docking software perform a search algorithm in which the conformation of the ligand is evaluated recursively until the convergence to the minimum energy is reached as the sum of the electrostatic and van der

Waals energies, obtaining an affinity score to classify the successful candidates. The driving forces for these interactions in biological systems aim toward complementarities between the shape and electrostatics of the binding site surfaces and the ligand[112].

In this work, ligand docking simulation were accomplished using the open-source programs for AutoDock Vina[113] and AutoDock4.2 in conjunction with AutoDock Tools (ADT)[114]. The human uroporphyrinogen III synthase structure (PDB: 1JR2, chain A)[51]. was used as a protein receptor. Virtual library (25000 compounds) were retrieved in SMILES format. Structure prediction, optimization and refinement was achieved through minimization by applying chemical groups (CGs) with a united force field by employing $25x10^6$ steps using Open Babel package (v 2.4.0). Receptor and ligand structures were adapted to AutoDock format using ADT tools, adding partial charges and atom types to the PDB format, a standard format for files containing atomic coordinates and provides the representation of a macromolecular structure. The Lamarckian geometric algorithm methodology was selected in the docking parameter.

For the blind docking simulation, we used the whole virtual library against the entire UROIIIS structure with a screening exhaustiveness of 200 and a number of binding modes defined as 15. A grid centred on the protein of 35x33.9x47.8 Å in the x, y and z directions was built. The virtual screening results were analyzed using in-house Matlab© scripts and visualized using PyMOL. The top scoring 10 % of molecules were selected and further analyzed in a second run increasing the exhaustiveness and the number of binding modes to 500 and 50 respectively.

For flexible-docking, the CPS information were analyzed from the NMR experiments and were implemented in the docking simulation by restraining the searching space to a 25x25x25 Å centred in the binding site and providing flexibility to the side-chains of the key residues. The screening exhaustiveness and the number of binding modes were defined as 500 and 50 correspondingly. Results were analyzed using in-house Matlab© scripts and visualized using PyMOL.

III.2. Protein Sample Preparation

The proteins used in this work were the enzymes corresponding to the heme pathway biosynthesis required for biophysical, enzymatic activity and NMR experiments; PBGD and WT or C73N version of UROIIIS. C73N is used instead of C73R version of UROIIIS due its highly instability complicating its purification and management. Previously, the proteins were already available in our laboratory produced by site-directed mutagenesis as described by Fortian, A. *et al.*[57] and checked by gene sequencing analysis. PBGD were cloned in a pETM-11 expression vector, whereas WT- or C73N-UROIIIS were cloned in a pET-16b expression vector. Proteins for biophysical and enzymatic activity assays were grown in regular LB (Lysogeny Broth, Pronadisa) media, whereas protein samples required for NMR experiments included a specific isotopic labelling scheme.

III.2.1. Culture growth and isotopic labelling

PGBD and UROIIIS protein samples were prepared by freshly transformation of the plasmid with the expression vector into *Escherichia coli* BL-21 (DE3) cells (Invitrogen), following the transformation protocol adapted from Stratagene QuickChange Mutagenesis Kit®. Approximately 100 ng of plasmid DNA are added to 50 μL of competent cells and the mixture is kept for 30 minutes at 4 ºC. A thermal shock is performed in a thermoblock (1 minute at 42 ºC) to facilitate plasmid entering the cell. The sample is chilled on ice for 1 minute and then 300 μL of LB media are added. The mixture is incubated at 37 ºC for an hour. 200 μL of transformed cells were plated in petri plates with 50 mg/μΛ of the corresponding antibiotic, Kanamycin (Kan) for PBGD and Ampicillin (Amp) for UROIIIS and incubated over night at 37 ºC. Cells were then grown at 37 ºC for 16 h in small preinocules of 100 mL of LB media for unlabelled proteins or M9 minimal media for isotopic labelled proteins. Cells were separated by centrifugation and resuspended into 1–1.5 L of corresponding cell culture media to grow at 37 ºC. Once cells reached optical density of 0.60–0.80 for LB cultures or 0.45–0.60 for M9 cultures, protein overexpression was induced with 1 mM IPTG (isopropyl-β-D-thiogalactopyranoside, Sigma-Aldrich) in both cases. Optimal induction conditions were found to be 12-14 h at 20 ºC for PBGD and UROIIIS. Cells were then separated by centrifugation and resuspended in 30 mL of resuspension buffer per litre of culture, in 20 mM Tris, 150 mM NaCl, pH 7.0 buffer for PBGD, and pH 8.0 for WT or C73N version of UROIIIS. Resuspended cells can be stored at -20 ºC prior to purification process.

Protein samples prepared for NMR experiments require specific isotopic labelling, in this work we used ^{15}N. M9 minimal media is a restrictive media in which the sources of nutrients are tightly controlled (Table 6). Ammonium chloride and glucose were used as the sole sources of nitrogen and carbon for protein synthesis. As a result, the addition of $^{15}NH_4Cl$ ensures that all nitrogen atoms in the protein are isotopically labelled.

Reactive	Quantity	Company
Na_2HPO_4	6 g/L	Sigma-Aldrich
K_2HPO_4	3 g/L	Sigma-Aldrich
NaCl	0.5 g/L	Sigma-Aldrich
$(^{15})NH_4Cl$	1 g/L	Cambridge Isotopes Labs.
$MgSO_4$	1 mM	Sigma-Aldrich
$CaCl_2$	0.1 mM	Sigma-Aldrich
Biotin	1 mg	Sigma-Aldrich
Thiamine hydrochloride	1 mg	Sigma-Aldrich
Antibiotic	0.5 mM	Sigma-Aldrich

Table 6. Composition of M9 minimal media. ^{15}N-labelled ammonium chloride.

III.2.2. Protein purification

Freshly or -20 ºC stored cells were resuspended and 1:100 diluted PIC (Protease Inhibitor Cocktail, Sigma) was added. The cells were then thoroughly sonicated and the lysate was centrifuged at 25000 g at 4 ºC for 30 minutes. After centrifugation, the proteins were obtained by nickel affinity chromatography following the protocol: the supernatant was mixed with 3 mL of His-tag resin (Ni-NTA; Invitrogen) and incubated for 1 h at 4 ºC being gently mixed/rotated. Previously, the resin is equilibrated with buffer A (20 mM sodium phosphate, 500 mM NaCl and 5 mM imidazole, pH 7.4). After incubation, the mixture was eluted with buffer A containing 500 mM imidazole. The eluate was then purified by size exclusion chromatography (Superdex 75; GE Healthcare) under isocratic conditions, in 20 mM Tris, 150 mM NaCl, pH 7.0 buffer for PBGD, and pH 8.0 for WT or C73N version of UROIIIS. All the purification steps proceeded at 4 °C to minimize proteolysis, and resulted proteins were concentrated and stored at 4 °C. Protein concentration was measured by UV spectrophotometer at 280 nm and quantified with extinction coefficients of 15970 and 25410 $M^{-1} \cdot cm^{-1}$ for PBGD and UROIIIS respectively[115].

III.3. Protein Thermal Shift (PTS) Assay; Stability Assay

The melting profiles for the stability assay with chemical library L1 for UROIIIS-WT purified by our laboratory, were recorded by Protein Thermal Shift (PTS) assay with a non-specific dye which fluoresces bind to hydrophobic parts of unfolding protein when starts to denature in response to an increase in temperature. PTS assays were performed in a Real Time PCR instrument (ViiA™ 7 Real-Time PCR System; Applied Biosystems, CA, USA). The samples were distributed in 384-well PCR plates loaded with 1X Dye (Protein Thermal Shift™ Dye kit, Applied Biosystems), 4 μM UROIIIS protein and 60 μM of each compound and heated from 25 to 90 ºC at 1 ºC/min. Each experiment was done in quadruplicate, reaction volumes were 15 μL/well, and controls without compounds were also included. The excitation wavelength of 580 nm and the emission wavelength of 623 nm, were adapted to detect our dye. Fluorescence data were processed using in-house Matlab© scripts. Comparisons of the resulting mid-point denaturation temperature of the protein (T_m) values with respect to the control were used to select potential pharmacological chaperones. The chemical compounds from library L1, originally at 200 mM in DMSO, were diluted to 1.2 mM in 50% DMSO and 50% Phosphate buffered saline (PBS) and diluted again in assay media for a final concentration of 60 μM in the screen. The final concentration of DMSO in each assay well, including all control wells was 0.89%.

III.4. Enzymatic Assay

Enzymatic assay was adapted from the method described by Jordan, P. *et al.*[60] using 96-well polystyrene plates (Corning Inc., NY, USA). The assay is divided in two parts or reactions; First, the plates were loaded with 5 μL of PBGD at 150 μM in 24 μL of 20 mM tris-HCl, NaCl 150 mM, pH 8 buffer. The first reaction starts with the addition of 12.5 μL of substrate porphobilinogen (PBG; Frontier Scientific Inc., UT, USA) diluted in the same buffer at different concentrations (0.1, 0.4, 0.8, 1.5, 2, 3, and 4 mM). This reaction was performed by incubation at 37 ºC for 1 minute and was then stopped by freezing the plates

at -80 ºC until the second reaction which occurs by the incubation with 12.5 µL of WT or C73N UROIIIS at 35 µM with different concentrations of the potential chaperones ranging between 1:80 to 1:5 (1:80, 1:50, 1:30, 1:15 and 1:5) at 37 ºC for 5 minutes. Controls included reaction without substrate PBG and reaction without any potential chaperone. The WT or C73N UROIIIS reaction was also stopped by freezing at -80 ºC. Uroporphyrinogens were then oxidized to uroporphyrins by adding 12.5 µL of I_2/KI solution and incubation on ice for 10 minutes. The excess of iodine was removed with 12.5 µL of sodium metabisulfite (saturated solution) and the protein was precipitated by lowering the pH with 125 µL of trichloroacetic acid (10 % w/v) and centrifugated at 13000 g for 5 minutes. Finally, the supernatant in 0.1 M of HCl were prepared to measure the change of absorbance at 405 nm (absorption max. of protein bound porphyrin) with respect to the control sample in an absorbance reader. Due the photosensitivity of porphyrins, all reactions were carried out protected by the light. Additionally, it is possible to obtain the product ratio formation which was calculated by absorbance values at 405 nm, while HPLC was used to separate and quantify uroporphyrin III/I products from UROIIIS enzymatic assays.

III. 5. Circular dichroism

Circular dichroism (CD) is one of the most commonly used techniques to monitor the chemical and thermal unfolding experiments and to report on the populations of the folded and unfolded protein state. It measures the difference in the absorption of left-handed circularly polarised light (L-CPL) and right-handed circularly polarised light (R-CPL) and is usually reported as ellipticity θ. This phenomenon occurs when a molecule contains one or more chiral chromophores (light-absorbing groups). In this sense, it is possible to analyze the secondary structure or conformation of macromolecules, particularly CD can be used to observe how secondary structure of a protein changes with environmental conditions or on interaction with other molecules obtaining structural, kinetic and thermodynamic information. In the present work, we used CD to monitor the unfolded and folded state populations at increasing temperature or denaturant concentration in order to estimate the global protein stability from stability curves in the presence or not of different compounds.

All experiments were collected in a JASCO J-810 spectropolarimeter, using a quartz cuvette of 0.2 cm of path length. Proteins tested were WT or C73N UROIIIS at 5 µM in 20 mM Tris, 150 mM NaCl, pH 8.0 buffer in presence or absence of potential chaperones ranging between 1:5 to 1:30 (1:5, 1:10, 1:15 and 1:30) in order to evaluate the stability interaction. Apparent melting temperatures were measured using temperature scans from 10 to 75 ºC. to ensure the proper determination of the baselines in both, the folded and unfolded states. Data were analyzed using in-house built scripts programmed in Matlab© (Simulink) assuming the linear extrapolation method: the molar ellipticity at each point of the transition can be described as a linear combination of the expected values for the folded (θF) and unfolded (θU) states. The values for θF and θU are obtained from extrapolations of the linear baselines.

III.6. Cell cultures

III.6.1. Cell lines

The following mammalian cell lines have been used for the present study:

M1: Human fibroblast and not commercial cell line. M1 are a non-tumor epithelial cells derived from apparently health human skin tissue.

MLP29: Mouse liver progenitor clone 29 (MLP29) is an epithelial cell line established from mouse embryonic liver. MLP29 are small cells with ovoidal nuclei, forming tightly packed colonies[116].

HEK 293: Human embryonic kidney 293 (HEK 293 or HEK) is a cell line transformed with sheared human Ad5 DNA[117] which possess high percentage of transfection. Provided by the laboratory of Dr. Emmanuel R., University of Bordeaux, France.

K562: Human erythroleukemic cell line from a human blood 53-year-old female patient with chronic myelogenous leukemia, established from pleural effusion during the blast crisis[118]. Provided by the laboratory of Dr. Emmanuel R., University of Bordeaux, France.

HuH-7: Human liver cell line is a well differentiated hepatocyte derived cellular carcinoma cell line that was originally taken from a liver tumor in a 57-year-old Japanese male in 1982[119].

Lymphoblastoid cell line (LCL) with CEP: Human LCL with CEP obtained from the NIGMS Human Genetic Cell Repository at the Coriell Institute for Medical Research, ID number: GM09666. LCL were established by Epstein - Barr virus (EBV) transformation of peripheral blood mononuclear cells from a patient with CEP using phytohemagluttinin as a mitogen. Infection with EBV leads to proliferation and subsequent immortalization of cells *in vitro*. The following cell line were obtained from the peripheral vain of a male 23-year-old patient with CEP diagnosed with hemolytic anemia; splenomegaly; skin photosensitivity; marked cutaneous scarring and deformity; porphyrinuria; erythrodontia; hypertrichosis and 4-10 % of normal UROIIIS activity.

III.6.2. Cell cultures conditions and reagents

M1, MLP29 and HEK cell lines were grown in complete DMEM medium (Dulbecco's modified Eagle's medium) supplemented with 10 % (v/v) Fetal Bovine Serum (FBS), 0.1 mg/mL streptomycin and 100 units/mL penicillin at 37°C with 5% CO_2 in incubator chamber. K562 and LCL with CEP cell lines were maintained with Roswell Park Memorial Institute (RPMI) 1640 medium supplemented with 10 % FBS, 0.1 mg/mL streptomycin and 100 units/mL penicillin and maintained at 37 °C with 5 % CO_2 in incubator chamber.

To maintain all cell lines in a properly confluence, they were count by an automated cell counter (Countess™, Life technologies) that performs cell count and viability (live, dead, and total cells) measurements using Trypan blue staining. First, the cells were harvested by trypsin treatment, this step is not necessary for cells in suspension RPMI medium. Cell sample in suspension were then diluted 1:10 in DMEM or RPMI medium and mixed 1:1 with Trypan blue. A fraction of 10 µL of the sample mixture was loaded into a Countess™

cell counting chamber slide. The camera of the equipment acquires cell images from the sample on the slide and the image analysis software automatically analyzes acquired cell images, and measures cell count and viability based on trypan blue exclusion method. The measurement provides live and dead cell concentration (per mL), total cell concentration (per mL) and viability (% of live cells). After the evaluation of viability which serve as routine control, the cells were then seed in a properly concentration in order to maintain or according to the experiment when is indicated.

III.6.3. Generation of stably transfected mammalian cell lines

For stable transfection of M1 and MLP29 cell lines were grown to 60–70 % confluency. The cells were transfected with C- or N-terminal GFP-tagged UROIIIS-WT or UROIIIS-C73R-encoding plasmids pEGFP-N3 or pEGFP-C2 (Takara Bio, Clontech, Mountain View, CA). Previously, these mammalian expression plasmids were already available in our laboratory produced and described by Fortian *et al.*[62] and verified by DNA sequencing analysis. The transfection was carried out by using FuGENE 6 (Roche Diagnostics, Manheim, Germany) and OptiMEM medium (Invitrogen) as described by the manufacturer's instructions. The medium was changed to complete DMEM 5 h post-transfection and to complete DMEM containing 2 g/L G418 (aminoglycoside antibiotic) 24 h later. About 2 weeks later, clones of stably transfected cells were isolated and maintained in complete DMEM containing 2 mg/mL G418. The same stable cell line from each of the different WT and C73R versions of the UROIIIS protein was selected to perform this work.

Human erythrocytic K562 cells were transfected at the unit of Biotherapy of genetic diseases, inflammatory disorders and cancer (BMGIC) in University of Bordeaux (France). For stable transfection, $1x10^6$ K562 cells were electroporated (Amaxa^{TM} Nucleofector^{TM} Technology, Lonza, USA) with 5 μg of C-terminal or N-terminal EGFP-tagged UROIIIS (WT-, C73R or P248Q) encoding plasmids and selected with G418 (0.5 g/L) for 3 weeks. Stably transfected cells were maintained in complete RPMI 1640 medium containing 2 mg/mL G418.

III.6.4. Generation of UROIIIS-C73R$^{+/+}$ and UROIIIS-P248Q$^{+/+}$ mutant HEK cells by CRISPR/Cas9

These experiments were carried out at University of Bordeaux (France) in collaboration with the group of Drs. Emmanuel R. and Jean Marc B.

Two *UROS* missense mutations (c.217T>C and c.743C>A) were introduced by targeted homologous recombination at the endogenous *UROS* locus in HEK cells. The cells were co-transfected by nucleofection (Nucleofector^{TM}, Lonza AG) with the p.X462-UROS-sgRNA plasmid (1 μg) and single strand oligonucleotide ssODN (3 μg) containing C73R or P248Q UROIIIS mutations as well as flanking sequences on each side of the targeted exon. The p.X462 plasmid was obtained from Addgen and expresses Cas9 (D10A nickase mutant) from *S. pyogenes*, puromycin resistance gene and cloning backbone for sgRNA. The targeted sequence was designed next to a NGG sequence named PAM (protospacer

adjacent motif, N can be any nucleotide). Two silent substitutions were introduced in PAM sequences of ssODN to prevent secondary CRISPR/Cas9 cleavage after homology directed repair (HDR) at *UROS* locus and enhanced recombination efficiency. Transfected cells were maintained for 2 days in a culture medium containing puromycin to enrich for modified cells followed by a limited dilution sub-cloning assay on 10 cm culture dishes. UROIIIS-targeted cellular clones were selected by fluorescent microscopy based on their red-fluorescence by UV-excitation due to the spontaneous accumulation of porphyrins. DNA and RNA were extracted from the individual UROIIIS-C73R$^{+/+}$ and UROIIIS-P248Q$^{+/+}$ clones for *UROS* gene sequencing to characterize genome editing at the molecular level. Targeted exons were PCR amplified and sub-cloned into T-easy vectors for individual allele analysis. Because of HEK cell are triploid, three independent genetic modifications were detected. One allele resulting from HDR modification was detected in each UROIIIS-C73R$^{+/+}$ and UROIIIS-P248Q$^{+/+}$ cellular clones. The two other *UROS* alleles presented major nucleotide deletions leading to shift in the reading frame that leads to the synthesis of a non-functional protein. Additionally, UROIIIS-targeted clones exhibited very low to undetectable residual UROIIIS enzymatic activity leading to the spontaneous accumulation of porphyrins that could be analyzed by flow cytometry.

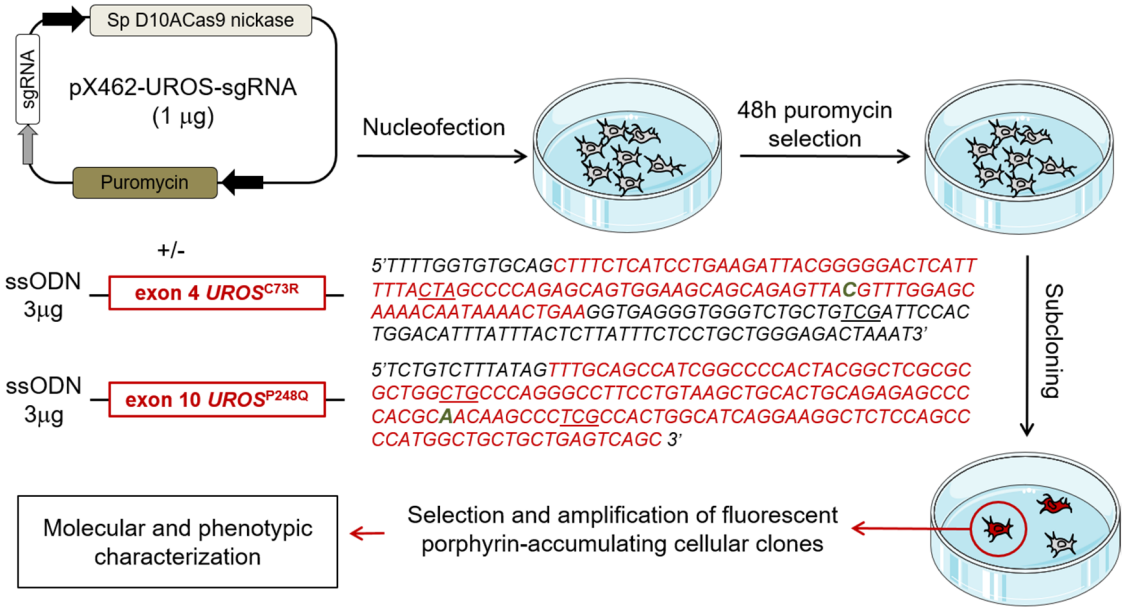

Figure 28. UROIIIS-targeted gene edition by CRISPR/Cas9-medited homologous recombination in HEK cells. HEK cells were co-transfected by nucleofection with the p.X462-UROS-sgRNA plasmid (1 µg) and single strand oligonucleotide ssODN (3 µg) containing flanking sequences on each side of the targeted exon as indicated. UROIIIS-targeted cellular clones were selected based on their spontaneous accumulation of porphyrins then characterized at the molecular level. DNA of *UROS* sequence is indicated as red character: exonic sequence, green character: *UROS* gene substitution corresponding to the C73R or P248Q UROIIIS mutants. Adapted from the original figure created by Dr. Emmanuel R., University of Bordeaux, France.

III.7. Cellular screening of L1 or L2 Library; Functional assay by HC automated fluorescent microscope

Functional assays *in cellula* were carried out in order to evaluate the intracellular UROIIIS homeostasis and its variation in the presence of chemical compounds from library L1 or drugs from library L2. GFP-tag fused to the mutant UROIIIS protein was suitable to monitor the interaction. The proteasome inhibitor MG132 were used as positive control of GFP based on the proof of concept of homeostasis rescue of UROIIIS mutant by blocking its main degradation pathway.

In Falcon® 96-well black/clear flat Bottom TC-treated imaging microplate (Corning Life Science), 25.000 cells of stably human M1 fibroblast C73R UROIIIS-GFP were seed per well. 2500 compounds from library L1 or 130 selected drugs from library L2 were added at the concentration of 500 μM or 100 μM respectively, in 100 μL of DMEM containing 10 % FBS and 1% antibiotics per well and incubated for 16 h at 37 ºC with 5% CO_2 in incubator chamber. The plates were removed from the incubator into laminar flow hood and were washed twice with PBS. The cells were then fixed adding 100 μL of formaldehyde 2 % for 10 minutes at room temperature. The plates were washed three times with PBS for 5 min each wash. Finally, 100 μL of PBS containing 0.7 mg/mL 4',6-diamidino-2-phenylindole (DAPI) with 0.2% of Azide was added and kept at 4 ºC. Negative control in absence of compounds or drugs and GFP positive control with MG132 at 5 μM were included in each plate. HC automated fluorescent microscope was used to evaluate the GFP fluorescence emitted by UROIIIS-GFP mutant protein in presence of the compounds. General conditions for the fixed cells and GFP intensity are indicated in Table 7.

Settings of HC Automated Fluorescent Microscope	
App. Min width	2 μm
App. Max width	100 μm
Area min. Stained	2 μm^2
GFP intensity above local background	1000 graylevels

Table 7. Setting of HC Automated Fluorescent Microscope established for functional assays of cellular screenings of pharmacological chaperones for CEP. App. Min or Max width as well as Area min. Stained are related to the DAPI staining in order to detect the nucleus of cells. Graylevels are arbitrary measure unit from HC automated microscope.

Picture data were analyzed using the HC automated fluorescent microscope software (MetaExpress ®). The output files obtained included the number fluorescent cells (NFC) and total cell number (NTC) detected by the microscope and later the data were processed using Excel Microsoft ® 2016 version. Four pictures were taken automatically per well and the analysis of data by MetaExpress ® spent about 7 h per plate. In total were 32 plates for library L1 and 2 plates for library L2. L1 compounds, originally at 200 mM in DMSO, were diluted to 10 mM in 5% DMSO and 95% PBS and diluted again in DMEM media for a final concentration of 500 μM in the screen. L2 drugs, originally at 10 mM in DMSO, were diluted directly in DMEM media for a final concentration of 100 μM in the screen.

III.8. Flow Cytometry

Flow cytometry is a laser-based technology to analyze the characteristics of cells or particles. Constitute a widely used method for analysing the expression of cell surface and intracellular molecules, characterizing and defining different cell types in a heterogeneous cell population, assessing the purity of isolated subpopulations and measuring cell size and volume. It allows simultaneous multi-parameter analysis of single cells as well as is predominantly used to measure fluorescence intensity produced by fluorescent-labelled, ligands or intrinsic cellular fluorescence. In the present work, we analyzed the fluorescence emitted by GFP-tagged from stably M1 or MLP29 WT- or C73R-UROIIIS-GFP and the intrinsic fluorescence from UROIIIS-C73R$^{+/+}$ and UROIIIS-P248Q$^{+/+}$ mutant HEK cell lines emitted by intracellular accumulated porphyrins for the characterization of the molecules or drugs assays. Flow cytometry analyses were performed using the BD FACSCanto^{TM} II system (BD Biosciences). Data were analyzed using the BD FACSDiva^{TM} software (BD Biosciences) and later processed using Flowing Software - a free flow cytometry data analysis software. All cells were harvested with TrypLE^{TM} (Gibco) treatment, the cells were then washed twice with PBS and finally resuspended with D-PBS (400 µL) for flow cytometry analysis. Porphyrin and GFP fluorescence were detected by APC (Ex-Max 650 nm/Em-Max 660 nm) or FITC (Ex-Max 494 nm/Em-Max 520 nm) channel respectively.

III.9. MTT cell viability assay

The MTT assay is a colorimetric assay for assessing cell metabolic activity. We used MTT assay to determine if the test molecules had effects on cell proliferation or showed direct cytotoxic effects that eventually lead to cell death. MTT (3-(4,5-dimethylthiazol-2-yl)-2,5-diphenyltetrazolium bromide) is a tetrazolium dye (yellow) which is reduced by the NAD(P)H-dependent oxidoreductase mitochondrial enzyme to its insoluble formazan (purple) Figure 29. The viability of cells is analyzed by the formation of formazan which concentration is determined by optical density.

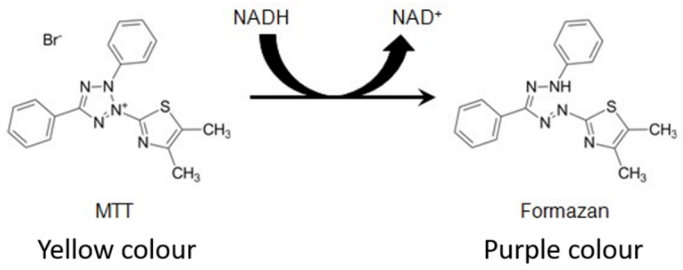

Figure 29. MTT assay. Conversion of the tetrazolium water soluble MTT into insoluble formazan dye in presence of mitochondrial reductase[120].

For the assay, the cells were seed in 96-well cell culture plate in 100 µL/well of DMEM containing 10 % FBS and 1 % antibiotics. The cells were treated with different compounds from L1 or L2 libraries at a series of concentration of 1/2 dilutions from 1 mM to 0 mM with 3 parallel wells in each group. The cells were cultured in an incubator at 37 °C, saturated humidity and 5 % CO_2 for 24 h. The plates were then washed twice with PBS, 10 µL of MTT (0.5 mg/mL) was added into each well in a final volume of 100 µL of DMEM complete and continued to culture for 1 h at 37 ºC in the incubator chamber. Then, all the medium was removed, 200 µL of DMSO was added to each well and mixed properly to solubilized the formazan. The absorbance was measured at 550 nm by a microplate reader (Spectramax M3 spectrophotometer) to determinate the concentration of formazan. The half maximal inhibitory concentration (IC_{50}) was calculated by linear regression method as described by Nevozhay[121].

III. 10. Western blot analysis

The cells pellets were lysed for 15 minutes on ice in the presence of 50-100 µL of lysis buffer (1 % Triton X-100, 300 mM NaCl, 50 mM Tris-HCl, pH 7.4) supplemented with protease inhibitor cocktails. After centrifugate the samples at 14000 g for 5 minutes, the supernatant was transferred to a fresh eppendorf tube. The protein concentration of the cell lysates was determined by a Bradford protein assay (Bio-RadLaboratories, Inc) using bovine serum album (BSA) as the standard. NuPAGE® LDS Sample Buffer (Life Technologies, Inc) was added and samples were incubated for 5 minutes at 37, 65 and 95 ºC in order to prepare protein samples for denaturing gel electrophoresis. The proteins were separated on 4-12 % pre-cast acrylamide gels (NuPAGE® Bis-Tris gel, Life Technologies, Inc). The proteins were then transferred to Polyvinylidene difluoride (PVDF) membrane (Millipore, Bedford, MA, USA) and blocking for 1 h (5 % milk and 0.05 % Tween 20 in PBS). The primary antibody was added overnight at 4 ºC, followed by PBS washes and incubated by horseradish-peroxidase (HRP)-conjugated secondary antibody for 30 minutes at room temperature. Chemiluminescent detection of bands was performed with ECL Plus reagent (GE Healthcare, Buckinghamshire, UK). All proteins were detected under non-reducing conditions.

Primary antibodies were purchased from the following vendors:

Antibody	Species	Clone	Suplier	ID	Work dilution
UROIIIS	Mouse	-	Abcam	ab58097	1:1000
GFP	Mouse	7.1 and 13.1	Roche	11814460001	1:1000
Ubiquitin (UQ)	Mouse	6C1.17	BD Biosciences	550944	1:2000
Lamp1	Rat	1D4B	Abcam	ab25245	1:1000
Annexin V	Rabbit	-	Abcam	ab14196	1:1000
PARP	Rabbit	46D11	Cell signaling	#9542	1:1000
Eea1	Rabbit	-	Invitrogen	PA1-063A	1:1000
Actin	Mouse	AC-15	Santa Cruz	sc-69879	1:5000
Tubulin	Mouse	DM1A	Sigma-Aldrich	T9026	1:5000
Hsp70	Mouse	BRM-22	Abcam	Ab6535	1:1000
GAPDH	Mouse	-	Abcam	ab9484	1:5000

Table 8. List of commercial antibodies used for western blot analysis.

The HRP-conjugated secondary antibodies used were: anti-Mouse; DαMo-HRP (Abcam, Ab205724), anti-Rabbit; DαRb-HRP (Abcam, ab205722) and anti-Rat; GtαRat-HRP (Abcam, ab205720). All cases diluted to 1: 6000.

III. 11. Immunofluorescence staining

The cells were seed to 50–80 % confluence on glass coverslips and after incubation at 37 ºC for 24 -48 h, cells were fixed for 10 minutes with 2% formaldehyde in PBS and then washed with PBS. Successive incubations with primary and fluorophore-conjugated secondary antibodies diluted in a PBS solution containing 0.1 % BSA and 0.1 % saponine were carried out for 30 minutes. After each incubation period, unbound antibodies were removed by washing the coverlips in PBS. Finally, the coverslips were mounted onto glass slides on Fluoromont G (Southern Biotechnology Associates, Birmingham, AL) containing 0.7 g/mL DAPI to stain DNA (nucleus). All procedure was carried out at room temperature. All immunostainings were analyzed in a fluorescent microscope (Zeiss Axioverte200).

III.12. Transcript Expression Analysis (qRT-PCR Assay)

Total RNA from cell lines was isolated using the RNeasy Mini Kit (Qiagen, Hilden, Germany) as described by the manufacturer's instructions, and quantitative real-time PCR (qRT-PCR) was performed in two steps. Single-stranded cDNA was synthesized from 300 ng of mRNA, treated previously with RNase-free DNase (Qiagen, Hilden, Germany), using qScript™ cDNA SuperMix (Quanta BioSicences, MA, USA). The real-time step was carried out with 4.5 µl of 1:18 cDNA dilution for the genes of interest or 4.5 µl of 1:90 dilution for the reference genes, and SYBR® Select Master Mix (Applied Biosystems, Thermo Fisher Scientific, Carlsbad, CA, USA) for 35 cycles (for 15 seconds at 95 °C, and 60 seconds at 60 °C) on a ViiA7 Thermocycler. The samples were examined twice in triplicate for expression of the eight human genes involved in the heme route biosynthesis (*ALAS1*, *ALAD*, *HMBS*, *UROS*, *UROD*, *CPOX*, *PPOX*, and *FECH*). The specific primers were purchased from Sigma Life Science (Sigma-Aldrich, St Louis, MO, USA) and sequences are shown in Table 9. The relative level of each transcript was calculated on the basis of the ΔΔCt method and normalized to *ACTB*, *TUBB* or *RPLS14* as reference housekeeping human genes.

Gene	Forward	Reverse
ALAS1	5′-gaaagagtgtctcatcttcttc-3′	5′- aggtgtggtcattctttttc-3′
ALAD	5′-ctacttccacccactacttc-3′	5′-tatgtcatcaggaacatccg-3
HMBS	5′-agaaaagcctgtttaccaag-3′	5′-ttttgggtgaaagacaacag-3′
UROS	5′- ggttcttttactgaaggatgc-3	5′- ctgggaagagacaaaaactc-3′
UROD	5′- atatctggtaggacaagtgg-3′	5′- agtgcaaacttgttgaagag-3′
CPOX	5′- catggaaatctttcagaggaag-3′	5′- attcttggggtggataacag-3′
PPOX	5′- cccagtatacactaggtcac-3′	5′- acagtcattaacagcaactc-3′
FECH	5′- gaccattttccacttgagaag-3′	5′- ttccatgacttttggacag-3′
ACTB	5′- gacgacatggagaaaatctg-3′	5′- atgatctgggtcatcttctc-3′
TUBB	5′- ctcagaatttgtgtttgctg-3′	5′- cagaaagaaatacagggtcac-3′
RPS14	5′- aaaagaaggaagaacaggtc-3′	5′- atatggtgagattcatctcg-3′

Table 9. Primers used for the transcript expression analysis.

III.13. Drugs

L1 and L2 molecules or drugs were used in the concentration under indicated conditions. Particularly, the following drugs have been the most used in this work:

Ciclopirox (CPX): 6-Cyclohexyl-1-hydroxy-4-methyl-2(1H)-pyridone, $C_{12}H_{17}NO_2$, MW: 207.27 from Sigma-Aldrich (ref: Y000040).

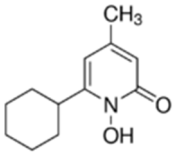

Scheme I. Chemical structure of ciclopirox.

Ciclopirox olamine (CPXol): 6-Cyclohexyl-1-hydroxy-4-methyl-2(1H)-pyridone; 2-aminoethanol, $C_{12}H_{17}NO_2 \cdot C_2H_7NO$, MW: 268.36 from LKT Labs (ref: C3208).

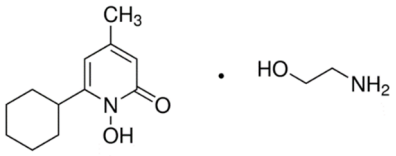

Scheme II. Chemical structure of ciclopirox olamine.

Ciclopirox glucuronated (CPXglu): Ciclopirox beta-D-Glucuronide, 1-[(6-Cyclohexyl-4-methyl-2-oxo-1(2H)-pyridinyl)oxy]-1-deoxy-b-D-glucopyranuronic Acid, $C_{18}H_{25}NO_8$, MW: 383.39, a metabolite of ciclopirox from Santa Crux Biotechnology (ref: 79419-54-8).

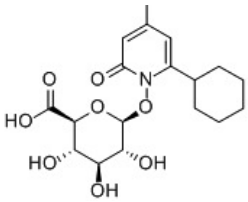

Scheme III. Chemical structure of ciclopirox glucuronated.

MG132: membrane-permeable proteasome inhibitor (Sigma-Aldrich), $C_{26}H_{41}N_3O_5$, MW: 475.62. When indicated, cells were treated for 16 or 18 h in the presence of 5 µM of MG132.

III. 14. Animals

In the development of this doctoral thesis have been used mice of pure genetic background and different ages:

- Transgenic (Tg) *Uros*$^{P248Q/P248Q}$ mice: Congenital Erythropoietic Porphyria *Uros*^{mut248} knock-in mouse model. These animals had a mixed 129/SV–C57BL/6 genetic background and expressed the P248Q missense recessive mutation of the *Uros* mouse gene (exon 10) with *Uros*$^{P248Q/P248Q}$ (*Mut/Mut*) genotype[122]. The phenotype of *Uros*^{mut248} mouse closely mimic the pathophysiology of CEP disease in humans. Homozygous mice display erythrodontia, moderate photosensitivity, hepatosplenomegaly, and hemolytic anemia. Uroporphyrin type I isomer is accumulated in urine, total porphyrins are increased in erythorcytes and feces, while UROIIIS enzymatic activity is below 1 % of normal level. The ages studied were 6-12 weeks.

- Control mice: Tg healthy heterozygous [*Uros*$^{P248Q/N}$ (*Mut/N*)] or Tg homozygous [*Uros*$^{N/N}$ (*N/N*)] mice of the same genetic background as previously, 129/SV–C57BL/6 as well as the same ages.

Animals were maintained on a 12 h light/dark cycle, in case of homozygous mice were maintained with special protections of light and had free access to food and water in the animal facility of CIC bioGUNE, Derio (Spain). All procedures involving animals were in accordance with the Spanish Guide for the Care and Use of Laboratory Animals, and with International Animal Care and Use Committee Standards. All procedures were approved by the CIC bioGUNE ethical review committee (Permit Number: P-CBG-CBBA-0117) accredited by AAALAC organizations.

III.14.1. Animal experimentation

III.14.1.1. Mice and CPX oral administration by food ingestion.

Mice were treated by CPX oral food ingestion (2 g of CPX per Kg of pellet) for 45 days. Assuming mice weights between 20-25 g, CPX intake was estimated at 400 mg per kg per day. To analyze the evolution of this study, porphyrins concentrations were measured from whole blood. The blood samples were taken by submandibular vein weekly and mice were weighted before each extraction.

III.14.1.2. Mice and CPX oral administration by gavage.

Mice were treated by CPX oral administration by gavage in order to evaluate the CPX dose-efficiency. Mice were organized in different groups of 25 mg/kg or 10mg/Kg or 5 mg/kg or 1 mg/Kg CPX or ORA-Sweet® (flavored Syrup Vehicle). CPX was administered every 24 h for 8 consecutive weeks. Porphyrins concentrations were measured from whole blood. The blood samples were taken by submandibular vein weekly and mice were weighted before each extraction.

III.15. Histology experiments

At the end of animal experiments liver, spleen and kidneys were collected in order to analyze the histopathology of these tissues damaged for the disease. The histological analyses were carried out by a service of CIC BioGUNE in collaboration with the histopathology service of the University of Bordeaux, France. Samples were fixed with enough volume of 10 % neutral buffered formalin during 24 h at room temperature. After fixation, formalin was replaced with 50 % ethanol until processing. Fixed tissues (liver, spleen and kidneys) were processed for paraffin embedding. Samples were incubated in an automatic tissue processor in 1h and 30 minutes cycles of 50 %, 70 %, 80 %, 96 % and 100 % (x 3) ethanol, followed by 45 minutes in Histo-clear and finally in two changes of 2 hours of paraffin. After processing, samples were embedded in paraffin, metallic molds were filled with liquid paraffin until solidification. Formalin fixed and paraffin embedded samples were sectioned at 5 microns. Sections were dewaxed in two changes of Histo-clear of 10 minutes each and hydrated in distilled water. Once the samples were properly fixed, the following protocol stains were carried out for the present study:

- Perls Prussian Blue Staining (PS): samples were incubated in two changes of ten minutes each of 4 % hydrochloric acid and 4 % potassium ferrocyanide solution. Used to detect the presence of iron in tissues.

- Sirius Red Stain (SR): samples were incubated in 0.01 % fast green FCF dye solution in saturated picric aqueous solution for 15 minutes followed by 15 minutes incubation in 0.04 % fast green FCF/0.1 % Sirius red in saturated picric aqueous solution. Dye used principally for collagen to observe fibrosis levels.

- F4/80: Endogenous peroxidase was blocked with 3 % H_2O_2 for 10 minutes and washed with PBS. Sections were unmasked 15 minutes with proteinase K, washed with PBS and blocked with 5 % normal goat serum for 30 minutes. Samples were then incubated overnight at 4 ºC with 1:50 primary antibody (F4/80 ref: Bio-rad MCA-497-BB). Samples were washed with PBS and incubated 30 minutes with Immpress anti-rat HRP-conjugated secondary antibody (Vector ref: 7404). Colour was developed with Vector VIP substrate (ref: SK-4600). Immunostaining used as mouse macrophage marker.

- Hematoxylin-eosin staining (HE): samples were stained with Harris hematoxylin (ref: HHS16) for 5 minutes, washed with running tap water for 5 minutes, stained 15 minutes with aqueous eosin (ref: HT110216), washed 3 minutes with running tap water and dehydrated briefly in 100% alcohol. The gold standard of histology staining techniques was used to analyzed porphyrin deposits and steatosis in the tissues.

III. 16. Porphyrins extraction

The cell lines were growth in complete DMEM medium treated for 16 or 24 h with the interest compounds from commercials libraries to analyze and collect for the porphyrins extraction. The blood samples were obtained from the submandibular vein and collected in ethylenediaminetetraacetic acid (EDTA) tubes (BD Microtainer®) weekly; the samples were aliquoted and stored in a freezer at -80 ºC. Cells and blood samples were treated by the same protocol. For the porphyrins extraction 300 µL of 6 M HCl were added for the cells samples and 200 µL for the blood samples, sonicated 3 cycles of 25 seconds each and incubated at 37 ºC for 30 minutes in a thermoblock. The samples were then centrifugated for 10 minutes at 10000 g. Following this step, the pellets were removed and the supernatants were transferred to a fresh centrifuge tube filter cellulose acetate membrane, pore size 0.22 µm (Corning® Costar® Spin-X®) and centrifugated for 10 minutes at 4000 g. The samples were then analyzed by HPLC. The porphyrins standards were obtained from Frontier Scientific Europe (Carnforth, UK) included a chromatographic market kit containing the number I isomers of 8,7,6,5,4 carboxylate porphyrins and mesoporphyrin IX. All porphyrin standards were reconstituted in 3 M HCl.

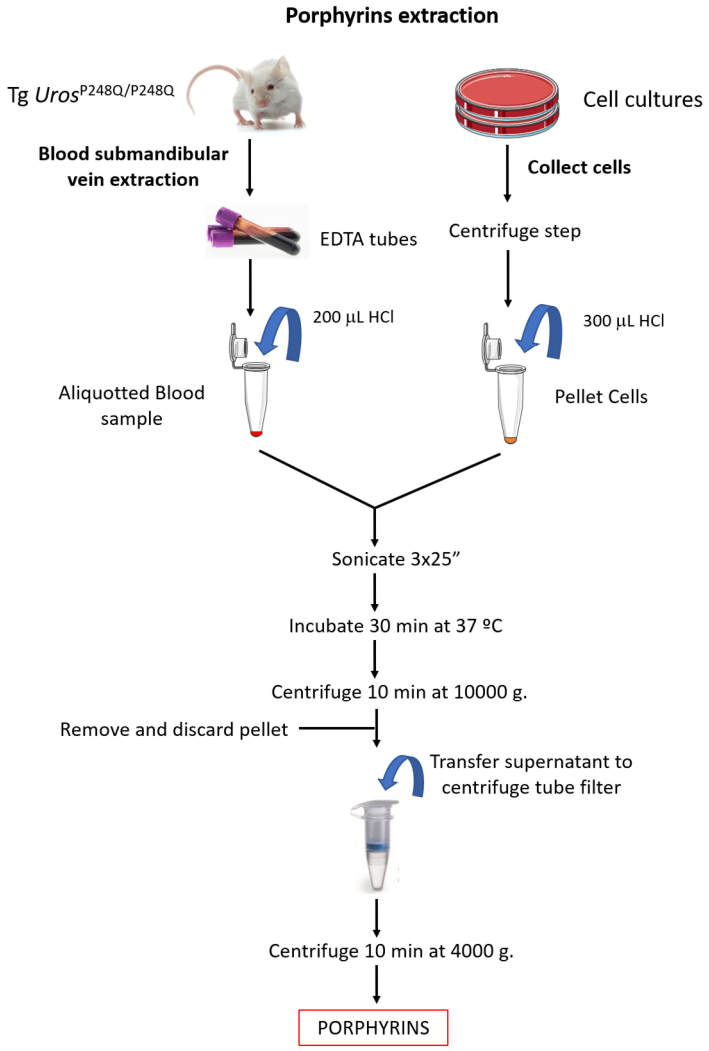

Figure 30. Schematic porphyrins extraction protocol. This figure shown porphyrins extraction for blood and cell samples.

III. 17. HPLC; Chromatographic Conditions

A high-performance liquid chromatograph (HPLC) (Shimadzu) with an autosampler was used for the assessment in order to separate and quantify porphyrins. The analytical column was BDS Hypersil C18 (250 x 3mm; 5 μm particle size) purchased from Thermo Scientific. The method to separate the porphyrins was facilitated by 60 minutes gradient elution and a two-component mobile phase consisting of ammonium acetate (1M, pH 5.16) filtered through 0.1 μm as solvent A and 100% acetonitrile as solvent B. Gradient elution commenced upon injection at 0 % B, increased to 65 % B for 30 minutes, remained for 5 minutes, returned to 0 % B in 15 minutes and remained for 10 minutes in order to re-equilibrate the column at 0 % B before the next injection. The flow rate was 1 mL min^{-1} and the sample injection volume was 20 μL. All analyses were performed at 20 ºC and the spectra were taken at an excitation wavelength of 405 nm and an emission wavelength of 610 nm. The concentrations of porphyrins were calculated with five-point calibration curve ranging from 0.0 to 100 pmole.

III.18. NMR-based method for the analysis of the active and glucuronated forms of CPX in serum and urine

NMR method has been developed by Chassys™ platform (Atlas Molecular Pharma S.L.) to determinate the concentration of CPX in biological samples. For the serum samples, 1,3 mL of Methanol: H_2O (2:1) were added in 200 μL of serum and incubated for 5-24 h with agitation at 4 ºC. The mixtures were then centrifuged at max-speed (~30000 g) for 30 minutes at 4 ºC. The supernatants were transferred to fresh eppendorf tubes and frozen with liquid N_2. Once the samples were frozen, the caps of the eppendorf were changed by new perforated caps in order to evaporate the buffer by lyophilization. The powder obtained was reconstituted by deuterated DMSO (DMSO-6d). In case of urine samples, first the volumes were measured and deuterated water (D_2O) were added till 450 μL. Finally, to analyze the samples by NMR, DSS (4,4-dimethyl-4-silapentane-1-sulfonic acid) were added to a final concentration of 1.66 μM. This method allows to distinguish between glucuronated or active CPX in a concentration limit between 10-15 μM.

III.19. Statistical analysis

The experiments were performed in duplicate or triplicate when indicated and, in each case, the data are expressed individually as the mean ± standard deviation. The relative units are expressed with respect to the control samples. Statistical analyses were carried out with Matlab®, Sigmaplot® version 12 software or Excel Microsoft® version 2016. The comparison of the data was carried out by paired student t-test or ANOVA analyses. The differences were considered significant for a value of $p < 0.05$ (confidence interval of 95 %). When indicated statistically significant differences are expressed by the symbol * ($p < 0.05$).

CHAPTER IV
RESULTS

“Science is not only a discipline of reason but,
also, one of romance and passion”

— Stephen Hawking

IV. RESULTS.

Previous studies from our laboratory demonstrate that C73R-UROIIIS, a hotspot mutation on CEP with deficient catalytic activity, can be rescued by modifying the side chains prone to interact with R73[61]. Particularly, enzyme's activity restoration was achieved with the double mutant L43D/C73R-UROIIIS. Based on this proof-of-concept experiment, we propose a new therapeutic approach based on the restoration of an appropriate kinetic stability of deficient UROIIIS by means of pharmacological chaperones. Specifically, the molecules are expected to increase the protein stability by binding the enzyme and stabilizing the folded conformation which corresponds to upregulated protein homeostasis *in cellula* and *in vivo*.

In the present work, we have combined *in silico* structural analysis with biophysical characterization and functional experiments to identify novel pharmacological chaperones. Figure 31 shows the selection strategy for the hit compounds identification than spans from molecular docking analysis up to the final validation of the selected compounds by *in vivo* experiments. The complete procedure allowed identifying ciclopirox (CPX) as potential pharmacological chaperone to stabilize deficient UROIIIS.

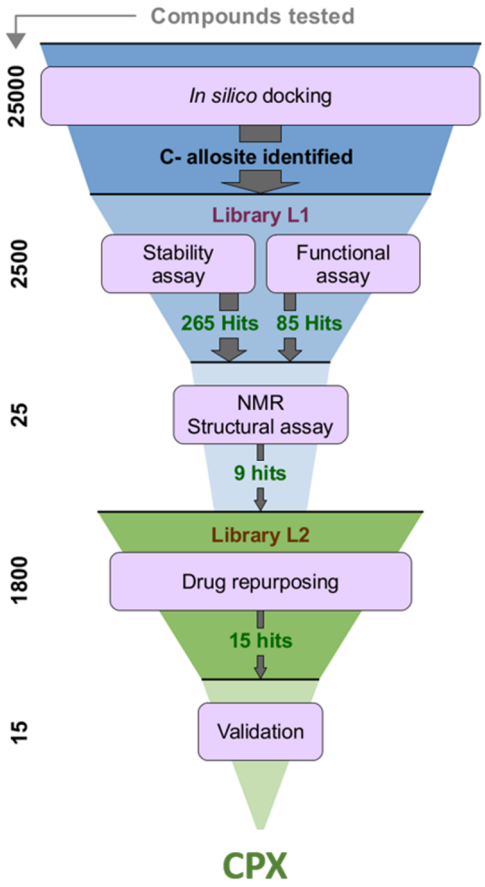

Figure 31. Flow chart that represents the hit identification strategy of pharmacological chaperones for deficient UROIIIS enzyme. The strategy includes in silico structural analysis and *in vivo*, *in cellula* and *in vivo* functional experiments. The complete procedure allowed identifying ciclopirox (CPX).

IV.1. Identification and Characterization of Pharmacological Chaperones for deficient UROIIIS enzyme.

IV.1.1. Identification of binding drugs sites for UROIIIS by computational simulation or *in silico* docking.

Molecular docking is a remarkable computational method in the design and discover of new drugs[123]. The docking process, by means of algorithms and simulations, allows us to study the interactions of a small molecule with a protein at the atomic level as well as to characterize the binding site of the protein-ligand complex and to elucidate biochemical processes[124]. In this context, we can perform *in silico* screening of chemical libraries based-fragments[125] and predict the ligands configuration in the complex, their relative position and orientation within these sites (usually referred to as pose) and the binding affinity[126]. Even the results obtained by virtual interactions are subject to the limitations of the computational forcefield, they facilitate the exploration of the chemical space and ease the process to find candidates for developing new drugs, constituting today as a powerful tool and first key in drug discovery[127].

In a non-canonical approximation, we have used a blind molecular docking approach, without any assumption about the binding site, to identify druggable binding sites in UROIIIS enzyme. As mentioned in the sections I.5.2 and I.5.3, the human isoform of UROIIIS is composed by 265 aa and folded in two domains connected by a flexible linker[51]. The active site of the enzyme is located in the cleft between the two domains, and substrate binding involves most of the residues in the hinge region[52]. In Figure 32 we show the *in silico* docking of up to 25000 molecules from a large virtual chemical diversity library of compounds.

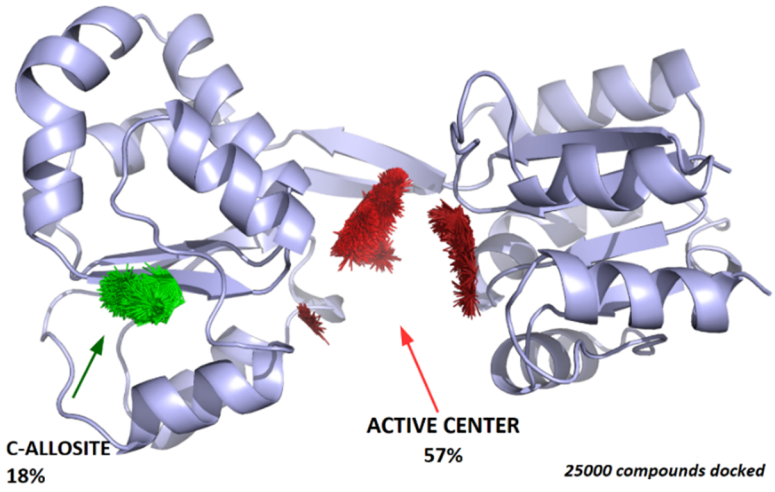

Figure 32. Representation of UROIIIS enzyme *in silico* docking results from virtual libraries. 25000 compounds tested and clustered in two locations: i) the active centre of the enzyme, docking 57 % (red) and ii) an allosteric binding site (denominated C-allosite), docking 18 % (green). The C-allosite is an ideal locus to screen drug candidates that may operate as pharmacological chaperones.

By analysing the interfaces of the obtained complexes, we conclude that the compounds cluster in two locations: i) the active centre of the enzyme, which is the most populated site, docking 57 % of the molecules and ii) an allosteric binding site (that we denominate **C-allosite**) located in the C-domain and defined by residues V96-V98 and T114, G116, T118, which is the targeted locus for 18 % of all compounds tested.

In 1965 the allostery process was introduced: a binding event at one site of a molecule affects the binding activity at another distinct functional site, enabling the regulation of the corresponding function[128]. In here, we define an allosteric site as a location on the surface of an enzyme other than the active site. The binding at an allosteric site enables function by increasing the overall stability of the biomolecule. The identification of the C-allosite as potential target for pharmacological chaperones is advantageous since it does not involve any residue hosting a CEP-producing mutation and it becomes an ideal locus to screen drug candidates that may operate as pharmacological chaperones, acting over a wide range of deleterious mutations.

IV.1.2. Organic molecules screening from the Ro3 chemical library L1 by WT UROIIIS thermostability assay.

In the field of drug discovery, at the end of the 90s, Lipinski formulated the called “rule of five (Ro5)” to evaluate drug-likeness by experimental and computational approaches, estimating the solubility and permeability of compounds to determine which properties make them more orally bioavailable for human uptake, basing on pharmacokinetics properties of ADME[107]. Assuming that the drugs are usually small and moderately lipophilic molecules, following the Ro5, the physicochemical properties predict that poor absorption or permeation is more likely when there are more than 5 hydrogens-bond donors (HBD), expressed as the sum of OHs and NHs; 10 hydrogens-bond acceptors (HBA), expressed as the sum of Ns and Os; the molecular weight (MW) is greater than 500 Daltons (Da); and the calculated Log P (cLogP) is greater than 5, being the algorithm that calculates the partition coefficient between n-octanol/water, measuring the hydrophobicity of compound. Compound classes that are substrates for biological transporters are exceptions to the rule[129]. More recently, these rules have been enhanced by others authors who included more key properties for oral bioavailability, as polar surface area (PSA)[130] and the number of rotatable bonds (NROT)[131]. Although these approaches allow identifying high value hits, many of them fail to progress into optimization, due to limitations of drug-sized compounds because they tend to actually reduce their initial drug likeness and therefore reduce the developability of the final optimized compounds[132]. Fortunately, alternative approach referred to as ‘fragment-based’ discovery extended the Ro5 to the rule of three (Ro3) (Table 10), with enhanced hit rate and the ability of drug optimization[108].

PROPERTIES	RULE OF THREE CRITERIA
MW	≤ 300
cLogP	≤ 3.0
HBA	≤ 3
HBD	≤ 3
NROT (Flexibility Index)	≤ 3
PSA	≤ 60Å²

Table 10. Rule of three (Ro3) Criteria. Physicochemical properties for reduced chemical complexity which achieves high quality compounds. MW=Molecular Weight (Da). cLogP=coefficient between n-octanol/water (hydrophilicity). HBA=hydrogen bond acceptors. HBD=hydrogen bond donors. NROT = number of rotatable bonds (Flexibility). PSA = polar surface area.

Based on the results from molecular docking, we have selected a library of 2500 chemical fragments with such enhanced chemical diversity that we have denominated as library L1, composed by fragments of organic molecules with high purity (≥95%) and improved properties according to Ro3 compliance, reducing chemical complexity and achieves high quality compounds (See Materials & Methods, Section III.1.1.2.). Range and average values of set library is shown in Table 11. The set of molecules have been selected to find compounds that might bind to the C-allosite domain, stabilize deficient UROIIIS enzyme and to identify candidates for further preclinical studies.

PROPERTIES	Ro3 Fragments RANGE OF VALUES	Ro3 Fragments AVERAGE VALUE
MW	93.1 - 298.4	178.3
cLogP	-2.5 - 3.0	1.5
HBA	0 - 3	2.4
HBD	0 - 2	0.9
NROT (Flexibility Index)	0 - 3	0.9
PSA	4.9 - 69.1Å²(99% <60Å²)	37.0Å²

Table 11. Range and average values of 2500 compounds from library L1 fragments upon Ro3 criteria.

In order to look for possible chaperones, in a first mechanistic approximation, we set up an *in vitro* **stability assay** that consists in the screening of the full library L1 for their capacity to enhance the thermodynamic stability of WT UROIIIS, monitoring changes in the mid-point denaturation temperature of the protein (T_m) which is a gold standard parameter for defining thermal stability[133]. From the technical point of view, the assays were performed using a thermal shift assay[134] in the multiwall peltier of a RT-PCR machine. An environmentally-sensitive fluorescent dye (Protein Thermal Shift™ Dye) was used to monitor changes in the T_m of the protein. Upon thermal unfolding of the protein, the hydrophobic core is exposed, then the dye detects this change and binds to the hydrophobic parts resulting in a significant increase in fluorescence emission.

Assuming a two-state model, the stability of the protein is defined as the thermodynamic equilibrium that exists between the concentration of unfolded protein (U) and the folded native protein (N), represented in the scheme:

$$N \underset{k_{UN}}{\overset{k_{NU}}{\rightleftharpoons}} U$$

where N is the native conformation and U is the unfolded state. k_{NU} and k_{UN} are the kinetic rate constant in the reversible equilibrium, being N state more stable than U state. Under this model, a ligand or any small molecule that binds specifically to native state should affect the unfolding equilibrium by decreasing the concentration of the unfolded state. Moreover, the combination of these thermodynamic model with the linear extrapolation method[135] allows estimating the concentrations of the conformational states of a protein as a function of temperature (T):

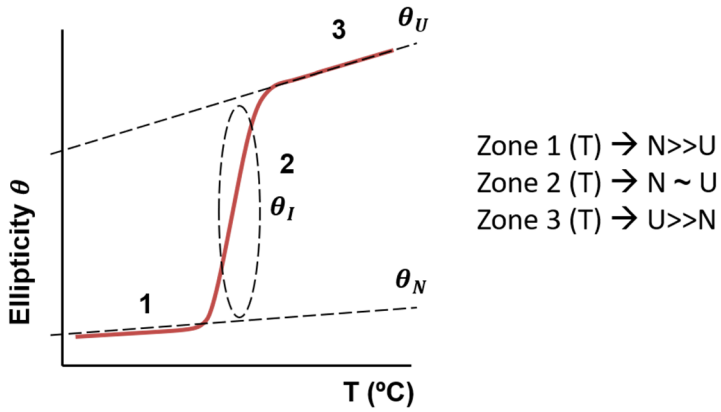

Figure 33. Theorical thermal denaturation curve. Ellipticity (θ) or the Fluorescence (F) as a function of temperature (T). Different zones (1,2,3) to estimate the concentrations of the conformational states of a protein are indicated.

Here, the ellipticity (θ) or the Fluorescence (F) is a magnitude that is proportional to the folded conformation of a protein, ultimately providing information about its state of denaturation. A typical thermal denaturation curve adopts the shape shown in Figure 33, where three zones can be clearly discriminated. Zone 1 can be associated to a state where all the concentration of protein is totally folded (N). The temperature dependence of the physicochemical property (ellipticity or fluorescence) with temperature is assumed linear and determined by the equation:

$$\theta_N = \theta_N + m_N[N]$$

where m_N is the slope of N variation with T. Equivalently, zone 3 corresponds to completely unfolded protein (U) with a temperature dependence determined by:

$$\theta_U = \theta_U + m_U[U]$$

where m_U is now the slope of U state with T. Zone 2 embraces mixed states where U and N states coexist, always fulfilling the mathematical expression:

$$\theta_I = \theta_N X_N + \theta_U (1 - X_N)$$

where X_N is the fraction of folded protein. Under these premises, the fraction of folded protein (FF) at a given temperature can be obtained from[135]:

$$FF = [F - (F_N + m_N T)]/[F_N + m_N T] + [F_U + m_U T]$$

where FF is the fraction of folded protein normalized, F is the experimental fluorescence (or ellipticity from a CD experiment), T is the temperature, and m_N and m_U (F_N and F_U) are the slopes (intercepts) for the linear dependence of the fluorescence values with T, for the native and unfolded states respectively, as shown in Figure 34:

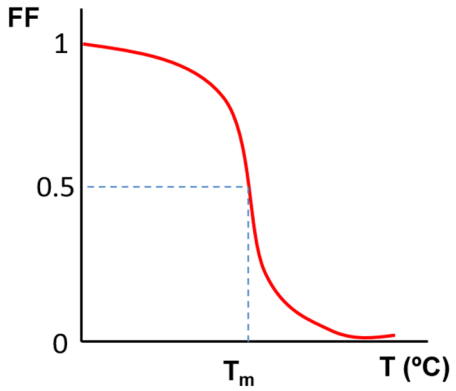

Figure 34. Representative thermal denaturation profile. FF is the fraction of folded protein normalized as a function of temperature (T). Mid-point denaturation temperature of the protein (T_m) is indicated (FF = 0.5).

T_m is then calculated as the T value at which half of the protein molecules are in the unfolded state (FF = 0.5). The data obtained can be further analyzed to extract the difference in free energy $\Delta\Delta G^0_{U-N}$ between unfolded and native state, using:

$$\Delta\Delta G^0_{U-N} = -RT\, lnK \; ; \; K = \frac{[U]}{[N]}$$

where R is the universal gas constant and K is the equilibrium constant defined by the concentration of U state divided by the concentration of N conformation. $\Delta\Delta G$ changes in the folding free energy are a good descriptor of the stabilization energies. Here, $\Delta\Delta G$ is used to quantify the magnitude of the ligand's effect on stability. These mathematical estimations constitute an excellent model to predict the effect of ligand binding on the protein's stability.

As previously indicated, fluorescence is able to monitor the loss of tertiary and secondary structure of the protein as a function of temperature. First, we set up the melting curves of UROIIIS enzyme in the absence of any ligand multiple times to appreciate the robustness of the T_m determination (Figure 35A) and to estimate the minimum confidence limits for the shifts in the T_m values induced by the potential pharmacological chaperones.

Subsequently, ligands that increased the T_m values of UROIIIS in, at least, 2.5 degrees, determined in the corresponding control experiments, were selected as, *a priori*, positive candidates to stabilize the protein. Furthermore, each experiment was compared with internal and external controls to assure the correct validation of the technical process (Figure 35B). Finally, the screening reported a total of 265 compounds (10.6% of the library) that significantly increased the T_m of WT UROIIIS which corresponds to a statistically significant increment of UROIIIS stability and is equivalent to $\Delta\Delta G^0_{U-N} > 1$ kcal·mol^{-1}, where $\Delta\Delta G^0_{U-N}$ is the variation of increment of ΔG^0_{U-N} from the unfolded conformation to the native folded state.

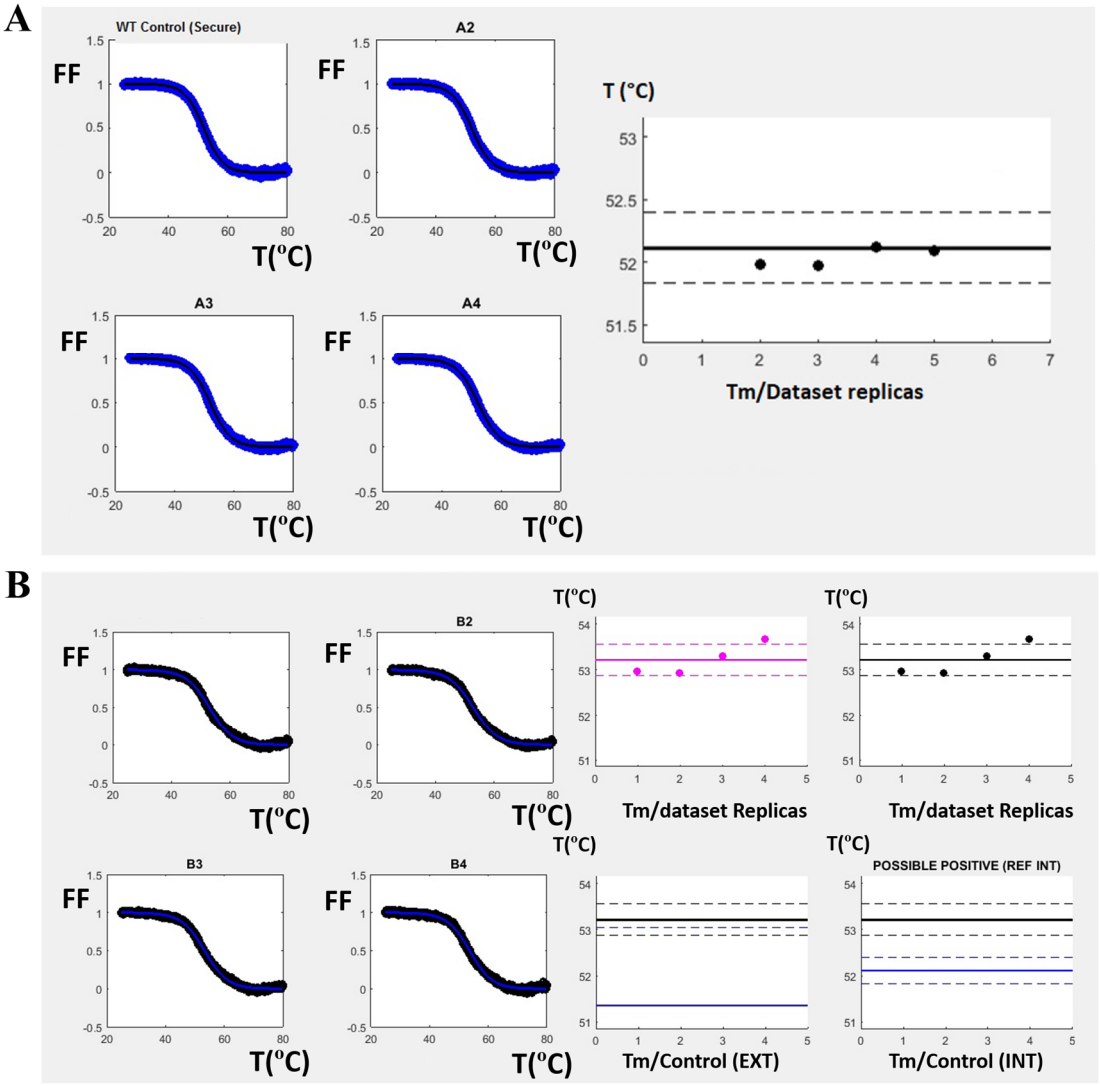

Figure 35. Outputs representation of melting curve of ligand-protein from inhouse bioinformatic program. Representation of melting curve by tetraplicate on the left; FF correspond to the fraction folded protein normalized temperature-dependent (in ºC). A) Setting up of negative control. WT UROIIIS (4 µM) protein without ligand. On the right is shown a graphic of the points distribution of T_m from the replicas, the average of T_m is represented as black line, the dashed lines are the range of distribution. B) Example of possible positive compound (60 µM) output data. On the right upper is shown the distribution of the T_m values; all T_m values represented (pink), validated T_m values represented (black). Graphics showed on right lower are the comparisons T_m values (black line) with respect to the negative control (blue line), increment of T_m in presence of ligand is appreciated; Data validation with external control (T_m/control Ext) and internal control (T_m/control INT) is shown.

IV.1.3. Generation of cellular models to investigate human UROIIIS homeostasis. Transient transfection of UROIIIS-GFP (WT or C73R) in mammalian cells.

In an orthogonal approach, based on a **functional assay**, we also performed experiments *in cellula*, targeting the same chemical library (L1) to assess their ability to raise the cytosolic enzyme concentration. The assay is based on the fact that UROIIIS when carrying the hotspot C73R mutation becomes highly unstable by misfolding and triggers a degradation mechanism via the proteasome. Consistently, the intracellular protein levels of C73R-UROIIIS-GFP (where GFP accounts for the green fluorescent protein) fall below detection limit, whereas WT-UROIIIS-GFP can be easily detected. Remarkably, the mutant protein levels can be restored upon cell treatment with the proteasome inhibitor MG132[62] or Bortezomib, a commercially proteasome inhibitor[105], through a mechanism by which the compound blocks the degradation proteasome pathway, abrogating the main pathway for this enzyme degradation and resulting in the accumulation of C73R-UROIIIS-GFP, which now can be monitored by its neat fluorescence emission.

To be able to perform the functional assay, several mammalian cell lines (MLP29, K562, M1 cell lines) were transiently transfected using the plasmids coding for WT- or C73R-UROIIIS-GFP to monitor the turnover of overexpressed proteins. All the constructs were verified by DNA sequencing and the resulting stable cell lines were characterized by fluorescence microscopy, cytometry and/or western blot. After cell transfection and under antibiotic selective conditions, resistant cells outgrow the non-resistant ones, resulting in a polyclonal population of stably-expressing cells. To obtain 100% clonal purity, the selection technique requires to pick, grow and dilute clones several times. The outcome is a mixed population of stably-transfected cell lines with undefined and genetically mixture, yet they are suitable for a wide range of applications such as drug discovery assays or the production of recombinant proteins[136].

IV.1.3.1. Characterization of stably transfected cellular models.

The biosynthetic heme pathway occurs in all mammalian cells but their expression levels vary significantly depending on the cell type and the tissue where they belong. Principally, hepatic and erythroid cells are the highest producers of heme due to high requirements as prostatic group of cytochrome P450 and hemoglobin, respectively[137]. As hepatic cell model, we use MLP29 cell line from progenitor epithelial cells of mouse liver. K562 is a human erythrocyte cell line, while M1 human fibroblast cell line were used as an experimental mimetic human skin.

To characterize the stably transfected cell lines, we proceeded to the identification of GFP-tagged version of UROIIIS WT or C73R mutant of the obtained clones by different fluorescence detection techniques. First, we analyzed the clones by flow cytometry to monitor the fluorescence emitted from the GFP protein tag (509 nm)[138]. The expression levels were quantified by western blotting, a technique that is able to ascertain the integrity of the UROIIIS-GFP expression. Finally, fluorescence microscopy was suitable to pinpoint the subcellular localization of the expressed protein. In all cases, the threshold was established according to the fluorescence measured in unmodified and/or transfected cells treated with MG132.

Stably transfected MLP29 cell lines were already available in our laboratory[62]. Following the characterization above described, we certified that the stable line remains fit and functional for the investigation. Figures 36A shows the fluorescence emitted by WT- and C73R-UROIIIS-GFP. First, by flow cytometry we observe the fluorescence at the GFP emission frequency, indicating proper transfection. As expected, WT and C73R mutant proteins increase the number of GFP-positive cells in the presence of MG132 compound (14,7 % and 9,15 %, respectively) after blocking the proteasome, the principal degradation pathway for UROIIIS. On the other hand, Figure 36B shows, by western blotting, the presence of GFP tagged proteins with specific antibodies against UROIIIS or GFP, clearly showing a band above at 50 kDa indicating the correct overexpression of the interested proteins (theoretical MW = 55 kDa). MG132 treatment is required to detect the C73R-UROIIIS-GFP, which shows a drastic change in intensity as a function of the MG132 treatment.

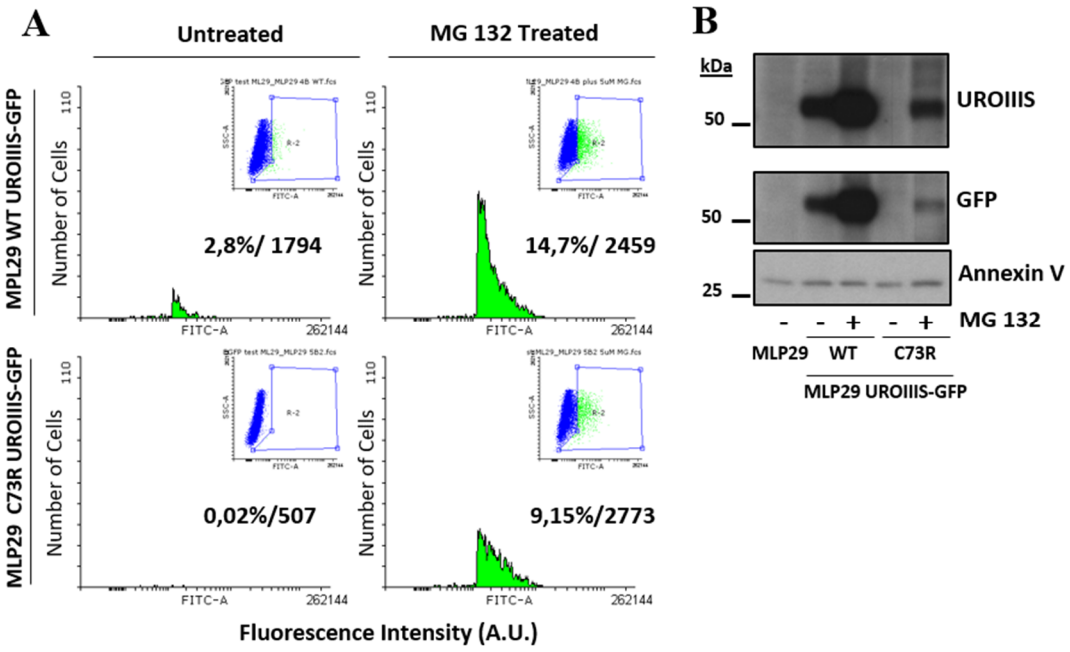

Figure 36. Characterization of stably MLP29 WT- or C73R-UROIIIS GFP. A) GFP fluorescence (FITC-A signal) of stably MLP29 WT or C73R UROIIIS GFP-tagged cell lines untreated or treated with MG132 at 5 μM analyzed by flow cytometry. Percentage and median fluorescence intensity of GFP-positive cells are indicated. B) Western blotting analysis of unmodified cell line (control) and cells stably expressing versions of WT- or C73R-UROIIIS protein GFP-tagged untreated or treated with MG132 (5 μM) in MLP29 cell line. Specific antibodies against UROIIIS and GFP were used to detect proteins from transfected vectors. Annexin V serve as protein loading control.

Human M1 fibroblast cell line is an immortalized non-tumoral line, rather convenient to avoid the problems derived from high metabolic activity and morphological and functional modifications that occur in the neoplastic cell lines[139]. Furthermore, since they derive from human skin they become a realistic model for the investigation of the pathological skin alterations in CEP patients. The stably transfected M1 versions of WT- or C73R-UROIIIS-GFP cell lines were obtained following the steps described previously (See Materials & Methods, Section III. 6.3.) for transient transfection and characterized by the same analysis as used with the MLP29 stably clones and described above. First, the clones were analyzed by flow cytometry (Figure 37A); the GFP expression observed after MG132 treatment indicates the correct cells transfection. The expression of WT- or C73R-UROIIIS-GFP at 55 kDa was confirmed by western blotting (Figure 37B).

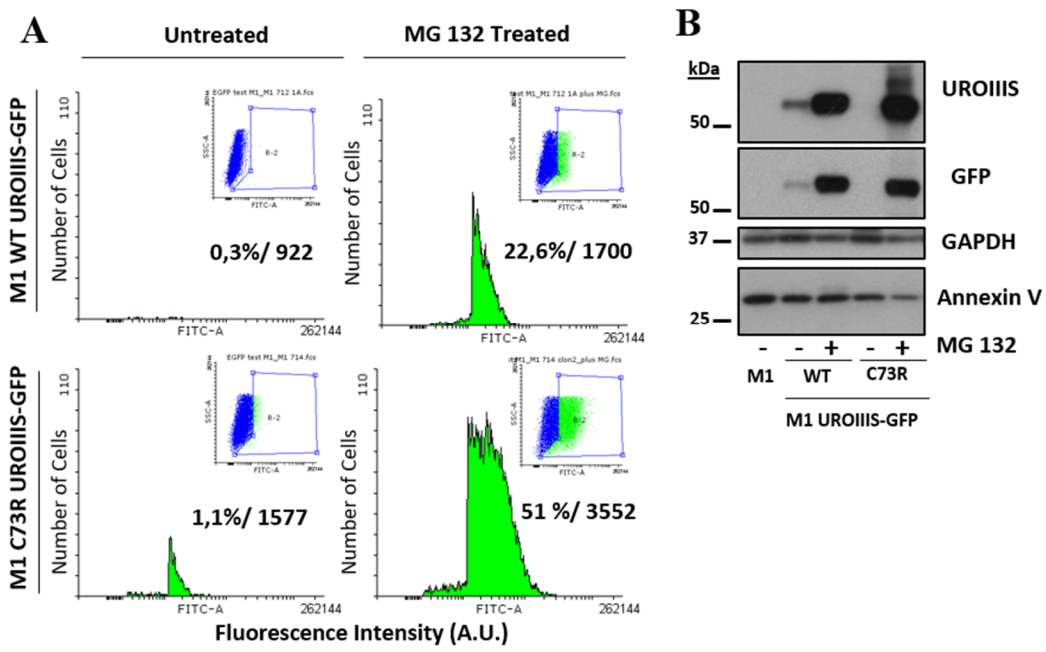

Figure 37. Characterization of stably M1 WT- or C73R-UROIIIS GFP. A) GFP fluorescence (FITC-A signal) of stably M1 WT or C73R UROIIIS GFP-tagged cell lines untreated or treated with MG132 at 5 μM analyzed by flow cytometry. Percentage and median fluorescence intensity of GFP-positive cells are indicated. B) Western blotting analysis of unmodified cell line (control) and cells stably expressing versions of WT- or C73R-UROIIIS protein GFP-tagged untreated or treated with MG132 (5 μM) in M1 cell line. Specific antibodies against UROIIIS and GFP were used to detect proteins from transfected vectors in both cell lines. GAPDH and Annexin V serve as protein loading controls.

Images obtained by fluorescence microscopy (Figure 38) reinforce the flow cytometry results, corroborating the presence of GFP fluorescence by conjugated Cy3 secondary antibody, emitting red fluorescence at 570/615 nm wavelength. MG132 treatment determine the accumulation of UROIIIS, increasing the number of positive cells observed. The immunofluorescence technique allows the localization of the protein that, in this case, accumulates in the cell cytoplasm. The distribution of the WT-UROIIIS-GFP protein is largely homogeneous for stably M1 cell lines (Figure 38, below), while C73R-UROIIIS-GFP showing a granular protein distribution in MLP29 (Figure 38, upper).

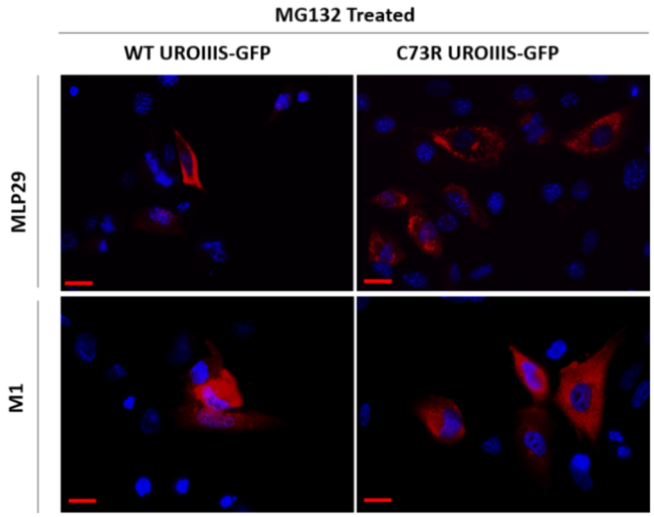

Figure 38. Fluorescence Microscopy (Zeiss Axioverte200), immersion oil objective 63X. Immuno-fluorescence of MLP29 (upper) and M1 (below) stably versions of WT- or C73R-UROIIIS-GFP protein. DAPI (blue) stain showing the presence of cells and location of nucleic acids. Expression of GFP is determined by primary GFP antibody conjugated by Cy3 dye secondary antibody (red). MG132 (5μM) treatment for 16 hours. Co-localization of nucleus and cytoplasm GFP expression in cells is shown. *Scale bar*, 20 μm.

Flow cytometry certified the stability of K562 cell lines. These cell lines were obtained at the University of Bordeaux, France (See Materials and Methods, Section III.6.1.). Figure 39 shows the results obtained when GFP is inserted at the C- or N-terminus of WT-, C73R- or P248Q- UROIIIS-GFP. P248Q is the second most frequently found mutation in CEP patients (See Introduction, Section I.5.3). C73R- and P248Q-UROIIIS show similar percentage of expression but in the case of GFP, when placed at the N-terminus, the transfection percentage is slightly higher: 8 % for C73R- and 11 % for P248Q-UROIIIS. The threshold was established at the fluorescence for unmodified K562 for control. Stably K562 WT UROIIIS cell lines in both cases are characterized by high GFP expression: 16 % for GFP C-terminal and 27 % for GFP N-terminal.

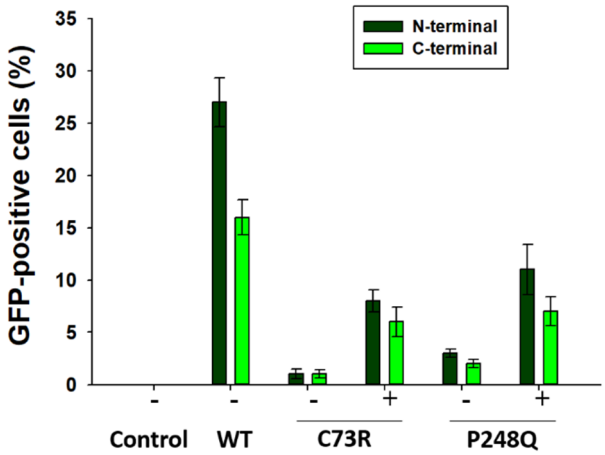

Figure 39. Percentage of GFP-positive cells (EGFP-A signal) of stably K562 WT-, C73R- or P248Q-UROIIIS GFP-tagged in N-terminal (dark green) or C-terminal (light green) cell lines in the absence or presence of MG132 at 5μM analyzed by flow cytometry. The threshold was established at the fluorescence observed for unmodified K562 cell line control. N=3.

IV.1.4. Functional assay *in cellula.* Screening of the L1 library in C73R-UROIIIS-GFP stably transfected human M1 cells to identify pharmacological chaperones.

The functional assay was performed on the library L1, using stably human M1 fibroblast C73R UROIIIS-GFP as cellular model. The stably cell line characterization, previously described, demonstrate that a GFP-tag fused to the mutant protein is suitable to monitor intracellular UROIIIS homeostasis and how it can vary in the presence of compounds. Based on this property and on previous studies from our laboratory[61,62], a GFP fluorescence monitoring system was designed by HC automated fluorescent microscope (See Materials & Methods, section III.7.). As shown in Figure 40, untreated cells do not show GFP intrinsic background, whereas MG132 treated cells show high GFP intensity.

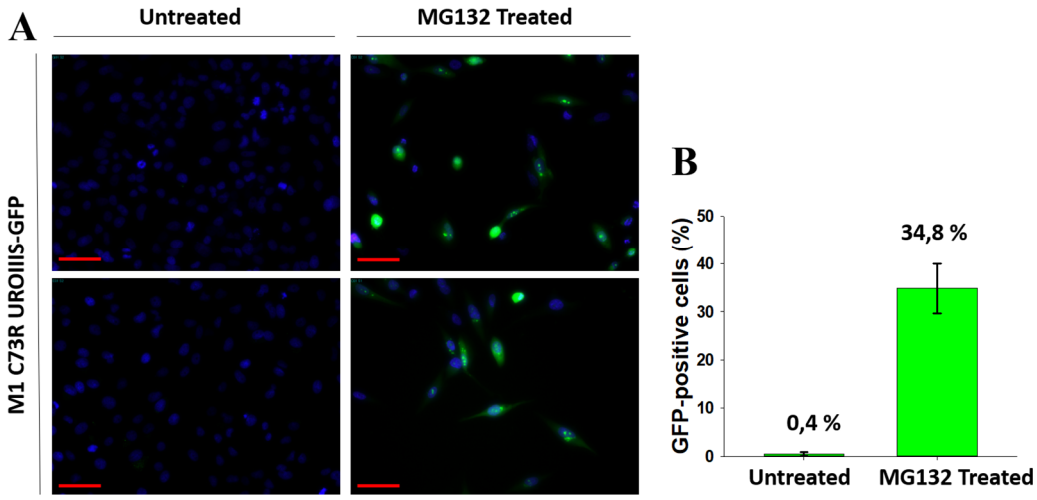

Figure 40. Setting up of functional assay. A) Fluorescence microscopy images. Setting up of GFP fluorescence of stably M1 C73R mutant UROIIIS-GFP. Untreated cells as negative control (low GFP background) and MG132 (5μM) treated cells for 16 h as positive control (high GFP intensity observed). N=2, cells were formaldehyde fixed. *Scale bar*, 50 μm. B) Percentage of intensity GFP-positive M1 stably C73R UROIIIS-GFP cells analyzed by HC automated fluorescence microscope. Untreated cells as negative control shown 0.4 % of intensity and 34,8 % for MG132 (5 μM) treated cells for 16 h as positive control. N=8, data record analyzed by MetaExpress software.

The intensity differences between untreated and MG132-treated cells were used to establish the GFP intensity threshold to analyze L1 molecules. After calibrating the fluorescence microscope parameters, we established a valid working system in order to check the interaction between C73R-UROIIIS-GFP and the putative ligand, where all the neat fluorescence was directly reporting on a neat increase in the intracellular protein concentration induced by the compound. In this context, 2500 organic molecules from the L1 library were tested at 500 μM during 16 hours, formaldehyde fixed and analyzed by HC automated fluorescence microscope (Figure 41). From the entire set, 85 compounds (3.4 % of the library) significantly increased the GFP fluorescence in the functional assay.

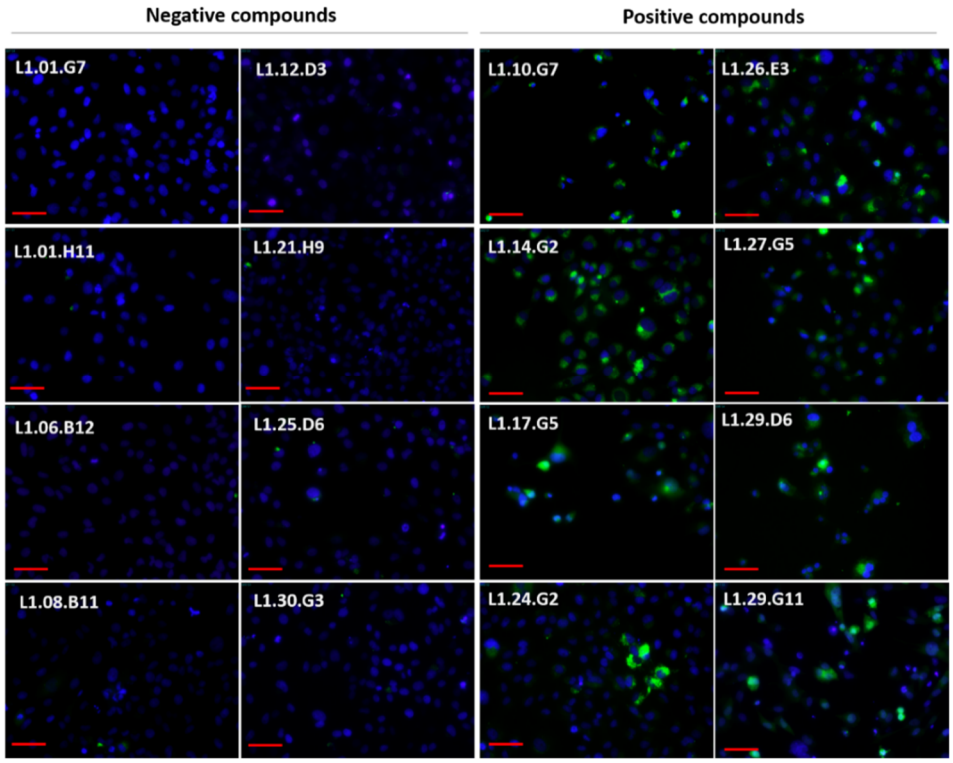

Figure 41. Fluorescence microscopy images of library L1 functional assay; negative (N=8) and selected positive (N=8) compounds at 500 µM for 16 hours. Cells were formaldehyde fixed. *Scale bar*, 50 µm.

IV.1.5. Library L1 hit compounds identification; cross-validated analysis, biochemical and structural characterization.

The results obtained from the orthogonal stability and functional assays were cross-validated to yield a reduced list of 25 selected compounds (Table 12). After in-depth analysis and assuming that the increasing GFP fluorescence is associated to a protein-ligand interaction in the cytosolic environment, the best performing compounds from the short list were characterized biochemically by flow cytometry and western blot (Figure 42).

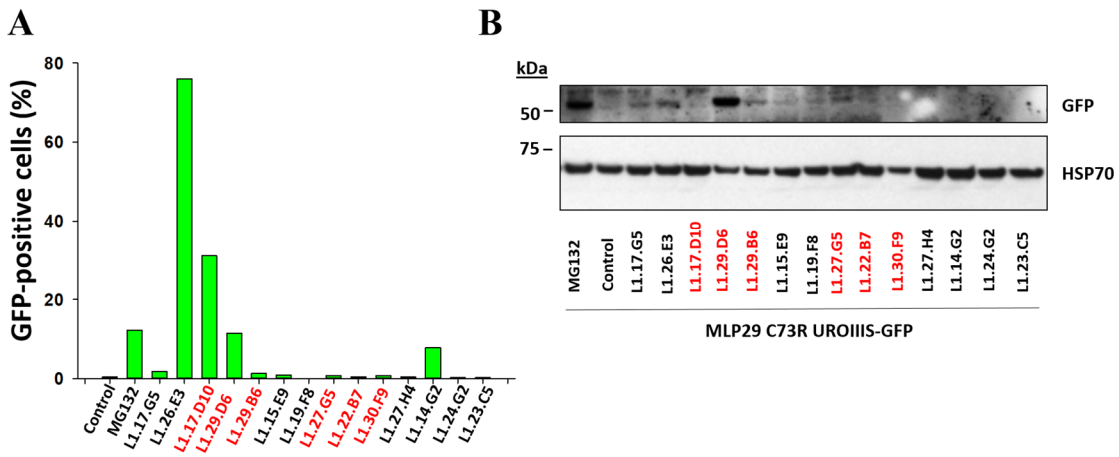

Figure 42. Biochemical characterization of library L1 selected compounds. Stably MLP29 C73R-UROIIIS-GFP library L1 treatments at 500 µM or 250 µM (depicted in red). A) Percentage of library L1 GFP intensity tested by flow cytometry. B) Western blot of library L1 treatments. Specific antibody against GFP was used to detect intracellular mutant protein at 55 kDa. Hsp70 serve as protein loading control.

The molecules were tested in the hepatic murine stably cell line MLP29 C73R-UROIIIS-GFP at a range of compound concentrations adjusted to avoid toxicity (between 500 μM and 250 μM). The level of mutant protein accumulated or restored is determined by western blot (Figure 42B), where the band at 55 kDa reflects the protein expression level. These results were used to select the compounds that most powerfully increase the intracellular levels of the protein.

	Stability assay (Scr.1)		Functional assay (Scr.2)	
Icode Name	ΔTm-ABS(n.e.)	ΔTm-EXP(n.e.)	FC (%)	NFC/NTC
1.H11	1.5 ± 0.4 (3)	1.3 ± 0.4 (3)	2.2	6/480
20.C3	3.0 ± 0.4 (3)	2.0 ± 0.4 (3)	15.9	62/385
26.E3	3.0 ± 0.9 (3)	2.7 ± 0.9 (3)	12	27/217
2.F9	1.3 ± 0.5 (4)	2.5 ± 0.5 (4)	19.8	66/396
2.F11	1.9 ± 0.2 (2)	3.2 ± 0.2 (2)	13.2	7/191
23.A9	1.4 ± 0.2 (4)	1.3 ± 0.2 (4)	1.5	4/497
2.C7	1.3 ± 0.2 (3)	1.9 ± 0.2 (3)	0.5	2/545
3.B10	1.2 ± 0.09 (4)	1.93 ± 0.09(4)	7.2	14/485
3.E5	1.6 ± 0.7 (3)	2.1 ± 0.7 (3)	3.7	9/397
14.G2	2.4 ± 0.3 (4)	2.0 ± 0.3 (4)	6.5	15/339
27.G3	2.4 ± 0.9 (2)	1.7 ± 0.9 (2)	50	6/17
15.E9	2.0 ± 0.7 (4)	1.0 ± 0.7 (4)	100	121/121
17.G5	2.9 ± 0.3 (2)	1.9 ± 0.3 (2)	17	9/231
17.D10	1.2 ± 0 (1)	0.7	100	6/6
19.F8	2.7 ± 0.7 (2)	2.1 ± 0.7 (2)	3	8/352
22.B7	3.3 ± 0.3 (2)	2.2 ± 0.3 (2)	18.2	2/73
29.D6	n.a.	n.a.	5.1	4/150
24.G2	2.3 ± 0.5 (4)	1.6 ± 0.5 (4)	2	7/300
23.C5	1.8 ± 0.1 (4)	1.7 ± 0.1 (4)	45.3	311/666
23.D5	3.9 ± 1.3 (2)	3.8 ± 1.3 (2)	8.6	37/445
24.D11	1.3 ± 0.2 (4)	1.0 ± 0.2 (4)	95	166/178
27.G5	1.9 ± 0.1 (3)	1.9 ± 0.1 (3)	23.3	14/95
27.H4	2.8 (1)	2.1 (1)	24	11/47
29.B6	1.7 ± 0.5 (3)	1.2 ± 0.5 (3)	86.8	102/118
30.F9	1.3 ± 0.3 (4)	0.7 ± 0.3 (4)	100	11/11

Table 12. Selected hit list of compounds after the stability and functional assays on the library L1. Cross-validated data from independent stability (Scr.1) and functional (Scr.2) assays. FC = Fluorescent Cells / n.a. = not available / n. e. = number experiments / NFC = number fluorescent cells / n. s. = no stabilization / NTC = total cell number / Scr. = screening.

After the biochemical characterization, the 10 best hits are further investigated using NMR spectroscopy to characterize their interaction site within the protein. NMR is a high resolution spectroscopic technique suitable for the elucidation of the tridimensional structure and flexibility of proteins[140], to study their segmental reorientations and the catalytic mechanism of enzymes[141]. The experiments obtained by NMR allow studying the biomolecular dynamics at a large number of time scales. There are examples described in the literature which, using NMR, the link between the conformational flexibility and the biological function of the protein is unraveled[142]. A characteristic feature of NMR is that the observed nuclear resonance frequencies (chemical shifts, δ) depend on the local environments of the individual nuclei, which can be measured with great precision and, therefore, are sensitive to minimal changes in the chemical environment. Chemical shift is

normally represented in parts per million, or ppm, which are determined through the following equation:

$$ppm = \frac{(Vo-Vref)x10^6}{Vref},$$

where ν_o is the frequency of the nucleus to be observed and ν_{ref} is the frequency of the reference nucleus.

Here, for the NMR experiments to study the complex protein-selected compound (library L1), the method used was the Chemical Shift Perturbation (CSP) using the ^{1}H,^{15}N-HSQC spectrum as a reporter, which is reasonably sensitive and the mapping of interaction site is generally well resolved. So, analysing the CSPs in the spectra (with and without the compound), we can pinpoint the residues of the protein that are in contact with the compound, determine the location of the binding site, the ligand affinity for the biomolecule and, eventually, the structure of the complex. As a result of the analysis, it was determined that 9 molecules bind UROIIIS, five of them in a non-specific mode or in multiple modes, two of them (L1.27.G5 and L1.29.D6) at the catalytic enzyme site and two of them (L1.17.G5 and L1.26.E3) specifically targeting the C-allosite (Figure 43).

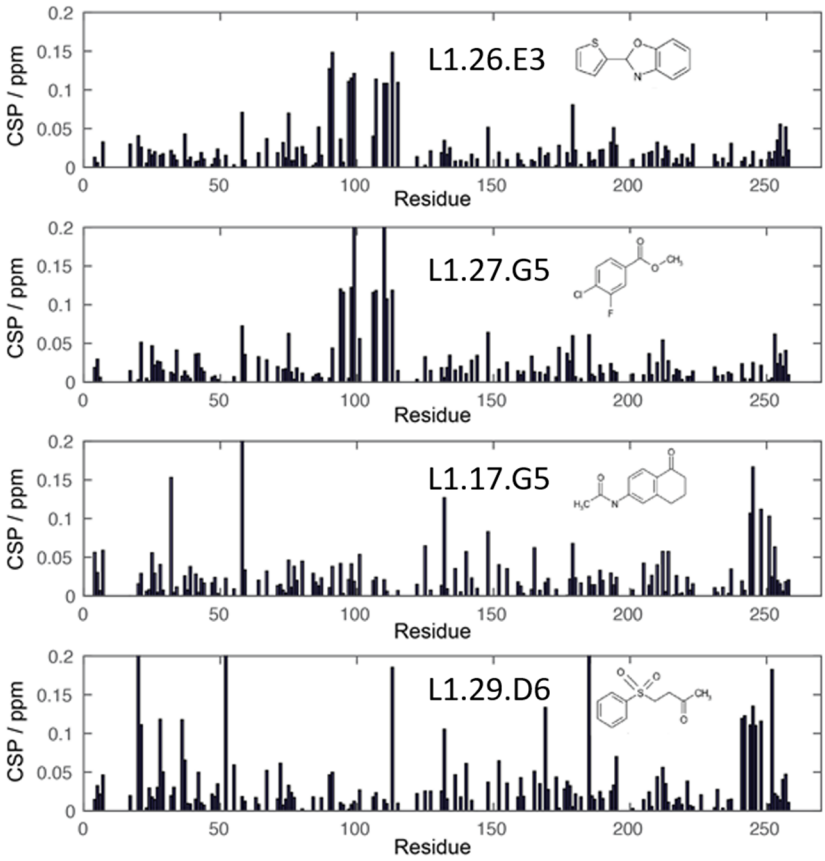

Figure 43. Chemical shift perturbation of library L1 hits selected compounds. CSP versus the residue number of UROIIIS for the top four compounds of the L1 library. The compounds L1.27.G5 and L1.29.D6 associate at the catalytic centre, whilst L1.17.G5 and L1.26.E3 specifically recognize the C-allosite.

On the other side, CSPs analyses also reveals that affinities are low (50-150 μM), consistent with the small sizes of the tested fragments but, once more, this is not in detriment of activity since western blot analysis confirms that the four molecules are functional and they are able to increase the intracellular levels of protein (Figure 44).

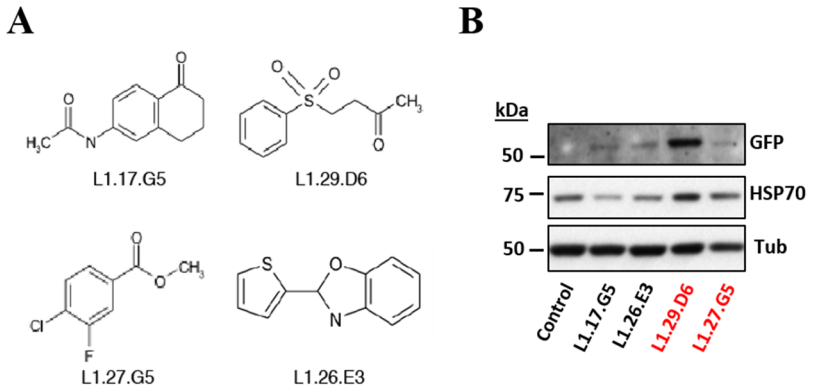

Figure 44. Library L1 hits selected compounds. A) Chemical structures of hits selected compounds, small fragments of organic molecules from the library L1. B) Analysis by Western Blot of library L1 selected compounds at 500 μM and 250 μM (compounds represented in red) by MLP29 C73R-UROIIIS-GFP cell line. Specific antibody GFP was used to detect the mutant protein associated to GFP at 55 kDa. Hsp70 and Tubulin (Tub) serve as protein loading controls.

The secondary structure of a protein, its folding thermodynamics and kinetics can be effectively investigated by measuring the chiral absorption of the circularly polarized light (circular dichroism, CD). Particularly, we were interested in how the protein's thermostability changes on the interaction with the selected compounds (library L1) as well as their kinetic stability. According to the current belief in protein folding theory, kinetic stability is related to a high free-energy barrier between the folded state from the non-functional forms (unfolded states, irreversibly-denatured protein). Such barrier may guarantee that the bioactive conformation of the protein is maintained, at least during a physiologically relevant time-scale, even if the native state is not thermodynamically stable as compared to non-functional forms[143]. In this context, previous studies in our laboratory show that the loss of UROIIIS catalytic activity parallels the exponential decay of the ellipticity, indicating that enzyme missfunction over time is due to protein unfolding. Specifically, at physiological temperature and *in vitro*, WT-UROIIIS has a half-life time of 61.1 h, a long time for the enzyme to exert its function in the cell, but the mutations accelerate the process of protein denaturation preventing them from exercising their function [16].

Through CD analysis we demonstrate that the molecules targeting the C-allosite of WT protein or a deleterious variant of UROIIIS (C73N-UROIIIS) are able to improve the thermostability (T_m) and also their kinetic stability as compared to the spontaneous and progressive degradation observed for the protein alone (Figure 45), therefore, improving the half-life of the protein which would allow it to exert its function.

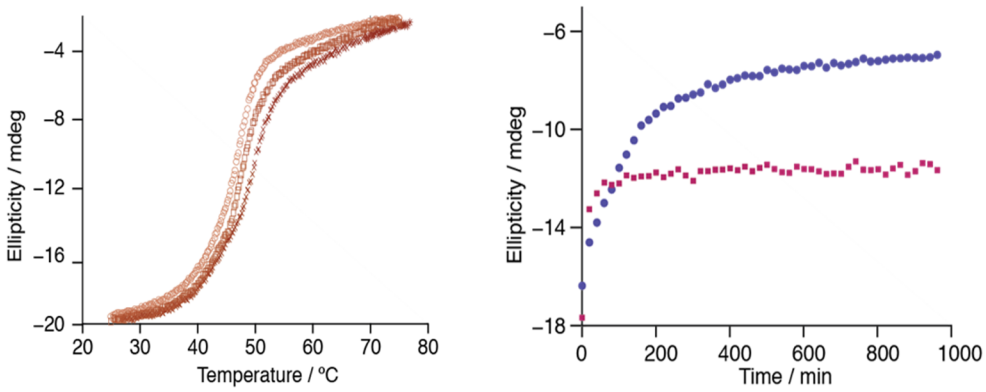

Figure 45. CD analyses of L1.26.E3 selected compound. Left) Representative curve protein mid-point denaturation temperature (T_m). Monitorization of WT-UROIIIS T_m shifts by interaction protein-ligand. T_m of WT-UROIIIS in the absence (circles) and in the presence of 5 equivalents (squares) and 10 equivalents (x symbols) of coded compound L1.26.E3. Ellipticity monitors the loss of secondary structure of the protein, shifts to the right of X axis (ºC) means a significant stabilization of WT protein version. Right) C73N-UROIIIS deleterious version is kinetically stabilized in the presence of L1.26.E3 (15 equivalents, purple squares), as compared to C73N-UROIIIS in buffer (blue circles).

Finally, with all the results together, we selected the best candidates from L1 compounds (L1.27.G5; L1.29.D6; L1.17.G5 and L1.26.E3), confirming that the screening strategy succeeded in finding organic molecules that act as pharmacological chaperones of UROIIIS *in vitro* and *in cellula.*

IV.1.6. Data integration and Drug repurposing analysis from FDA-approved (Food and Drugs Administration) compound Library.

The Food and Drug Administration (FDA) is an agency from Unites States responsible for protecting the public health by assuring the safety, efficacy, and security of human and veterinary drugs, biological products, medical devices, food supply, cosmetics, and products that emit radiation, so all the drugs approved by the FDA have passed rigorous safety measures for human consumption. This constitutes a key advantage when looking for chaperones since in minimizes preclinical studies and ensures reduced toxicity after human intake. Although most of them have indications for specific diseases, they can be used for different targets not yet described (drug repurposing). The two validated fragments (L1.17.G5; L1.26.E3) targeting the C-allosite, identified and characterized previously as potentially pharmacological chaperones, were used as templates for a structural comparison against an FDA approved library of 1800 drugs (library L2) (See Materials & Methods, Section III.1.1.2.).

The *in silico* analysis was carried out through a service offer by the Chassys^{TM} platform from the company Atlas Molecular Pharma S.L. (Basque Country, Spain). The comparison of the libraries was performed based on the similar properties of the chemical compounds, and a close skeleton topology and it was normalized by the molecular weight to avoid biases, resulting in a score from which the most qualified compounds were selected. The top 15 FDA-approved molecular entities with higher score (Table 13) were further evaluated for their chaperone activity in UROIIIS with different techniques.

Name	MW	Indication	Target
Ciclopirox (Penlac)	207,27	Neurological Disease	
Phenylephrine HCl	203,67	Endocrinology	Androgen Receptor
Isoxicam	335,34	Inflammation	
Betamipron	193,2	Infection	
Octopamine HCl	189,64	Immunology	
Oxaprozin	293,32	Inflammation	
Atomoxetine HCl	291,82	Neurological Disease	5-HT Receptor
Procyclidine HCl	323,9	Neurological Disease	
Dydrogesterone	312,45	Endocrinology	
Estrone	270,37	Endocrinology	
Darifenacin HBr	507,46	Infection	AChR
Furosemide (Lasix)	330,74	Cardiovascular Disease	
Probenecid (Benemid)	285,36	Metabolic Disease	
Candesartan (Atacand)	440,45	Cardiovascular Disease	RAAS
Thiabendazole	201,25	Vermifuge	

Table 13. FDA selected compounds as positive pharmacological chaperone. 15 FDA selected compounds from library L2 repurposing drugs.

The goal now is to validate the computationally repurposed compounds. First, the selected repurposing compounds were tested *in cellula*, monitoring the fluorescence of stably M1 UROIIIS-C73R-GFP cell line by fluorescence microscope, following the same methodology as when screening the L1 library, thus performing a second functional assay. In this case, the concentration of treatment was 100 μM for 16 hours. A total of 5 FDA approved entities (ciclopirox, phenylephrine, procyclidine, atomoxetine and dydrogesterone) were selected by their successful increase in the intracellular fluorescence, as it can be observed in the pictures taken from the microscope:

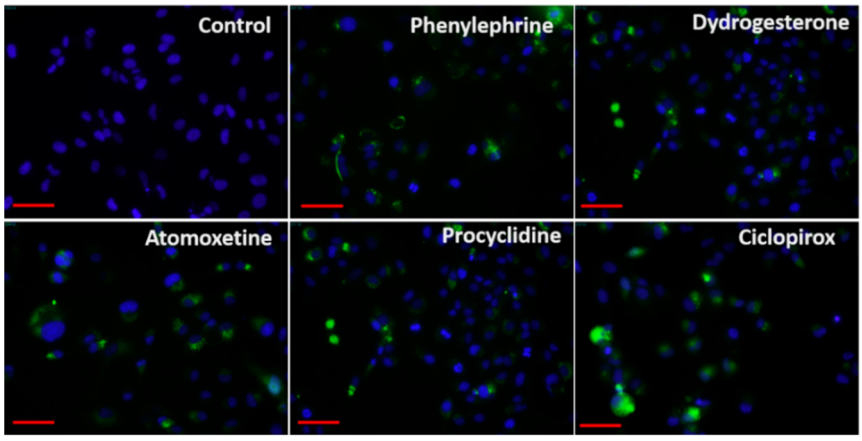

Figure 46. Fluorescence microscopy images of library L2 functional assay; negative control and selected positive FDA drugs at 100 μM for 16 hours. Cells were formaldehyde fixed. *Scale bar*, 50 μm.

Despite the obvious green fluorescence radiation, other non-UROIIIS specific mechanisms may activate the intracellular fluorescence of the GFP, thus producing false positives. Hence, we analyzed the GFP fluorescence emitted by the cells after treatments by flow cytometry (Figure 47A) and we performed western blot to distinguish GFP protein with a specific antibody (Figure 47B). These experiments are suitable to validate whether the compounds are able or not to accumulate the deficient protein associated to GFP after the treatment. As shown in Figure 47B, only ciclopirox shows a band at 55 kDa corresponding to UROIIIS-C73R-GFP, accumulating the protein above the detection level by western blot corroborated by flow cytometry where is the only drug that shows high GFP fluorescence (7,2 %). In all cases, the treatment by the proteasome inhibitor MG132 is the positive control by the accumulation deficient protein known effect blocking the degradation protein pathway.

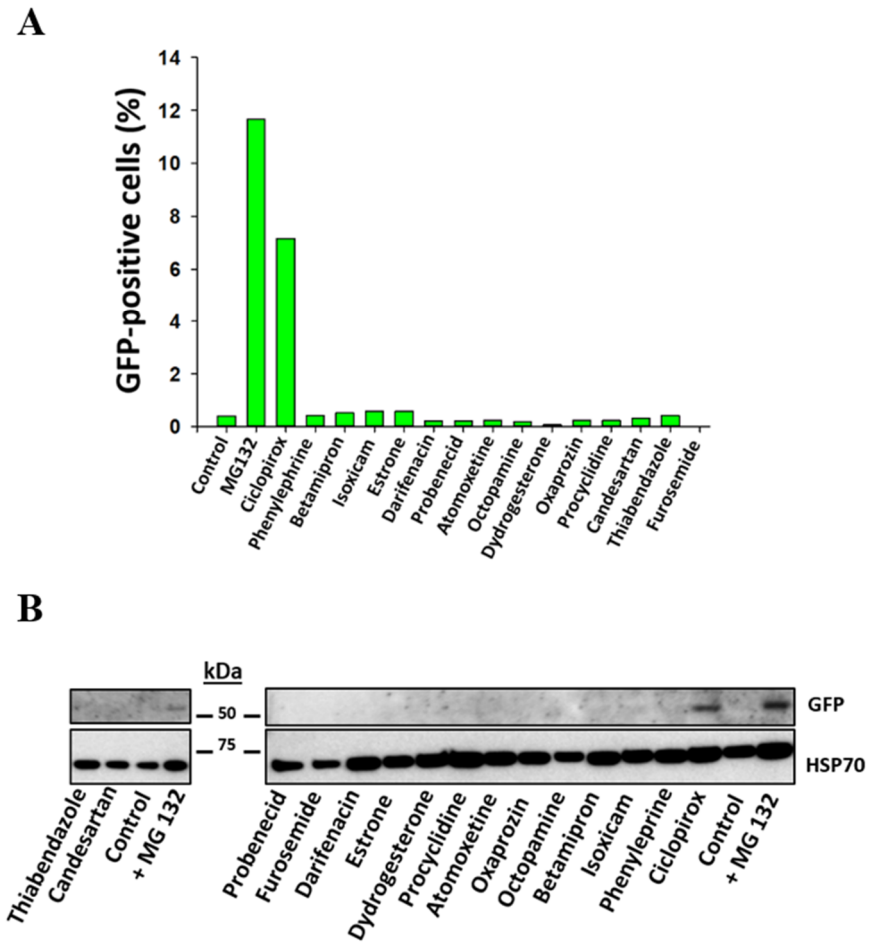

Figure 47. Biochemical characterization of library L2 drugs selected. A) Flow cytometry analysis of stably MLP29 C73R-UROIIIS-GFP L2 library treatments at 100 μM for 16 hours. MG132 proteasome inhibitor was used as positive control treated at 5 μM. B) Western Blot of L2 library treatments at 100 μM by MLP29 C73R-UROIIIS-GFP cell line. Specific antibody GFP was used to detect the mutant protein associated to GFP at 55 kDa. Hsp70 serve as protein loading control. MG132 proteasome inhibitor was used as positive control treated at 5 μM.

In parallel to the biochemical characterization, to study in detail the interaction site of the complex protein-drug, we analyzed by NMR spectroscopy the selected L2 compounds, focus on the C-allosite domain monitoring *in vitro* the changes in the catalytic efficiency of the protein. The NMR results analysing the chemical shifts perturbation (CSPs) of $^{1}H,^{15}N$-HSQC spectra were used to determine the drug binding pocket and the key residues involved in the binding phenomena. This information was implemented in the docking simulation by restraining the searching space centred in the binding site and providing flexibility to the side-chains of the key residues. Flexible-docking results were analyzed using in-house software and revealed that only ciclopirox (6-cyclohexyl-1-hydroxy-4-methyl-2(1H)-pyridone, CPX) specifically binds at the C-allosite, the structural model for the association is shown in Figure 48. The N-hydroxy-pyridone moiety actively interacts with the protein pocket through interactions with Asp113, Ser95 and Tyr97, while the ciclohexyl group fits in a hydrophobic pocket conformed by Tyr128.

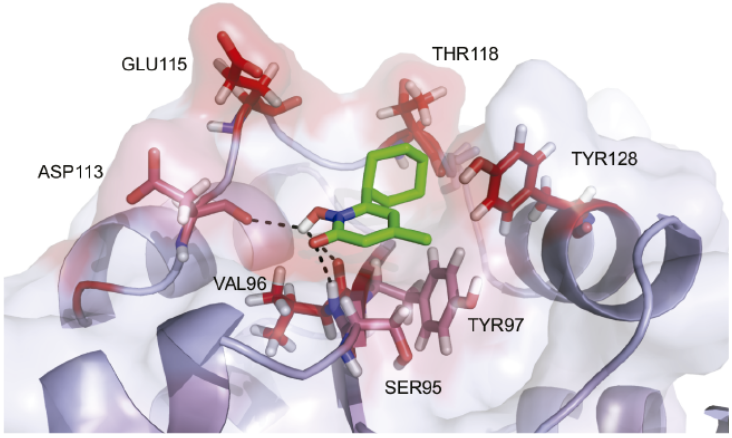

Figure 48. Structural model for the interaction of CPX (in green) to the C-allosite of UROIIIS, highlighting the involved amino acids. Residues with chemical shift perturbation upon CPX addition are shown in red. The hydrogen bond interactions are depicted by black dashed lines.

IV.1.7. CPX is the best candidate to stabilize deficient UROIIIS. Validation of CPX with a CRISPR/Cas9 generated CEP cellular model (UROIIIS-C73R$^{+/+}$).

IV.1.7.1. Cross-validation of L1 and L2 hits as potential pharmacological chaperones.

According to the data obtained so far, a set of compounds from the L1 and L2 libraries are already hits that stabilize deficient UROIIIS. For this set, Table 14 compares their chemical structures, analysing the interaction site, the accumulation of fluorescence GFP and the amount of protein detected intracellularly. All the results indicate that the strategy is capable to find putative pharmacological chaperones that rescue the deficient protein.

Based on the previous screenings whose results are reflected in Table 14, we selected four organic molecules from the library L1 (L1.17.G5; L1.26.E3; L1.29.D6; L1.27.G5) and one from the repurposed library L2 (CPX). Despite of the obvious advantage to associate to the C-allosite, we also selected two hits that bind in the active site (and compete with the

substrate), because the active site is evolutionary designed to host small organic molecules and some of these hits may show extraordinary potency.

Compound	Name	DT_m	Fc/%	GFP_int	WB/%	CSP
L1.17.G5	'N1-(5-oxo-5,6,7,8-tetrahydronaphthalen-2-yl)acetamide	2.9±0.3	17	+++	28	C-allosite
L1.26.E3	2-(2-thienyl)-2,3-dihydro-1,3-benzoxazole	3.0±0.9	12	+	90	C-allosite
L1.17.D10	'[2-(2-furyl)phenyl]methylamine	2.2±0.1	100	++	5	Non-specific
L1.22.B7	''4-[(4-methylphenyl)sulfonyl]butan-2-one	3.3±0.3	18.2	++	3	Non-specific
L1.29.D6	4-(phenylsulfonyl)butan-2-one	n. a.	5.1	+++	200	Active site
L1.29.B6	'2-(benzylthio)-5-methyl-4,5-dihydro-1H-imidazol-3-ium hydrochloride	2.7±0.5	87	++	47	Non-specific
L1.15.E9	'8-Hydroxyjulolidine	2.9±0.7	100	++	15	Non-specific
L1.19.F8	'isoxazole-5-carbothioamide	2.7±0.7	3	+++	13	Non-specific
L1.27.G5	'methyl-4-chloro-3-fluorobenzoate	2.3±0.1	23	++	26	Active site
L2.7.D7	ciclopirox	1.2±0.1	8	+++	36	C-allosite
L2.7.H10	phenylephrine	n. a.	2	+++		-
L2.11.E10	procyclidine	n. a.	1.8	+++		-
L2.10.E3	atomoxetine	n. a.	2	+++		-
L2.9.H2	dydrogesterone	n. a.	3.6	+++		Non-specific

Table 14. Summary of the biochemical and biophysical characterization of the L1 and L2 libraries selected compounds. ΔTm = the variation of half thermal denaturation of protein/ FC/% = percentage of fluorescent cells / n.a. = not available / GFP_int = GFP fluorescent intensity / WB/%= percentage of Western Blot analysis / CSP = chemical shifts perturbation.

The molecules, shown in Figure 49, display very similar chemical structures, demonstrating by western blot once more their capacity to accumulate the deleterious protein in the cytosol.

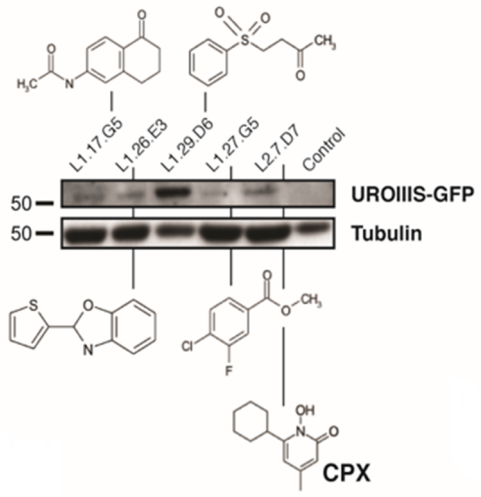

Figure 49. Western blot of putative selected compounds. MLP29 cells stably expressing UROIIIS-C73R-GFP protein cultured in the presence of DMSO (control), or pharmacological chaperones, analyzed by Western blotting. Tubulin is included as a housekeeping protein.

The molecule L1.29.D6 seems the most active compound as compared to the other hits (Figure 48) but it was excluded from the study due to the high toxicity showed in the MTT assay, which is used to analyze cell viability at half maximum inhibitory concentration (IC_{50}) (Figure 50). This quantitative measurement indicates how much of a particular drug or compound is needed to reduce the cell viability by half and the values are reported in molar concentration. Despite the inclusion of the Ro3 criteria of the L1 library of compounds, it is clear that they are not certified for human or animal consumption and their toxicity is not known. The above mentioned viability test shows that L1.29.D6 is potentially toxic (IC_{50} = 60 μM), while the IC_{50} values for L1.26.E3 and L1.17.G5 are around 1 mM, way above the bioactive concentration range.

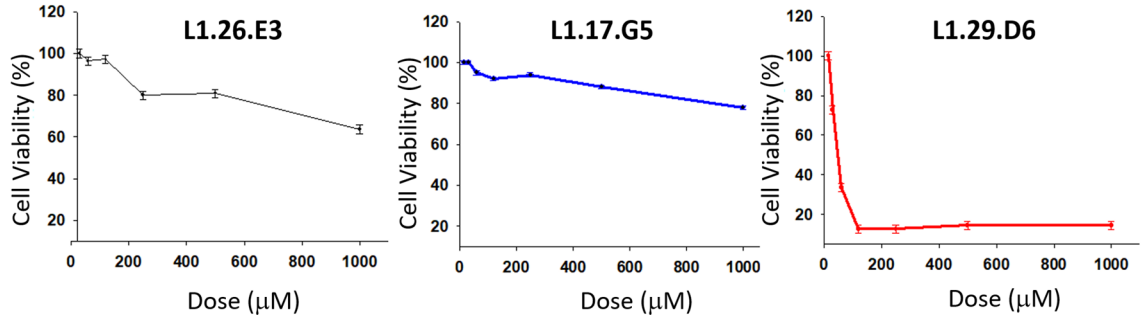

Figure 50. Cell viability assay for different compounds: the chemicals L1.26.E3, L1.17.G5 and L1.29.D6. The IC_{50} has been determined in human fibroblast M1 cell line. Absorbance at 550 nm is due to the tetrazolium reaction in the mitochondria and is a reporter of cell viability. N=3.

To complete the characterization of the hits, we analyzed their kinetic stability by circular dichroism, by monitoring the kinetic profile of the deficient C73N-UROIIIS. Specifically, the loss of secondary structure is monitored versus time, at physiological temperature. L1.26.E3 and CPX are able to stall protein's aggregation *in vitro* (Figure 51), which reinforce the idea that these molecules have chaperonin activity in UROIIIS.

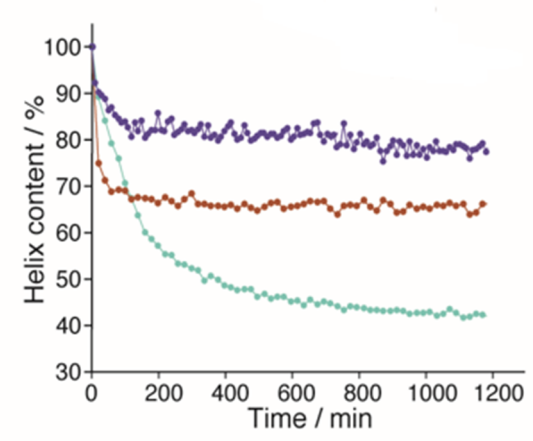

Figure 51. Comparison of kinetic stability of L1.26.E3 and CPX. UROIIIS-C73N is kinetically stabilized in the presence of L1.26.E3 (10 equivalents, red circles) or CPX (10 equivalents, purple circles), as compared to UROIIIS-C73N in buffer, which losses secondary structure over time (blue circles).

IV.1.7.2. Rescue of catalytic activity of mutated enzyme by the hit compounds

One essential issue is to ascertain whether the increase in the protein's stability is also translated into a gain in functionality. To that end, we need to evaluate the catalytic activity of the enzyme in the presence of the stabilizing compounds. In this context, we take CPX as a case study. According to the biosynthetic group heme pathway, the substrate catalysed by UROIIIS is hydroxymethylbilane (HMB), a highly unstable tetrapyrrole[48]. Therefore, to perform the enzymatic assay it is necessary to start at the previous step of the route, using porphobilinogen (PBG) as substrate. The assay is divided in two parts; the first reaction is carried out by incubation of the PGB substrate at different concentrations (from 0.1 to 4 mM) catalysed by the enzyme porphobilinogen deaminase (PBGD), followed by a second incubation by the enzyme WT or C73N-UROIIIS.

Figure 52 shows how the enzyme activity is increased in presence of CPX, manifesting the partial restoration of the reduced apparent catalytic activity of a mutated enzyme compared to the assay in absence of the drug, raising levels of activity to similar values than the WT enzyme. This study is an irrefutable proof of the direct CPX association on the deficient enzyme, reinforcing its role as pharmacological chaperone. Equivalent results have been obtained with other compounds from the L1 library.

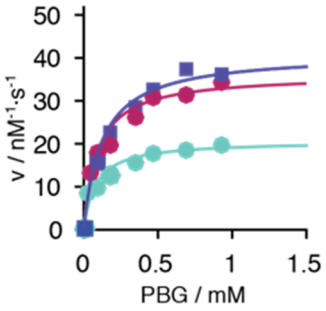

Figure 52. Substrate versus enzymatic rate plot for WT UROIIIS (purple), C73N-UROIIIS (green) and C73N-UROIIIS plus 15 equivalents of CPX (blue). Due to the instability of the substrate, it is generated in situ enzymatically from porphobilinogen (PBG) in a tandem assay. The lines correspond to the best fittings to the Michaelis-Menten equation.

IV.1.7.3. CRISPR/Cas9 cellular models of CEP (UROIIIS-C73R$^{+/+}$ and UROIIIS-P248Q$^{+/+}$).

The revolutionary genetic technology known as CRISPR/Cas9 (Clustered Regularly Interspaced Short Palindromic Repeats and CRISPR-associated protein 9) allow us to modify the cellular DNA, adding genetic material, removing, or altering at particular locations in the genome. It constitutes a powerful tool in molecular biology since it is faster, cheaper, more accurate, and more efficient than other existing genome editing methods[144]. In collaboration with the University of Bordeaux (France), we have employed CRISPR/ Cas9 technology (See Materials and Methods, Section III. 6.4) to transform human embryonic kidney 293 (HEK 293 or HEK) cells into human cellular models of CEP by modified the endogenous UROIIIS WT version by enzymes carrying either C73R or P248Q mutations, the two most frequent deleterious inborn errors in CEP.

HEK cell line was chosen due to is reported propensity to transfection (99 %) and efficient expression of proteins transfected [145], being a useful human cellular system. Consistently, the mutated replacing protein mimicks the disease, driving the toxic accumulation of porphyrins (URO I and COPRO I). HEK WT and mutant HEK UROIIIS-C73R$^{+/+}$ cells or HEK UROIIIS-P248Q$^{+/+}$ were characterised for their heme group biosynthesising properties by measuring the accumulation (or not) of toxic porphyrins in the cytosol. Porphyrins have a characteristic pattern of fluorescence, emission wavelength from 600 to 730 nm[146], therefore flow cytometry analysis at APC channel (Ex-Max 650 nm / Em-Max 660 nm) is able to distinguish between the non-fluorescent WT HEK cells and the fluorescent porphyrin-filled cytosol of the UROIIIS-mutated CEP cells, as shown in Figure 53.

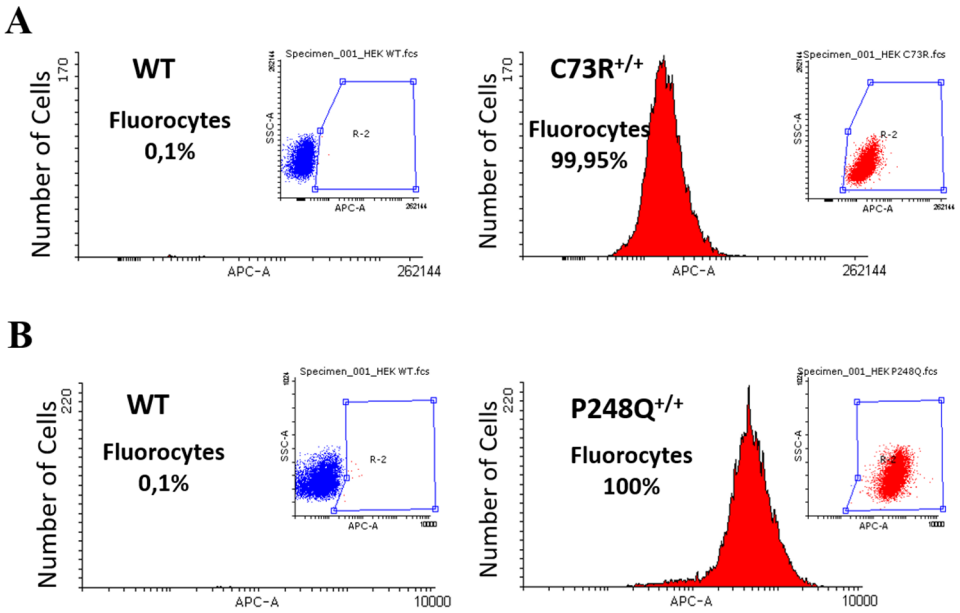

Figure 53. Characterization of HEK cell lines modified by CRISPR/Cas9. Fluorescence activated cell sorting (FACS) analysis. A) HEK WT cells (left), HEK cells with the UROIIIS-C73R endogenously introduced by CRISPR/Cas9 (HEK C73R$^{+/+}$, right). B) HEK WT cells (left), HEK cells with the UROIIIS-C73R endogenously introduced by CRISPR/Cas9 (HEK P248Q$^{+/+}$, right). The accumulation of porphyrins generates an intrinsic fluorescent phenotype of the cellular CEP models (fluorocytes). Emission wavelength from 600 to 730 nm.

We used HEK UROIIIS-C73R$^{+/+}$ cells to determine which selected molecules are the best candidates as pharmacological chaperones. Because HEK C73R$^{+/+}$ are a bona fide cellular model of CEP, it is possible to monitor the accumulation of porphyrins into the cells similarly to the experiments with knock-in CEP mouse models. This is an essential pre-clinical tool that beautifully mimics what happens at the patient level. Thus, instead of overexpressing the UROIIIS protein variants, in CRISPR/Cas9 CEP model we monitor the intrinsic fluorescence of the porphyrins themselves. For the experiments, the cell line was treated for 16 hours with two compounds (120 μM): L1.26.E3 and CPX and the experiments analyzed the total porphyrin fluorescence emitted by the cells by flow cytometry. Remarkably, CPX decreases the concentration of intracellular porphyrins in an 89,5 % as compared to the less than a 1% of reduction when using L1.26.E3 (Figure 54).

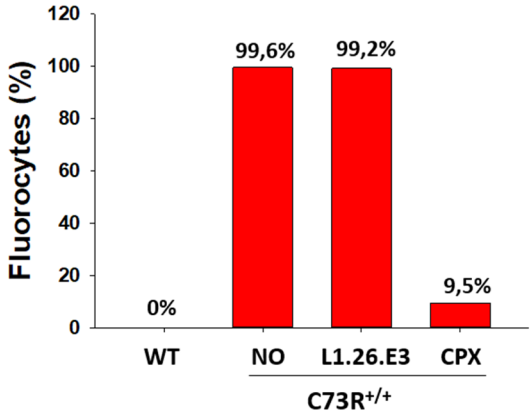

Figure 54. Intracellular porphyrins accumulation (percentage of fluorocytes). Flow cytometry analysis of HEK C73R $^{+/+}$ cell line of L1.26.E3 and CPX treatment at 120 μM for 16 hours.

Despite the great expectations of L1.26.E3, raised by previous experiments, the CPX performance with HEK UROIIIS-C73R$^{+/+}$ positions the repurposed drug as a really promising candidate for CEP treatment, acting as pharmacological chaperone, so all the efforts are focused in further characterizing CPX.

IV.2. Characterization of CPX as pharmacological chaperone against CEP.

IV.2.1. Analysis of the modulation of deficient UROIIIS homeostasis by CPX in multiple cellular models.

CPX was selected as potential pharmacological chaperone against CEP after the results showed in the previous sections, revealing its association to the C-allosite domain of UROIIIS, the accumulation of the deficient protein after the treatment in two different stably transfected cell lines monitored by GFP fluorescence, corresponding to fibroblast M1 and MLP29 hepatic cell lines, and finally the reduction of porphyrins in a CEP model genetically modified, all together evidencing its possible role as pharmacological chaperone. In addition, CPX is a repositioned drug which means that it is suitable for human consumption approved by FDA association, being of obvious advantage for future study in animals and subsequent clinical studies. To confirm the modulation of deficient UROIIIS homeostasis by CPX as a pharmacological chaperone, we funnelled our efforts towards a thorough analysis of the effect of CEP in different cellular models, also expanding the study by adding a second mutation (UROIIIS-P248Q, the second most common CEP-causing mutation). First, we tested CPX over a plethora of mammalian cell lines transfected with C73R- or P248Q-UROIIIS-GFP. The cell set includes: human fibroblast M1 cells, murine hepatocytes MPL29 cells, human immortalised myelogenous leukemia (K562) cells and human embryonic kidney (HEK). Fluorescence emitted by cells was measured by flow cytometry following the same protocol for the libraries screening, where the untreated cells does not show GFP fluorescence whereas the CPX-treated cells ought to increase the fluorescence if there is an increment in the intracellular protein concentration induced by the compound. As shown in Figure 55, this is actually the case and a large increase in fluorescence is induced by CPX treatment over C73R- or P248Q-UROIIIS-GFP transfected cells:

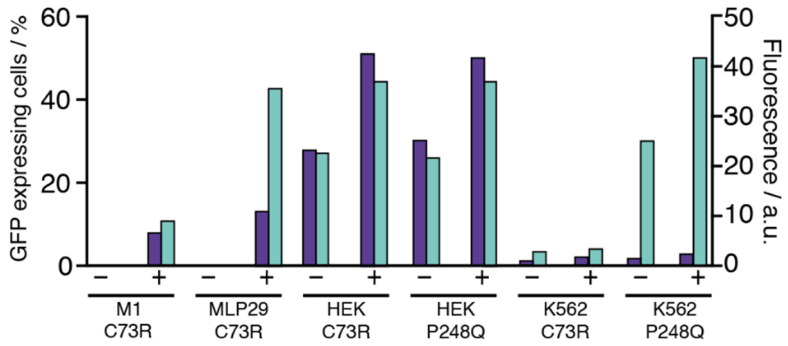

Figure 55. A dose of 60 μM CPX increases the number of GFP expressing cells (blue bars, left y-axis) and also the average fluorescence (green bars, right y-axis) by flow cytometry, for a set of eukaryotic cell lines.

HEK is a cell type with high metabolic rate and have been transiently transfected without subsequent selection of clones, so basal GFP fluorescence is expected. Yet, a significant raise in the fluorescence is observed when the cells are treated with CPX and identical results are obtained when the cells are transfected with the C73R- or P248Q-UROIIIS. The effect of CPX on both mutations indicates that it is not limited to the C73R mutation alone, opening possibilities that it could serve for an amplitude of mutations and even paving the way for its use in other types of Porphyria. Moreover, the positive result on the P248Q mutation validates the use of CPX with the available murine CEP model (Tg *Uros*$^{P248Q/P248Q}$ mice). Finally, the results obtained for the human erythrocytes K562 cell line reproduce an improvement in the protein's homeostasis in a cellular line that is a good producer of heme group.

As previously reported, the proteasome inhibitor MG132 is able to restore deficient protein levels by blocking its main degradation pathway. This compound is also cytotoxic, activating apoptosis. Using specific markers of polyubiquitination (UQ antibody) and cell death as the protein PAR-Polymerase (PARP antibody), we verify that the accumulation of the deficient protein on CPX treatment is **not** produced by an inhibition of the proteasome. Specifically, poly-ubiquitinated proteins are not more overexpressed than the control nor the integrity of the PARP is affected, as shown by western blot in Figure 56A-B. PARP antibody detects the PARP1 protein involved in cell viability, presenting a full length at 116 kDa as well as the large fragment (89 kDa) of PARP1 resulting from caspase cleavage facilitates cellular disassembly undergoing apoptosis[147]. Moreover, further protein markers were analyzed to demonstrate that CPX is not modulating other cell systems pathways. Early endosome antigen 1 (Eea1) is localized exclusively in early endosomes, and lysosome-associated membrane glycoprotein 1 (Lamp1), a highly-glycosylated glycoprotein associated to later endosomes, are not significantly altered (Figure 56A-B), which means that the glycosylation processes, closely associated to ER, and the endosomal trafficking are not apparently affected, reinforcing the idea that CPX is not modulating the endoplasmic reticulum pathways. Two different cell lines, human M1 and murine MLP29, confirm the same CPX effect on the stably overproduction of deficient protein UROIIIS at 60 μM, small concentrations of CPX around 6 μM are not effective doses as shown in Figure 56A.

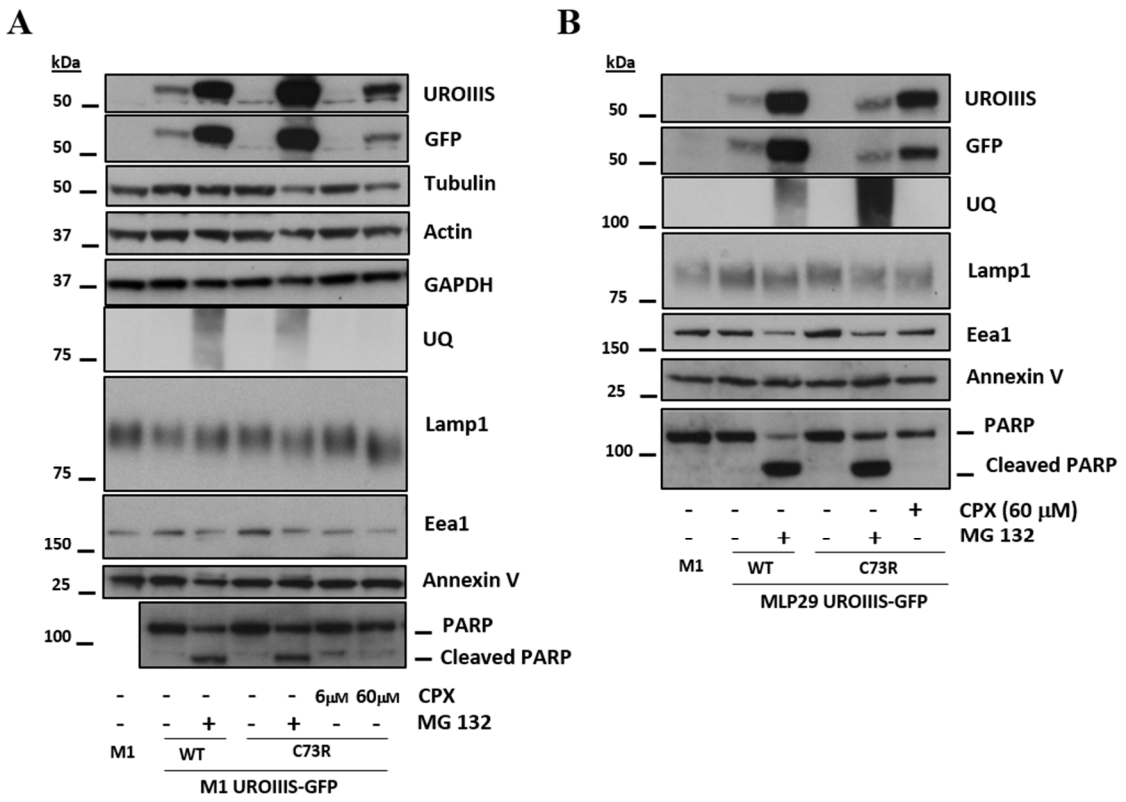

Figure 56. Western blot analysis of the CPX- of MG132 (5μM)-induced accumulation of UROIIIS-C73R-GFP in M1 human cells (A) and in MLP29 mouse cells (B). In all cases, the proteins were detected by using specific antibodies. Lam1 reports on post-translational modifications (glycosylation) in the endoplasmic reticulum; UQ displays the polyubiquitinylated proteins and is related to proteasomal degradation while Eea1 is a reporter for the endosomal vesicular trafficking. PARP is involved in the cell viability; cleaved PARP indicates cellular disassembly undergoing apoptosis. Actin, GAPDH, annexin V and tubulin serve as a protein loading controls.

Interestingly, CPX also presents the same effect on the WT version of human UROIIIS since it is able to accumulate UROIIIS-WT-GFP overexpressed protein not induce apoptosis confirmed by the absence of cleaved PARP (Figure 57). The fact that CPX treatment modulates the homeostasis of both WT and deficient UROIIIS version proteins equally supports a direct stability effect without apparently and significantly altering other cellular systems, acting as pharmacological chaperone.

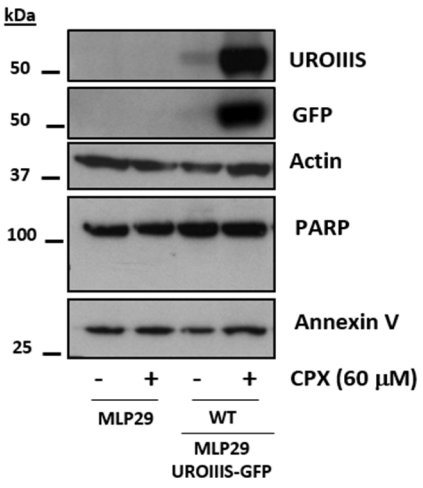

Figure 57. Western blot analysis of the CPX-induced accumulation of UROIIIS-WT-GFP in stably MLP29 mouse cells and non-stably MLP29 cells. The proteins were detected by using UROIIIS and GFP specific antibodies. PARP is involved in the cell viability; cleaved PARP indicates cellular disassembly undergoing apoptosis. Actin and annexin V serve as a protein loading controls

IV.2.2. Analysis of the CPX effect in heme metabolism.

IV.2.2.1. CPX reverts the CEP metabolic phenotype in cellular models.

To gain further insight in the CPX effect on UROIIIS and following the same procedure as in section IV.1.7.1, we tested different concentrations of CPX from 500 µM to 6 µM during 24 hours and monitored the accumulation of porphyrins by measuring the fluorescence in a flow cytometry experiment. Figure 58 shows a drastic decrease in the fluorescence at all concentrations tested and compared to the untreated negative control, reflecting an evident shift of the cellular population towards a cell pool that resemble native HEK cells. At 120 µM of CPX occurs the maximum fluorescence reduction, as detected by cytometry (14,5% vs 98% of untreated control). Yet, an equivalent effect can be observed at lower doses up to 30 µM with a gradual apparent increase of fluorescence.

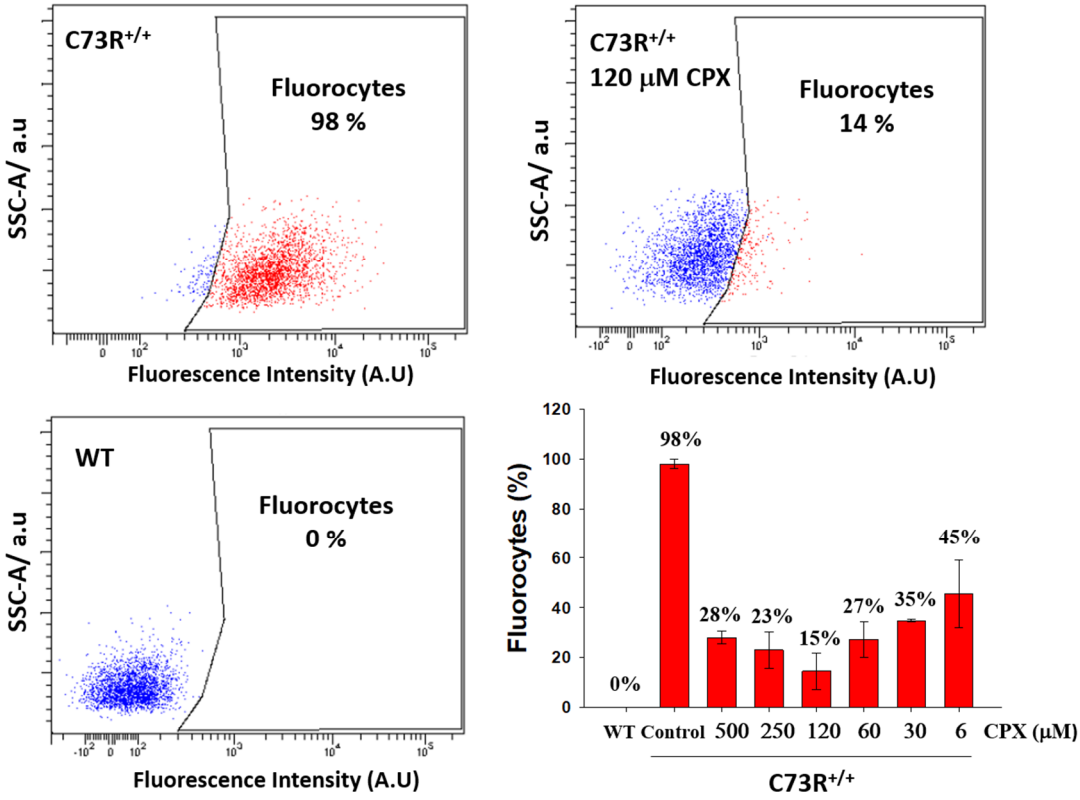

Figure 58. Analysis by flow cytometry of HEK UROIIIS-C73R$^{+/+}$ in the presence of CPX treatments at different concentrations from 500µM to 6 µM for 24 hours. The accumulation of porphyrins generates an intrinsic fluorescent phenotype of the CEP cellular model (fluorocytes). Intracellular porphyrins accumulation (percentage of fluorocytes).

On the other hand, we compared the CPX treatment with the inhibition of the proteasome, proposed in previous studies [105], CPX shows an effect 6-fold greater than MG132 (Figure 59).

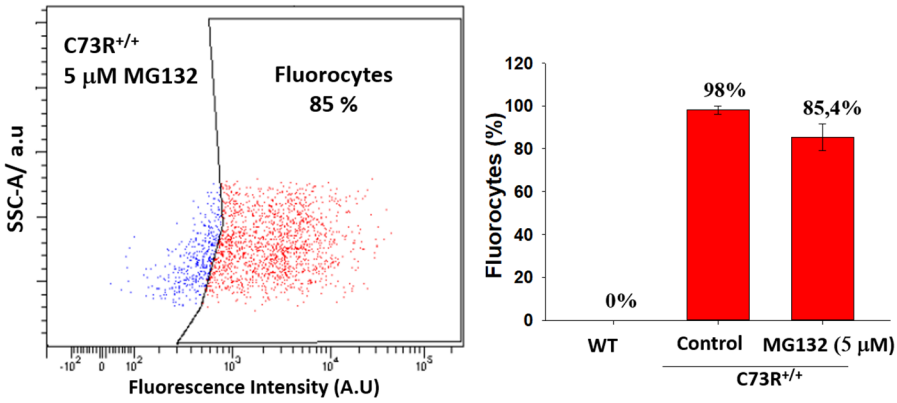

Figure 59. Analysis by flow cytometry of HEK UROIIIS-C73R$^{+/+}$ in the presence of 5 µM of MG132, a proteasomal inhibitor.

Figure 60 shows the analysis by flow cytometry of HEK UROIIIS-P248Q$^{+/+}$ cell line where we observe the shift of the cellular population to a similar WT profile (non-fluorescence cells). Concentrations from 3 to 120 µM of CPX were used to demonstrate that in both cellular models we obtain the same effect on the accumulation of porphyrins and their phenotypes. The maximum effect is also observed between 30 and 120 µM of CPX.

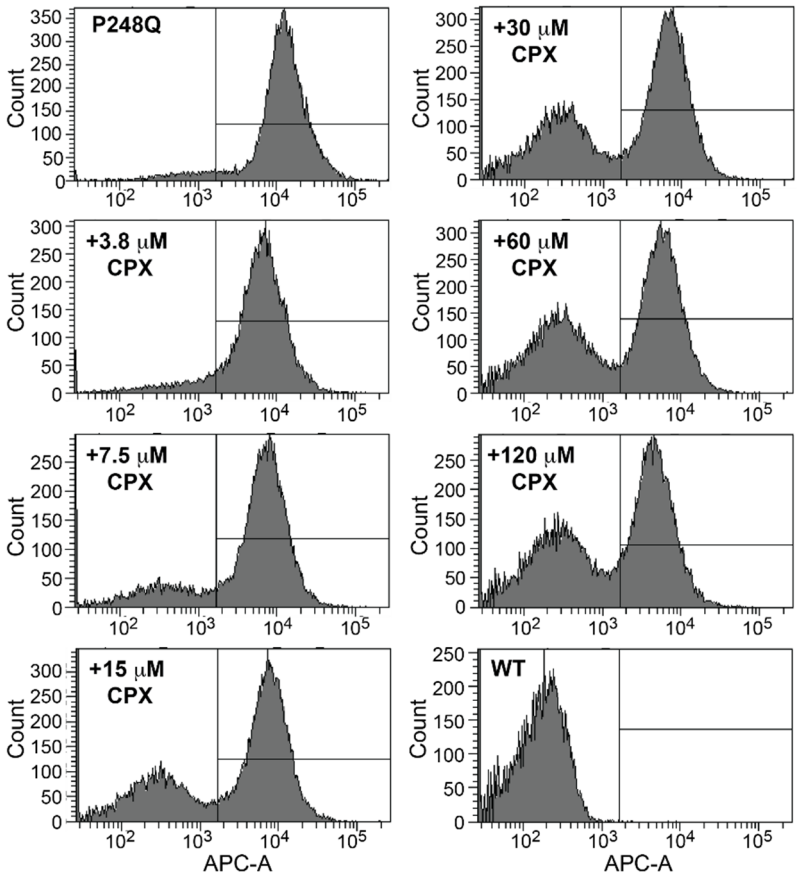

Figure 60. Analysis by flow cytometry of HEK UROIIIS-P248Q$^{+/+}$ in the presence of increasing amounts of CPX, as indicated. The accumulation of porphyrins generates an intrinsic fluorescent phenotype of the CEP cellular model (fluorocytes, right part of the histogram), whilst CPX reverts it towards normal phenotype. Part of the fluorescent phenotype is also due to the heme group production.

We conclude that the observations of the population shift in both lines by flow cytometry are associated with the decrease in fluorescence, which is due to the decrease in the accumulation of porphyrins induced by the CPX effect. The evident change from fluorescence to non-fluorescence cells, showing a similar WT profile, indicates the reversion of CEP phenotype to the WT one, as a result of the potential of CPX as a therapy against CEP.

IV.2.2.2. CPX effect on the decrease of porphyrins accumulation by separation and quantification of porphyrins. Study on cellular models and CEP-patient derived cell lines.

As shown in previous results, we postulate that the effect induced by CPX is associated to the recovery of deficient UROIIIS stability for both mutations (C73R or P248Q). To verify this fact, porphyrins were separated and quantified by HPLC analysis. HPLC is a chromatographic technique that, under high pressure, it enables separation and quantification or organic substances, depending on their retention time. The retention time reflects the partition equilibrium between the mobile phase (buffer) and the stationary phase (the matrix of the column) and reflects the distinctive chemical properties of the analyte. The HPLC characteristic profile of porphyrin analysis of a blood or urine sample of a CEP patient is dominated by the excess of the isomers URO I and COPRO I[64,148]. As shown in Figure 61 and compared to the porphyrin standards (Figure 61A), the CRISPR/Cas9 derived cellular models of CEP (Figure 61C) differ from WT cells (Figure 61B) and match the HPLC profile observed in patient samples, showing a large accumulation of URO I followed by a much smaller (yet very large) accumulation of COPRO I.

As expected, HPLC analysis confirmed that the decrease in fluorescence observed in the flow cytometry experiments is due to a reduction in the porphyrin concentration (Figure 60E, F), which drops up to an 80-90% of the value in absence of CPX. The drug-induced porphyrin reduction is noticeable already at low concentrations (between 1 and 6 μM of CPX) and the effect is maintained up to doses of at least 250 μM (Figure 61H). Remarkably, at the higher doses, URO I reduction is also accompanied by uroporphyrin III (URO III) accumulation (Figure 61G), confirming the effect of CPX on the deficient UROIIIS protein and supporting the idea of acting as a pharmacological chaperone.

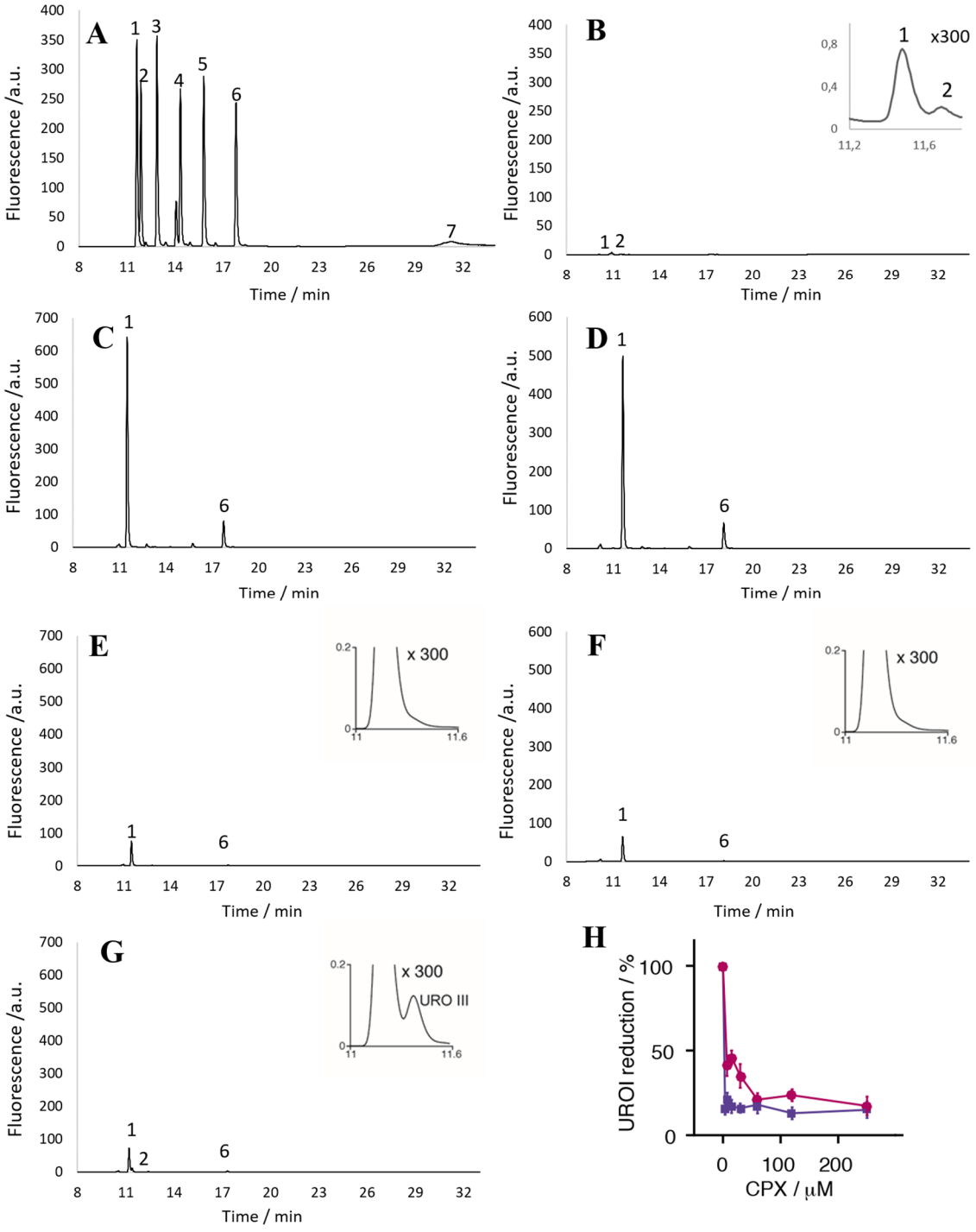

Figure 61. HPLC profile of porphyrins and CPX treatments. Porphyrin standards (A). Porphyrin separation of HEK WT mimic a normal profile (B); HEK UROIIIS-C73R$^{+/+}$ cells (C) or HEK UROIIIS-P248Q $^{+/+}$ cells (D) in absence of CPX; HEK UROIIIS-C73R$^{+/+}$ (E) or P248Q$^{+/+}$ cells (F) in presence of 60 μM CPX and HEK UROIIIS-C73R$^{+/+}$ cells in presence of 250 μM CPX (G). CPX dose dependent URO I reduction for HEK UROIIIS-C73R$^{+/+}$ (purple) and P248Q$^{+/+}$ cells (blue) (H). [1] Uroporphyrin I, [2] Uroporphyrin III (URO III), [3] Heptaporphyrin I, [4] Hexaporphyrin I, [5] Pentaporphyrin I, [6] Coproporphyrin I [7] Meso/Protoporphyrin IX.

The reduction of porphyrin accumulation was further corroborated by the analysis of CEP patient human primary cell line. Lymphocytes from a patient suffering from CEP (4-10% of WT's UROIIIS activity) responded to treatment with 60 and 250 µM CPX (Figure 62) and reduced the abnormal levels of the toxic porphyrin URO I by 2-fold, as compared to the untreated lymphocytes. No significant effect was observed in human lymphocytes from an apparently healthy individual. These preliminary results constitute promising effects as alternative therapy for CEP in humans.

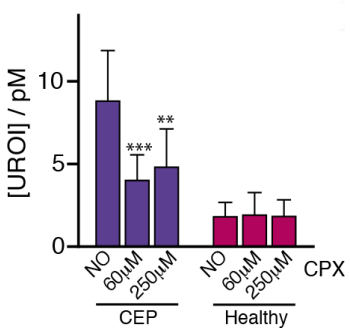

Figure 62. Effect of CPX in human lymphocytes from a 24-years-old CEP patient (blue) and an apparently healthy individual (purple). Treatment for 24 hours. N = 3, * p <0.05.

IV.2.2.3. CPX effect on the genetic regulation of heme biosynthesis pathway. Implications of CPX as a putative iron chelator.

The response induced by CPX on cellular models clearly indicates that improves the intracellular homeostasis of the deficient protein UROIIIS. Yet, one possibility is that the compound is acting at the transcription level so we studied the expression of the heme group pathway genes after treatment. Moreover, CPX has also been reported to be an iron chelator[149] and the heme pathway is intimately coupled to the iron cycle so we also investigated the effect of iron in the CPX-induced UROIIIS intracellular stabilization.

The expression of the eight genes involved in the heme biosynthesis pathway (*ALAS1*, *ALAD*, *HMBS*, *UROS*, *UROD*, *CPOX*, *PPOX* and *FECH*) were studied by RT qPCR in CEP cellular models HEK-C73R$^{+/+}$ and HEK-P248Q$^{+/+}$ with HEK WT cells used as control. The expression of each gene was normalized with the equivalent value in the untreated gene of WT HEK cells. The analysis revealed that there are no significant differences in any gene expression of the pathway after CPX treatment in the cell models and WT (Figure 63), thereby, the effect induced by CPX on the porphyrin levels depletion is not produced by changes in the pathway regulation. According to the literature, the biosynthesis of the heme in non-erythropoietic cells is mainly controlled by ALAS1 whose synthesis is regulated with negative feedback mechanism by a "free" heme group reserve to maintain appropriate intracellular heme level[44]. As expected, Figure 62 shows how the cellular CEP models upregulate the *ALAS* gene as compared to WT cells due to heme-deficiency cause by the unstable UROIIIS enzyme, whilst CPX exerts a negligible effect on the regulation of the pathway.

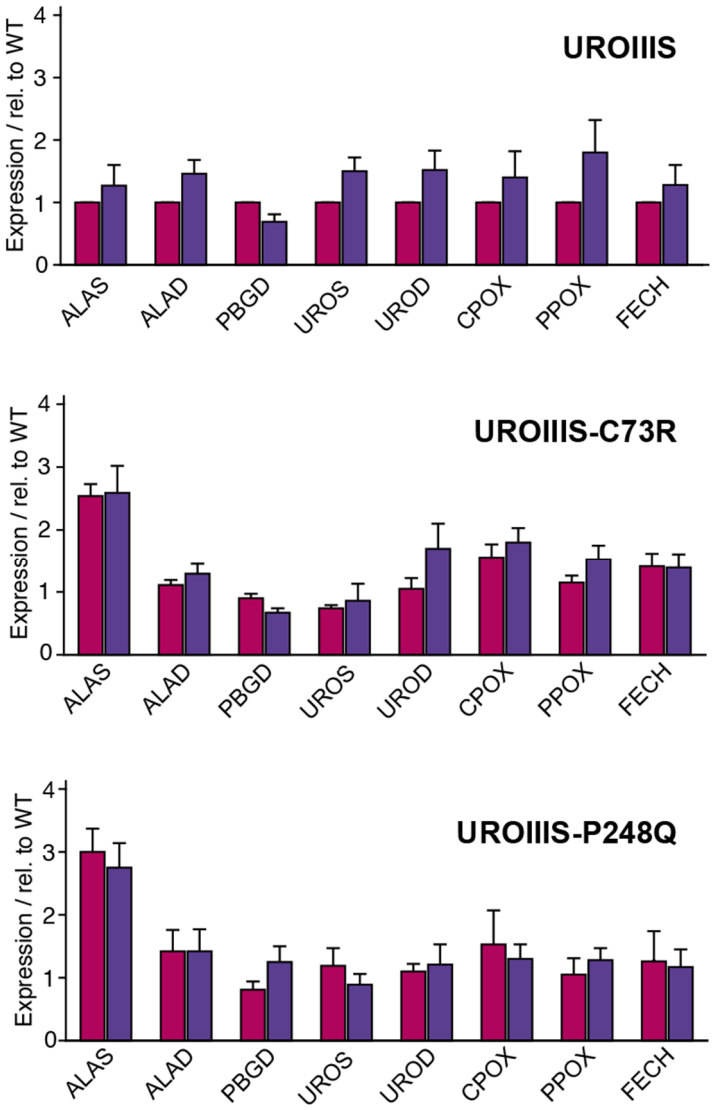

Figure 63. RT qPCR analysis of HEK cells (WT, UROIIIS-C73R$^{+/+}$ and UROIIIS-P248Q$^{+/+}$ as indicated) for the different human genes of the heme biosynthetic pathway in the absence (brown) and in the presence (blue) of 120 μM CPX. The main difference observed is the upregulation of the *ALAS* gene for the cellular models of disease, as previously reported.

Another interesting aspect to study is the consideration of CPX as an iron chelator, this property may constitute an alternative mechanism to modulate the heme group metabolism[150], a pathway tightly regulated by iron. This fact was studied testing two different concentrations of iron chloride (6 and 60 μM) in absence or presence of CPX at 30 or 60 μM incubated for 24 hours in HEK UROIIIS-C73R$^{+/+}$ cells. Under normal condition, the heme biosynthesis is dependent on iron uptake by the cells regulating mainly the expression of FECH, which is an iron-sulfur cluster protein[44]. The results shown that the incorporation of iron increases the amount of URO I in the cellular model due to upregulation of the pathway, however we conclude that CPX capability to reduce URO I levels is independent of iron chloride (Figure 64).

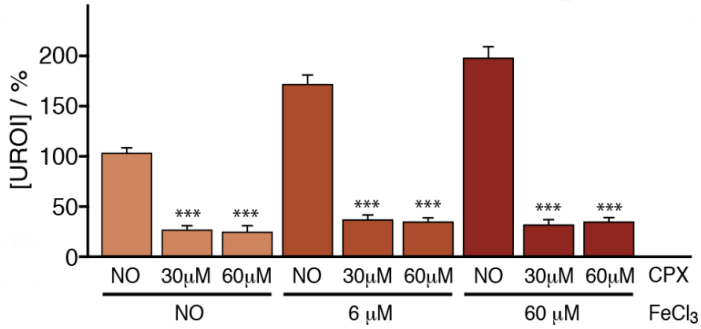

Figure 64. Effect of Iron chloride in the accumulation of URO I by HEK C73R$^{+/+}$ cells and its ulterior reduction induced by CPX. All bars have been normalized to the no iron, no CPX control group (100%). * p <0.05.

On the other hand, to investigate whether the CPX iron chelant properties could ultimately compete with iron of the heme group, we carried out studies about affinity by NMR. Actually, as compared to other drugs that act through the chelation mechanism like deferoxamine[151], we demonstrate that CPX weakly coordinates iron but it is unable to compete for the metal in the heme group nor in any of the main iron-containing prosthetic groups (Figure 65). Thus, as shown in Figure 64, CPX is not able to compete with the iron of heme but it seems to coordinate to it, stabilizing it to ultimately regulate the excess of iron that increases the accumulation of URO I in CEP cells.

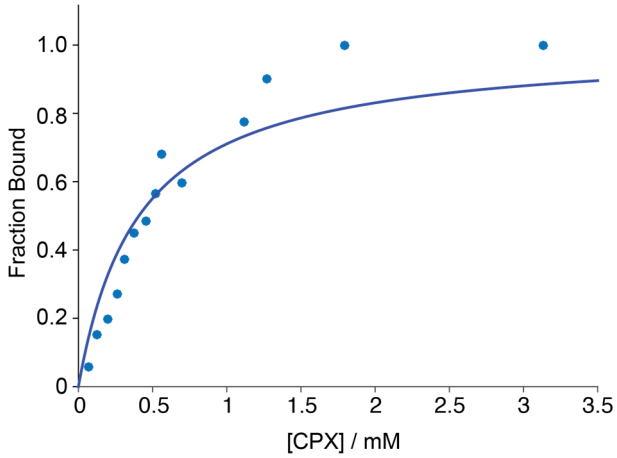

Figure 65. The signal intensity change in the 1D ^{1}H-NMR (6.2 ppm) can be used to determine the affinity constant of the complex. The best fitting to the experimental data provides a value of 380 μM.

IV.2.3. Affinity and cytotoxicity; the common formulation as CPX olamine (CPXol).

Once the beneficial effects of CPX have been characterized and demonstrated, pre-clinical studies in model animal of CEP disease becomes the next step. To ensure safety, a preliminary toxicity study of CPX in different cell lines was performed (Figure 66), concluding that its IC_{50} is around 120 μM for human cells (HuH7 and M1) and 64 μM for mouse cells (MLP29), concentrations that are above the effective optimum values characterized previously.

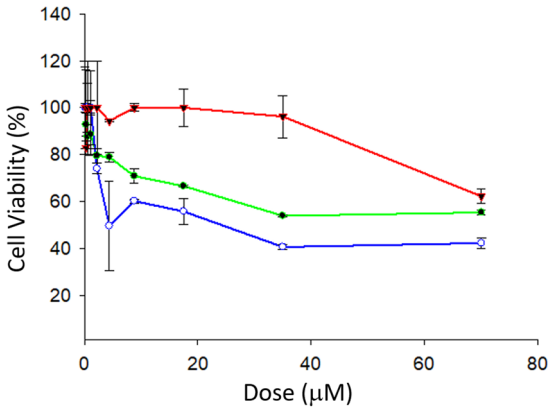

Figure 66. MTT cell viability assay for the approved drug CPX. The IC_{50} has been determined in three different cell lines: MLP29 (blue), M1 (green) and HuH7 (red). Due to the tetrazolium reaction in the mitochondria absorbance at 550nm is measured and is reporter as cell viability (%).

Observations on the HEK WT or UROIIIS-C73R$^{+/+}$ version cell lines by optical microscopy corroborate that there are no obvious serious alterations in the cellular phenotype, therefore not revealing signs of high toxicity (Figure 67). The only observation is the apparent decelerate of cell growth compared to untreated controls, perhaps due to the anti-tumor activity of CPX described by inhibiting the proliferation arrests in G1 phase of the cell cycle in mammalian cells[152] , which may induce the cells to present a larger aspect occupying the free space by the decrease of cellular growth.

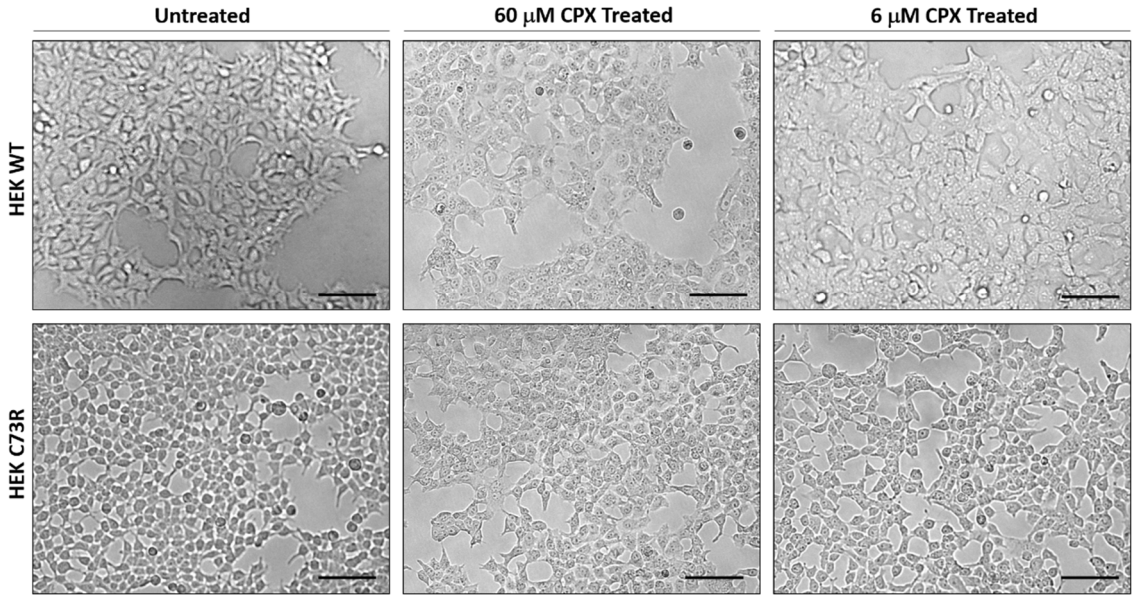

Figure 67. Optical microscopy images. HEK WT or UROIII-C73R$^{+/+}$ cell lines untreated or CPX treated (6 or 60 μM). CPX treatments not show obvious signs of major serious alterations compared to untreated control. *Scale bar*, 50 μm.

Finally, one of the problems commonly found with the compound is the solubility of CPX which may preclude an eventual oral administration of the drug at the desired concentrations. In this context, we also tested the activity for the most common formulation of CPX, CPX olamine (CPXol), which is sufficiently lipophilic with approximately neutral pK_a, being suitable for buccal administration[153]. As we could check in cell studies analyzed by HPLC, CPXol produce identical results in the reduction of toxic metabolites, underlining the fact that the active principle is the CPX entity (Figure 68).

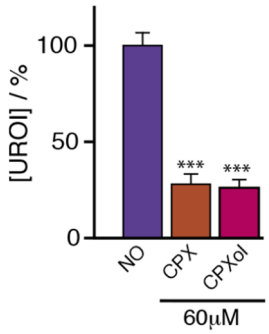

Figure 68. URO I reduction induced by 60 μM CPX (brown), 60 μM ciclopirox olamine (CPXol, purple). All bars have been normalized to the no CPX control group (blue, 100%). * p <0.05.

IV.3. Study of CPX effect in a mouse animal model of CEP disease.

The extensive dataset compiled on the effect of CPX in the heme metabolism, justifies an *in vivo* test of CPX with an animal model of CEP, a significant step forward in the pre-clinical dossier and a prerequisite to perform assays in humans. In this section, we present the results with the murine CEP model, highlighting the effects on pathology and symptomatology as well as the pharmacokinetic properties of the drug.

IV.3.1. Ciclopirox improves the phenotype of a mouse model of CEP.

We evaluated the activity of CPXol in a murine model of CEP (Tg *Uros*$^{P248Q/P248Q}$ knock-in mouse model). The CEP mouse model is a *bona fide* model of human CEP since it shows the metabolic defect, reflected in the isomer I porphyrin accumulation in blood as well as skin lesion defects upon irradiation with UV light[122]. A total of 16 animals (mouse model of CEP) were used to evaluate the effect of CPXol administered in the food pellets; 7 animals were fed with CPXol while 9 animals had food with regular pellets. The isomer I porphyrin levels were monitored in the blood weekly and the porphyrin were obtained by the porphyrin extraction protocol (See Materials & Methods, Section III.16.).

After a basal (pre-treatment) sample (day 0), treatment was started on day 2 and the first post-treatment sample was obtained on day 3, followed by weekly monitoring by HPLC. Isomer I porphyrins URO I (Figure 69A) and COPRO I (Figure 69B) in the blood were significantly reduced in the group treated with CPXol when compared with the control group.

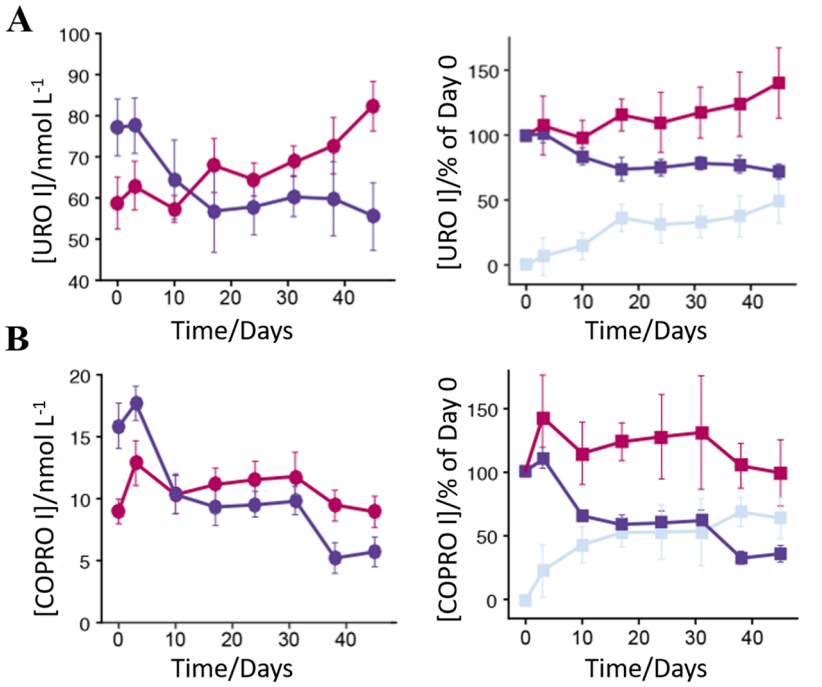

Figure 69. Change in porphyrin levels in red blood cells (RBCs). URO I (A) and COPRO I (B) porphyrin concentration in RBCs as determined by HPLC analysis for the mouse group treated with CPX (N=7, blue) and the control group (N=9, purple). Graphs on the right represent the same porphyrin levels but are compared to their respective values at day 0 for the mice treated with CPX (blue) and the untreated mice (purple). The reduction of porphyrins between the two groups is shown in green (in percentage).

The reduction in porphyrins in RBCs appeared to be greatest in the first 20 days following treatment, after which there was a slow-to-steady reduction until the last evaluation (day 45). Similar results were observed for the hepta-, hexa-, and penta-isomer I porphyrins (Figure 70). Preliminary data suggests that CPXol would continue reducing the porphyrin levels after 45 days (if administration is continued). Upon treatment disruption, the porphyrin levels are slowly restored (Figure 70D).

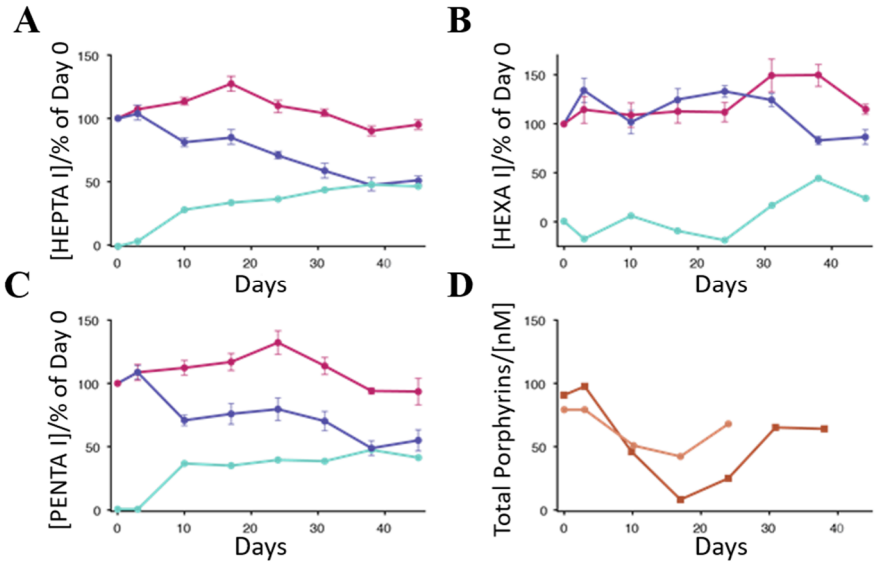

Figure 70. Levels of Hepta (A) Hexa (B) and Penta (C) porphyrin I. D) Increase of porphyrin levels upon interruption of CPX treatment.

Remarkably, CPXol is able to increase the concentration of protoporphyrin IX, an important precursor of the heme group downstream of UROIIIS activity, thus demonstrating the pharmacological chaperone activity in the mouse metabolism (Figure 71).

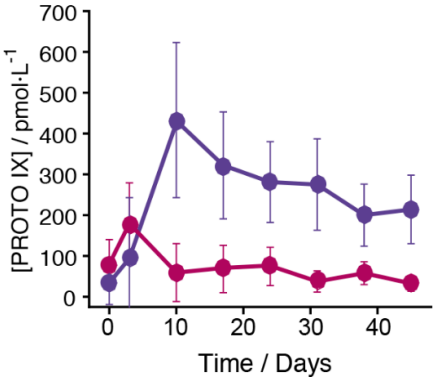

Figure 71. Variation in the protoporphyrin IX concentration over time in the mouse group treated with CPX (blue) and the control group (purple).

Additionally, porphyrins from the liver of the animals were measured after 45 days of treatment. The porphyrin was obtained by the extraction protocol with one modification, homogenizing the tissue previously to the extraction. The results showed that CPXol reduced the porphyrin levels in liver tissue by 40 % (Figure 72A for URO I). On the other hand, splenomegaly is clearly reduced (Figure 72B), a strong evidence of reduced hemolysis and decreased porphyrin deposition. Consistently, there was a significant weight reduction in the spleen in the CPX group (mean 410 ± 86 mg, Figure 72B bottom row) compared to the untreated group (mean 985 ± 204 mg, Figure 72B top row).

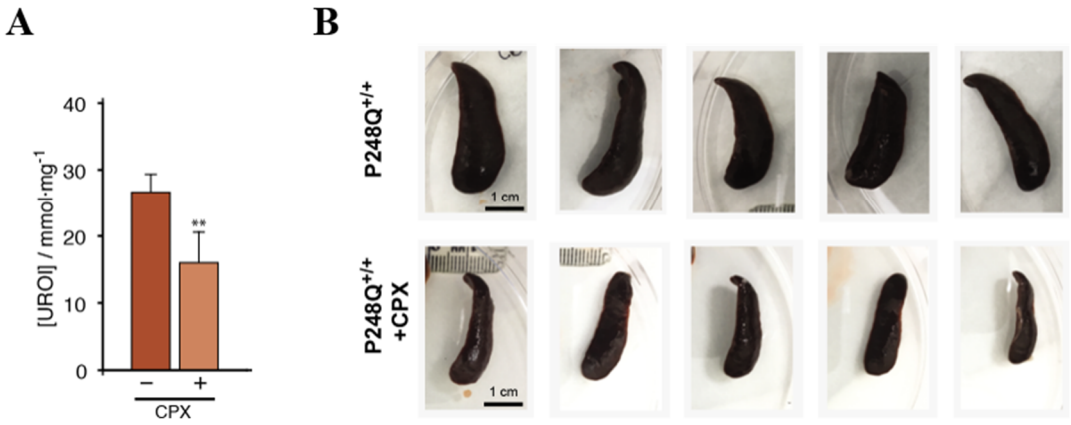

Figure 72. A) Change in URO I levels in the liver at day 45 of treatment (weight normalized). B) CPX reduced splenomegaly after 45 days of treatment since the spleen volume in the untreated mice (top row) was greater than that in the CPX-treated mice (bottom row). *Scale bar* 1 cm.

Liver, spleen and kidney histology was also performed. To that end, the tissues were fixed in parafilm and marked by different stains that allowed the study of iron deposits (Perls staining, PS), porphyrin deposits and steatosis (hematoxylin-eosin staining, HE), inflammation (F4/80 marker) and fibrosis (Sirius red, SR). The results obtained for the liver histology (Figure 73) shows reduced steatosis (white arrowheads in HE staining), a reduction in the cluster of erythroid cells in the sinusoids (circles in HE staining) and a reduction in the porphyrin deposits (pigment accumulation observed as dark spots, black arrow in HE staining). PS staining identified iron deposits (black arrows, blue staining), which become attenuated upon CPXol treatment both in liver and kidney (Figure 73).

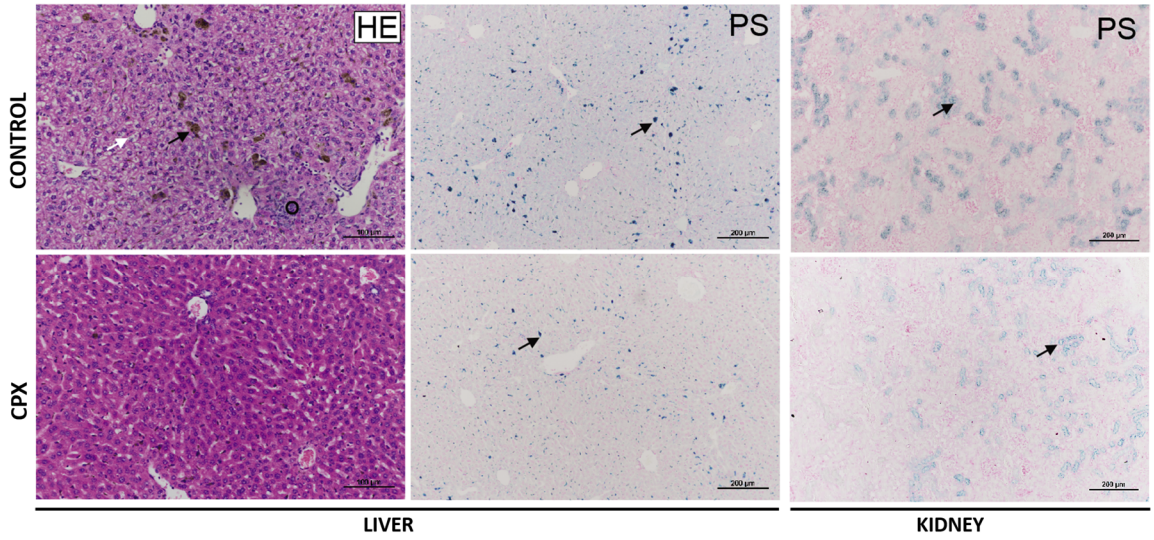

Figure 73. Histology of liver and kidney from mice as indicated. Stains: hematoxylin-eosin (HE) and perls (PS). Liver and kidney HE: steatosis (white arrowheads), clusters of erythroid cells in the sinusoids (dotted circles), pigment accumulation due to porphyrin deposits (black arrowheads). Liver and kidney SP: iron deposits (black arrows, blue staining). *Scale bar*, 100 μm (HE) or 200μm (PS).

We have also analyzed inflammation in spleen and liver tissues by inmunohistochemistry using F4/80 antibody, which recognizes a macrophage-specific glycoprotein in mice connective tissues. The recognition of these macrophages (F4/80, white arrow) allows their visualization as well as their quantification. In both, liver (Figure 74A-B) and spleen (Figure 74A-C) there is a decrease inflammation after CPX treatment, also related to the volume decrease observed previously. Furthermore, quantification of fibrosis by collagen estimation (SR, white arrow) indicates a CPX-driven tendency to reduce fibrosis in the liver after the treatment of the drug (Figure 74B).

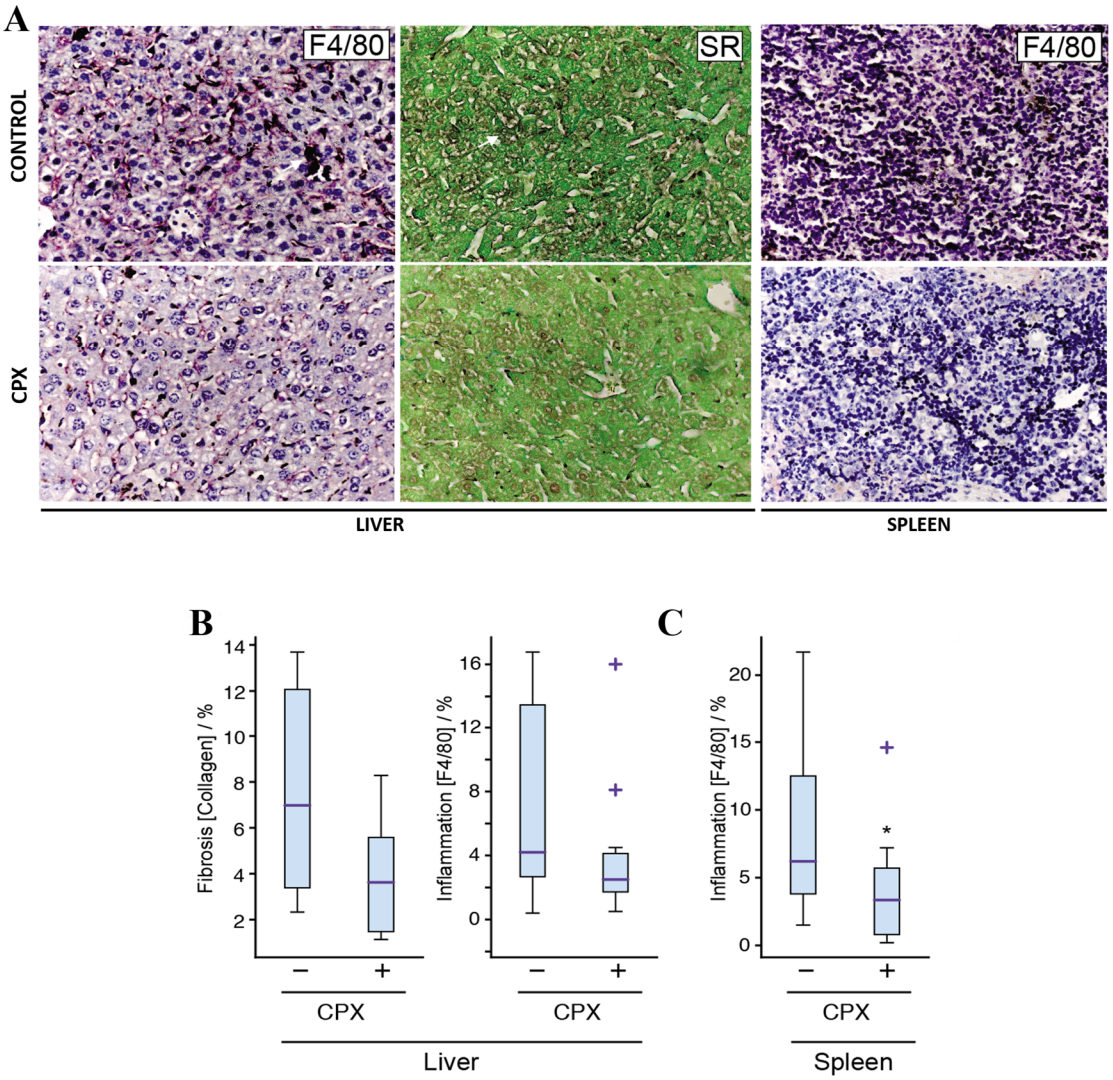

Figure 74. A) Histology of liver from mice as indicated. Stainings: F4/80 inmunohistochemistry (F4/80) and Sirius red (SR). Liver and spleen F4/80 is indicated by a white arrow. Liver SR: collagen fibrils (white arrow). B, C) Quantification of the fibrosis as measured by the collagen content and the inflammation as determined by F4/80 inmunohistochemistry, in the spleen (B) and liver (C) as indicated.

In general, there is a reduction of porphyrin and iron deposits in the tissues, alleviating the fisiopathology of the tissues which should have an effect on the symptomatology, being the histological analysis consistent with the hematological results. All together, these studies are quite determinant and promising for a possible clinic assay in human CEP patients.

IV.3.2. Preliminary pharmacokinetics and dose-response studies.

Once observed the effect of the medicine on the organism, in this section we now investigated how the organism affects the drug, specifically the study of the time course of drug absorption, distribution, metabolism, and excretion (pharmacokinetics). According to the literature, pharmacokinetic experiments showed that CPX's lifetime in the organism is short, with strong affinity for serum albumin and fast catabolism mediated by a glucuronation reaction[154,155].

Glucuronation occurs at the hydroxyl moiety and glucuronated CPX (CPXglu) inactivating it. This reaction inactivates CPX to reduce the porphyrins levels, verified by HPLC on the CEP cellular model HEK UROIIIS-C73R$^{+/+}$, where there is no significant effect with respect to the untreated control (Figure 75).

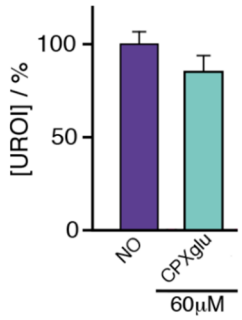

Figure 75. Effect of Glucuronated ciclopirox on URO I levels. No significant reduction induced by 60 μM glucuronated ciclopirox (CPXglu). The bars have been normalized to the no CPX control group (NO, 100%).

In the previous study of the CPX effect in CEP animals, the drug was administered in the food pellets, so its concentration was unknown depending on the intake of each animal. Hence, to quantify the effective concentration of CPX administered within the pellets, we have developed an NMR-based method for the analysis of the active and glucuronated forms of CPX in serum and urine (See Materials and Methods, Section III.17.). The average concentration of active CPX in serum was CPX = 2.79 ± 0.6 μM, CPXglu = 12 ± 1.2 μM, which is equivalent to an intake (gavage) of 100 mg/Kg and on the toxicity limit for the drug[156]. Consistently, a small fraction of the animals showed bowel inflammation, a clinical sign also observed in a clinical trial with humans at equivalent doses.

In a second independent experiment by gavage administration with wild type Tg mice (N = 8), tested CPX doses in the range of 1 to 100 mg/Kg (N = 2 for each dose) and CPXglu was determined by NMR spectroscopy. This species always peaks concentration (C_{max}) at 1h after administration (with C_{max} concentrations ranging between 1 and 15 μM); with a 30 % of remaining substance in serum after 6h of administration ($t_{1/2}$). Glucuronation of the drug increases its solubility, favouring its excretion: a peak of CPXglu in the mM concentration range was observed in urine within the first 24 h after administration. Finally, the ratio CPXglu/CPX was much higher in WT mice (with 94 % of glucuronated species) than in CEP mice (with 84 % of glucuronated species), as determined from serum analysis by NMR spectroscopy.

IV.3.2.1. CPX minimum effective dose (MED) and the maximum tolerated dose (MTD).

To try to determine what dose would be appropriate, we studied the minimum effective dose (MED) and the maximum tolerated dose (MTD) through a third experiment administered CPX to 30 CEP mice using oral administration by gavage during 35 days (control, 1, 5, 10 and 25 mg/Kg, N = 6 per dose). The isomer URO I porphyrin levels were monitored in the blood weekly and the porphyrin were obtained by the porphyrin extraction protocol.

The results are presented in the Figure 76, while 1 mg/Kg showed no effect as compared to the control, the MED is < 5 mg/Kg since, at this dose, a 22 % reduction in the URO I content is observed. A similar effect was observed at the higher dose (25 mg/Kg, 28 % reduction) so it can be concluded that 25 mg/Kg < MTD < 100 mg/Kg. Thus, CPX acts as a pharmacological chaperone in CEP mice in a concentration range below the toxicity limit of the drug.

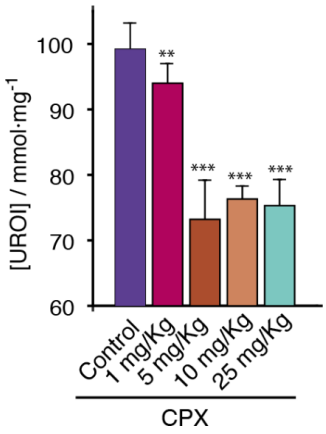

Figure 76. URO I variation in RBCs in mouse after 35 days of treatment of CPX at the indicated doses.

To conclude the results section, we confirm that the search strategy of pharmacological chaperones presented at the beginning, is well planned and has been successfully tested. All the results point in the direction of a promising therapy against the pathology suffered by this devastating disease, being closer to a clinical study in human patients.

CHAPTER V
DISCUSSION

“La ciencia es todo aquello sobre lo cual siempre cabe discusión”

— José Ortega y Gasset

V. DISCUSSION

The use of pharmacological chaperones in misfolding diseases represents, from the pharmaceutical and clinical points of view, a promising therapeutic strategy in terms of cost, efficacy, and patient's compliance to therapy. From the clinical point of view, the use of pharmacological chaperones promises to be a more efficient and safe alternative therapy than other therapies proposed to date. For instance, enzymatic replacement by intravenous application or genetic therapy entail high cost, safety and delivery issues[157,158] or do not adequately address the underlying mechanistic pathogenesis of the disease. Yet, the intrinsic complications of the drug discovery process and the specific features of the protein intracellular homeostasis has precluded its complete and final validation and, to date, no pharmacological chaperones are in the market yet (even though there are several in Phase III stage).

CEP disease is caused by loss-of-function inherited mutations, a feature that could be reverted by the use of chemical entities that stabilize the protein. The landmark of CEP pathophysiology is the abnormal and high toxic levels of porphyrins that accumulate throughout the body and impact in many organs, particularly in the skin. CEP is potentially devastating and can be life-threatening. Currently there are no curative treatments available, with the only management for CEP consisting in visible-light photoprotection. In summary, this severe disease is in high-demand of effective and accessible pharmacological treatments at the curative level. This work is focused on the search and development of pharmacological chaperones for congenital erythropoietic porphyria.

The results obtained in the present work are grounded on a comprehensive strategy of drug screening that integrates computational and structural approaches, said NMR, in combination with functional *in cellula* and *in vivo* experiments. This strategy yielded different hit compounds that can potentially act as pharmacological chaperones, stabilizing the UROIIIS protein upon binding. In this work, we have demonstrated that the repurposing drug ciclopirox acts as an allosteric pharmacological chaperone capable to reduce the levels of porphyrins, improving the homeostasis of UROIIIS as well as the phenotype of a *bona fide* murine CEP model. The versatility of our strategy is already being demonstrated by the adaptation of the platform for other rare missfolding-disease such as type I tyrosinemia, with ongoing research currently carried out in our laboratory to target human fumaryl acetoacetatehydrolase and that it already has provided some promising preliminary results.

Mechanistically, CPX acts as allosteric pharmacological chaperone in CEP. In the development of this thesis the screening platform used for the search of pharmacological chaperones for CEP has been validated. All the compounds have been analyzed in detail employing a wide range of methodologies, which has allowed to categorize compounds according to their thermodynamic properties and to simplify the choice of the lead molecules acting as allosteric pharmacological chaperones. In this context, the data obtained from CPX confirm that the mode of action in relation to CEP is by binding to UROIIIS at the C-allosite location and stabilises its folded conformation, increasing UROIIIS activity, modulating its proteostasis and reducing the subsequent toxic levels of porhyrins.

The *in vivo* studies in this work show how the treatment of CPX improves the clinical manifestations in CEP animals. The analyses show a reduction in the toxic levels of porphyrins in blood, directly related to the impact on the tissues and organs, being especially relevant the improvement in the pathology of liver and spleen, mainly related to the regulation of the heme group. Due to the importance of the spleen as the main blood filter, the clear reduction of splenomegaly strongly supports that, upon treatment, there is a reduction in hemolytic anemia which indicates an improvement in the biosynthetic production of the heme group. In turn, this is endorsed by an increase of the heme precursor PROTO IX in RBCs reinforcing a restoration of homeostasis of the heme pathway. This supports the observed reduction of porphyrin deposits in liver that can explain the reduction of steatosis and fibrosis as well as inflammation. Furthermore, due to the water-solubility properties of the porphyrins accumulated in CEP, the main elimination route is excretion, mainly by urine. Contrary to expectations, there is no greater accumulation of porphyrins in the kidneys in order to their elimination. The decrease of porphyrin deposits in the kidney suggests a relief in the production of porphyrins in the body supported by the previous results in liver and spleen. On the other hand, the data provided from the treatment of CPX in a lymphocyte hematopoietic cell line from a patient with CEP indicates that CPX would be able to act on the main heme producer of the body, the bone marrow. Thus, all the results obtained point that there is an improvement of the homeostasis of heme synthesis pathway *in vivo* that improves the erythropoiesis in both bone marrow and liver, so the treatment would cover 100 % of the body's heme production cells, which suggests reduction of hemolysis and ultimately the regulation of homeostasis of the heme group in the body, which translates into a significant therapeutic effect on the damaged tissues.

It is also expected that CPX may act positively on the skin lessions produced by CEP. Even though we do not have sufficient data of an improvement in photosensitivity, the data provided by *in vivo* experiments with Bortezomid have remitted skin problems[105]. Bortezomid acts as an indirect unspecific chemical modulator for UROIIIS by inhibiting its main degradation pathway, whereas CPX is a specific modulator, in comparison it is expected that there will be a remission of photosensitivity upon CPX treatment in CEP.

CPX is effective in two different mutations C73R or P248Q with practically identical results so it is expected that CPX may be applicable to the majority of pathogenic missense mutations causing CEP. On the other hand, an allosteric modulation is highly advantageous since it does not affect the catalytic site, minimizing its effect on the enzymatic activity. This is in contrast to the more canonical strategies to discover pharmacological chaperones which are directed against to the active site or at a given mutation site, often facilitated by focus on molecules with structural similarity to the substrate in the transition state of the complex with the enzyme, as it has been proven successful in Fabry, Tay-Sachs or Gaucher diseases[159] but at the expense of conflicting with the intrinsic catalytic activity. This differential impact of the search of allosteric pharmacological chaperones on misfolding diseases is also supported by recent studies following a similar screening strategy in which a molecule has been identified to regulate and stabilize lysosomal alpha-galactosidase *in vitro* in Fabry disease by allosteric binding[160]. Thus, the recognition of the potential of allosteric pharmacological chaperones open novel perspectives in the screening approaches and therapy of misfolding diseases.

CPX in the context of other treatments. Our results contrast with another therapeutic intervention based on bone marrow transplantation, although this therapy tries to solve the underlying mechanistic cause of CEP, it is used for the most severe cases and is rarely justifiable due its high safe risk[35]. On the other side, theoretically, the bone marrow transplant would only solve part of the problem, the accumulation of porphyrins in the liver would remain unresolved, which lead to a mosaicism of CEP. Our proposed therapeutic alternative through CPX would not generate this type of mosaicism since it may act in all the cells of the body as mentioned above, besides it does not entail security risks nor does require operations and has already passed safe administration tests. Together, all these data strongly support a further clinical trial of this drug in CEP patients.

Afamelanotide, an α-melanocyte stimulating hormone (α-MSH) analogue[161] is an approved treatment for EPP in Europe based on a drug with phototherapeutic properties and it could potentially be used on CEP patients. Yet, in contrast to CPX, afamelanotide just acts on melanocytes causing tanning skin, moreover its very long-term safety is not yet known, the studies of its benefits are diffuse and the most importantly, does not address the underlying cause of the disease. Actually, the possible use of afamelanotide on other cutaneous porphyrias is quite doubtful and debatable, whereas CPX in principle, as we have discussed above, could be an alternative therapy with good prognosis from the biochemical, pharmaceutical and clinical point of view.

Alternative therapeutic molecular mechanisms of CPX. CPX and often in the form of its olamine salt, is a repurposing drug off-patent fungicide with already proven efficiency for the treatment of cutaneous fungal infections, vaginal candidiasis, seborrheic dermatitis and onychomycosis[162]. Several studies have demonstrated that CPX also possesses anti-proliferative activity in tumor cells[152,163–166]. This anticancer activity of CPX has been attributed to intracellular iron chelation which, in turn, disrupts iron-dependent pathways and inhibit of iron-containing enzymes, such as ribonucleotide reductase and ultimately suppresses expression of the antiapoptotic gene surviving to induce cell death[163]. Iron also regulates the heme pathway and strong iron chelators like deferoxamine have been investigated for their potential use as drugs against porphyrias[150]. Yet, our experimental evidence suggests that CPX does not affect the regulation of the heme group: the mRNA levels of the pathway remain unaltered in the presence of CPX and most importantly, the CPX-induced URO I reduction observed in cellular experiments remains unaltered in the presence of a large excess of iron III chloride. This is likely the case because CPX is only a weak binder of iron and it does stabilize the heme group instead of competing with it for the metal chelation.

Interestingly, there are several studies that support an anti-inflammatory effect of CPX. Small clinical studies demonstrated that a 1 % ciclopirox cream suppresses the erythema response following UV irradiation in healthy volunteers and improves the inflammation associated with infective disorders, mainly caused by the release of ROS[167,168]. Indeed, using electron paramagnetic resonance, it has been demonstrated that CPX has a potent capacity to directly scavenge hydroxyl radicals[169]. This is supported by studies in mouse inflammatory cells[170] as well as antidiabetic studies where has been observed that CPX reduced the levels of ROS during culture high glucose[171]. In this sense, the release of ROS

in CEP is closely related to the accumulation of porphyrins, since toxic levels of porphyrins are likely determinants of ROS generation. The data provided demonstrate that the restored UROIIIS homeostasis by CPX-induction decrease dramatically the toxic levels of porphyrins which suggest that the production of ROS will also be reduced. This is supported by the significant reduction of the inflammation in the liver and the spleen observed in our *in vivo* experiments. Yet, the evidences on the anti-inflammatory effect of CPX could suggest that CPX act in synergy by scavenging of ROS and as a pharmacological chaperone of UROIIIS strengthened the therapeutic effect in CEP.

CPX ADME, pharmacokinetics and pharmacodynamics. The dosage at which the drug is administered could also be a potential obstacle; ciclopirox needs to preserve a good efficacy and show some activity at low concentration without compromise the safety of the patient. In this respect, several studies have addressed the potential toxicology of CPX at the regulatory level. For instance, three-month repeat-dose toxicity studies have been performed in rat and dog with the no-observed adverse effect level being determined at 10 mg/kg/day in both species, demonstrating no toxic effects or changes in electrocardiography[154]. Furthermore, numerous assays in animals have been performed to determine the carcinogenic, mutagenic and dysmorphogenic effects of topical, oral and subcutaneous administration of CPX. In all studies, there was no potential in drug-related for any of the above effects and no teratogenicity and embryotoxicity effect was also reported[172–174]. Additionally, a Phase I study used CPX administered orally in patients with advanced hematological malignancies. The data presented showed that the oral dosing of 40 mg/m^2 was well tolerated in patients with no dose-limiting toxicities, and it exhibited a sustained pharmacodynamic effect (on levels of survivin mRNA) and resulted in hematological improvement and/or disease stabilisation in 2 out of 3 patients[156]. In this context, we have demonstrated that CPX is active against CEP at sub-toxic concentrations.

From the pharmacokinetic point of view, CPX has a short lifetime in the organism, highly affected by circulating serum albumin and with an efficient and simple catabolic pathway constituted by a glucuronation reaction followed by urine excretion[156]. The glucuronation reaction occurs in the liver and it is more efficient in WT than in CEP mice, probably due to liver ill-functioning in porphyria patients. Such catabolic dependence on the liver sets a frame for the exploration of alternative pharmacological formulations to defer the glucuronation reaction, optimizing the effect of the active compound.

Potential use of CPX in other porphyrias. Presently, none of the therapeutic approaches for other porphyrias have proven suitable or totally safe. In this work, we have demonstrated how CPX has efficacy and safety in the experiments *in vitro* as well as *in vivo* for CEP. Yet, the mechanistic rationale of the therapeutic intervention suggests that CPX could extend its therapeutic value to be used in other porphyrias. The accumulation of by-products heme precursors is not exclusive of CEP, inherited or acquired defects in other enzymes in the porphyrin-heme biosynthetic pathway also produce toxic accumulation of porphyrins, even though the accumulated porphyrins are not the same or in the same proportions as in CEP (Figure 77). For instance, all the porphyrias except acute intermittent porphyria and the exceptionally rare aminolevulinic acid dehydratase deficiency porphyria (Doss porphyria) will affect the skin, classified as cutaneous porphyrias. Porphyrias with dermatologic implications include (Table 15): porphyria cutanea tarda (PCT),

hepatoerythropoietic porphyria (HEP), erythropoietic protoporphyria (EPP), hereditary coproporphyria (HCP), Harderoporphyria and variegate porphyria (VP). For all these cutaneous porphyrias the management mainly consists of visible-light photoprotection and as occurs in case of CEP, a treatment that reduces porphyrin levels would be therapeutically beneficial.

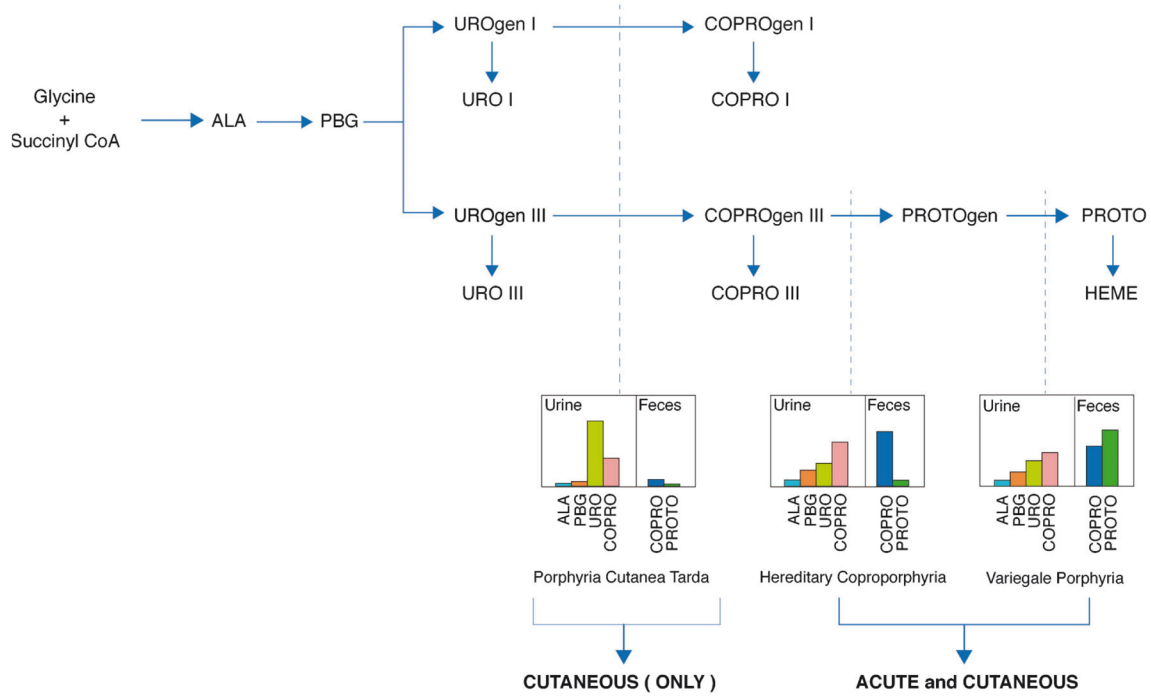

Figure 77. Profile of heme precursor excretion for different types of porphyria expected to extend the therapeutic value of CPX. The pathway of heme synthesis is represented by arrows. Profile of heme precursors in urine and/or stool (vertical dashed lines) is characteristic of the specific type of porphyria. The vertical bars depict the relative change in each metabolite, not the absolute amount. Adapted from[175] .

The heme group biosynthetic pathway is upregulated by ALA and iron and feedback downregulated by heme. Since all the porphyrias are characterized by hemolitic anemia, a common feature is the overstimulation of the biochemical pathway (erythropoiesis) due to the lack of heme. Erythropoiesis is responsible for most associated symptoms and is the central landmark in an attack of an acute porphyria. In this context, we hypothesize that an increase in the heme production may ultimately increase the heme production (by action-mass law), ultimately resulting beneficial to restore the normal metabolite homeostasis. Specifically, UROIIIS is located in the Y-junction of the metabolic pathway and an overexpression of the enzyme may avoid the accumulation of the type I isomers, thus optimizing the chemical efficiency of the pathway. In this context, our results show that CPX also is able to improve the homeostasis on WT version of human UROIIIS protein (See Figure 57 in Results, Section IV.2.1.), reinforcing the idea that CPX could act ultimately as a modulator of the heme pathway for other porphyrias. This approach may be particularly suitable in PCT, produced by a reduction in the activity of UROD, which is the next enzyme to UROIIIS in the heme pathway resulting in an accumulation of URO I and COPRO I (as well as URO III and COPRO III) and representing the closest metabolic scenario to CEP.

Porphyria Type	Putative Symptoms covered	Prevalence
Congenital erythropoietic porphyria	Severe photosensitivity, blistering. Hemolytic anemia, splenomegaly	< 1 in 1.000.000
Porphyria cutanea tarda	Photosensitivity, vesicles and bullae	1 in 10.000
Hepatoerythropoietic porphyria (HEP)	Photosensitivity, blistering,scarring and hemolytic anemia	Approximately 40 cases reported
Hereditary coproporphyria	Photosensitivity,	1 in 500.000
Harderoporphyria	Late photosensitivity	< 10 cases reported
Variegate porphyria	Photosensitivity	1 in 75.000 -100.000 but 1 in 300 in South Africa.

Table 15. Cutaneous porphyrias and potential symptoms that CPX may address.

The porphyrias HCP as well as its variant Harderoporphyria and VP could also be beneficiaries of the effect of the CPX, although the affected enzymes are further away from UROIIIS in the heme pathway. It is expected for CPX to benefit such phenotypes through homeostasis regulation of the heme pathway, ultimately producing a partial decrease in porphyrins (or a favourable redistribution of their composition). Therefore, it is also expected that the modulation effect of CPX on heme explained above will be able to remit the phototoxicity in the mentioned cutaneous porphyrias. This is unlikely the case for EPP, where the accumulation of the precursor PROTO IX is due to reduced ferrochelatase activity. In there, the effect of CPX could not regulate the homeostasis of the route by production of heme and the reabsorption of the metabolites could increase PROTO IX, being counterproductive. Furthermore, in the case of other non-cutaneous porphyrias such as AIP the toxic accumulated metabolites are porphyrin precursors (ALA and PBG) and not porphyrins so no beneficial effect of CPX is expected.

In summary, ciclopirox is a broad-spectrum antifungal agent that also exhibits anti-inflammatory activity. We have shown that this synthetic drug is able to stabilize UROIIIS by binding the enzyme in an allosteric site, constituting a novel class of pharmacological chaperone. Our results clearly demonstrate that the drug is able to improve the pathogenic phenotype of a *bona fide* mouse model of the disease at sub-toxic concentrations, establishing a novel therapeutic intervention line against congenital erythropoietic porphyria, applicable to the majority of pathogenic missense mutations causing CEP. Its preclinical efficacy coupled with its prior safety and toxicity record support a further clinical trial of this drug in CEP patients. Finally, future research will be directed toward to the application of CPX to treat in principle, the skin photosensitivity in other cutaneous porphyrias.

CONCLUSIONES/
CONCLUDING REMARKS

“The most incomprehensible thing about the world
is that it is at all comprehensible.”

— Albert Einstein

CONCLUSIONES

- Hemos establecido un **sistema de trabajo de válido** mediante la creación de una **plataforma de detección de chaperonas farmacológicas** para la porfiria eritropoyética congénita, aplicable a otras enfermedades relacionadas con el mal plegamiento proteico, tales como la tirosinemia tipo 1.

- El fármaco repositorio ciclopirox ha sido identificado como una chaperona farmacológica alostérica activa frente a CEP. Demostramos que el **tratamiento con ciclopirox** a diferentes dosis **puede modular la homeostasis** tanto de la proteína **UROIIIS** WT como las versiones deficientes C73R o P248Q sin que aparentemente se vean afectados otros sistemas celulares. El tratamiento podría ser aplicable a la mayoría de las mutaciones nonsense que causan CEP. Además, nuestros resultados apoyan que el ciclopirox es capaz de **mejorar el fenotipo patogénico *in vivo*** en un modelo murino de CEP a concentraciones sub-tóxicas.

- Todos los resultados obtenidos apoyan firmemente un **estudio clínico** de ciclopirox en pacientes con CEP.

- Valor terapéutico de **ciclopirox en otras porfirias cutáneas**. La regulación de la homeostasis del hemo por inducción de CPX sobre la homeostasis de la proteína UROIIIS WT, podría tener un efecto terapéutico sobre la acumulación de porfirinas en otras porfirias cutáneas reflejado en la mejora de la fotosensibilidad.

- **Nuestros resultados indican que las chaperonas farmacológicas se pueden utilizar de manera efectiva como una novedosa línea de intervención terapéutica contra enfermedades raras, cuando éstas derivan del mal plegamiento de proteínas.**

CONCLUDING REMARKS

- We have established a **valid working system; screening platform** to seek for pharmacological chaperones for Congenital Erythropoietic Porphyria, also applicable to other diseases produced by misfolding mutations, such as type I tyrosinemia.

- The drug repurposing ciclopirox has been identified as an allosteric pharmacological chaperone, active against CEP. We demonstrate that the **treatment with ciclopirox** at given concentrations **can modulate the homeostasis** of WT and deficient version C73R or P248Q of **UROIIIS** without apparently and significantly altering other cellular systems. Such treatment may be applicable to the majority of pathogenic missense mutations causing CEP. Our results support that ciclopirox is able to **improve the pathogenic phenotype *in vivo*** mouse model of the CEP at sub-toxic concentrations.

- All the data strongly support a further **clinical trial** of ciclopirox in CEP patients.

- Therapeutic value of **ciclopirox in other cutaneous porphyrias**. The regulation of heme homeostasis by induction of CPX on the homeostasis of the UROIIIS WT protein could have a therapeutic effect on the accumulation of porphyrins in other cutaneous porphyrias reflected in the improvement of photosensitivity.

- **Our results indicate that pharmacological chaperones can be effectively used as a novel therapeutic intervention line against rare diseases, when derived from protein misfolding.**

“The very essence of instinct is that
it's followed independently of reason”

— Charles Darwin

PUBLICATIONS

Jean-Marc Blouin, Ganeko Bernardo, Emma Sasso, Julie Esteve, Cécile Ged, Magalie Lalanne, Arantza Sanz-Parra, Pedro Urquiza, Hubert de Verneuil, Oscar Millet and Emmanuel Richard. **Missense UROS mutations causing congenital erythropoietic porphyria reduce UROS homeostasis that can be rescued by proteasome inhibition.** Hum. Mol. Genet. 26, 1565–1576 (2017).

Pedro Urquiza, Ana Laín, Arantza Sanz-Parra, Jorge Moreno, Ganeko Bernardo-Seisdedos, Pierre Dubus, Esperanza González, Virginia Gutiérrez-de-Juan, Sandra García, Hasier Eraña, Itxaso San Juan, Iratxe Macías, Fredj Ben Bdira,Paula Pluta, Gabriel Ortega, Julen Oyarzábal, Rosario González-Muñiz, Juan Rodríguez-Cuesta, Juan Anguita, Emilio Díez, Jean-Marc Blouin, Hubert de Verneuil, José M Mato, Emmanuel Richard, Juan M. Falcón-Pérez, Joaquín Castilla and Oscar Millet. **Repurposing ciclopirox as a pharmacological chaperone for the treatment of congenital erythropoietic porphyria**. *In progress.*

PATENTS

2018

INTERNATIONAL APPLICATION No: PCT/EP2018/060847
INVENTORS: MILLET AGUILAR-GALINDO Oscar, FALCON PÉREZ Juan Manuel, CASTILLA CASTRILLÓN Joaquín, SANZ PARRA Arantza, LAIN TORRE Ana, URQUIZA ORTIZ Pedro David, SAN JUAN QUINTANA Itxaso, BERNARDO-SEISDEDOS Ganeko.
TITLE: USE OF CICLOPIROX AS MODULATOR OF HEME GROUP BIOSYNTHESIS AND IN THE TREATMENT OF PORPHYRIA AND OTHER DISEASES
PRIORITY DATE: 10-05-2018
APLICANT: Centro de Investigación Cooperativa en Biociencias – CIC bioGUNE.

2016

EUROPEAN PATENT APPLICATION: EP 3 315 129 A1
APPLICATION No: 16382493.1-1466
INVENTORS: MILLET AGUILAR-GALINDO Oscar, SANZ PARRA Arantza, LAIN TORRE Ana, URQUIZA ORTIZ Pedro David, FALCON PÉREZ Juan Manuel.
TITLE: USE OF CICLOPIROX FOR THE TREATMENT OF CONGENITAL ERYTHROPOIETIC PORPHYRIA
PRIORITY DATE: 28-10-2016
APLICANT: Centro de Investigación Cooperativa en Biociencias – CIC bioGUNE.

ORPHAN MEDICAL PRODUCT

2018

Confirmation and approval by the European Commission of Ciclopirox as an Orphan Medicinal Product for the treatment of Congenital Erythropoietic Porphyria.

EU OPRHAN DESIGNATION NUMBER: EU/3/17/1960

ACTIVE INGREDIENT: CICLOPIROX

INDICATION: TREATMENT OF CONGENITAL ERYTHROPOIETIC PORPHYRIA

DATE OF DECISION: 17-01-2018

SPONSOR: Atlas Molecular Pharma S.L. Parque Tecnológico de Bizkaia, Building 800, 48160, Derio, Spain.

Can be found more information of this current orphan drug designation on European Medicines Agency's (EMA) website (http://www.ema.europa.eu/ema/), on the medicine's rare disease designations page.

ORPHAN DRUG DESIGNATION BY U.S. FOOD & DRUG ADMINISTRATION

2018

Confirmation and approval by the U.S. Food & Drug Administration of Ciclopirox as an Orphan-Drug for treatment of Congenital Erythropoietic Porphyria.

DESIGNATION REQUEST: # DRU-2018-6297

GENERIC NAME: CICLOPIROX

DATE DESIGNATED: 17/04/2018

ORPHAN DESIGNATION: TREATMENT OF CONGENITAL ERYTHROPOIETIC PORPHYRIA

ORPHAN DESIGNATION STATUS: DESIGNATED

SPONSOR: Atlas Molecular Pharma S.L. Parque Tecnológico de Bizkaia, Building 800, 48160, Derio, Spain.

Can be found more information of this current orphan drug designation by FDA on FDA U.S. Food and Drug Administration website (https://www.fda.gov/), on the Designating an Orphan Product: Drugs and Biological Products Databases page.

BIBLIOGRAPHY

1. Battersby, A. R. Tetrapyrroles: the pigments of life. *Nat. Prod. Rep.* **17,** 507–526 (2000).
2. Layer, G., Reichelt, J., Jahn, D. & Heinz, D. W. Structure and function of enzymes in heme biosynthesis. *Protein Sci. Publ. Protein Soc.* **19,** 1137–1161 (2010).
3. Puy, H., Gouya, L. & Deybach, J.-C. Porphyrias. *The Lancet* **375,** 924–937 (2010).
4. Gasson, T. & Klein, K. Porphyria: Pathophysiology, diagnosis, and treatment. *Nurse Pract.* **40,** 1–6 (2015).
5. Schultz, J. H. (Thesis) Inaugural dissertation, Griefswald. (1874).
6. Baumstark, F. *Physiologie* **9,** 568–584 (1874).
7. Hoppe-Seyler, F. *Med Chem Untersuchungen* **4,** 924–937 (1871).
8. Gunther, H. *Dtsch Arch Klin Med* **105,** 89–146 (1912).
9. Gunther, H. *Ergeb Allg. Pathol Pathol. Anat* **20,** 608–764 (1922).
10. Garrod, A. E. Inborn Errors of Metabolism. in 136–163 (Oxford University Press: London, 1923).
11. Madan, P. *et al.* Hans Gunther and his disease. *Photodermatol. Photoimmunol. Photomed.* **23,** 261–263 (2007).
12. Goldberg, A. *Clin Dermatol* 189–193 (1998).
13. Schmid, R., Schwartz, S. & Sundberg, R. D. *Blood* **10,** 416–428 (1955).
14. Di Pierro, E., Brancaleoni, V. & Granata, F. Advances in understanding the pathogenesis of congenital erythropoietic porphyria. *Br. J. Haematol.* **173,** 365–379 (2016).
15. Desnick, R. J. & Astrin, K. H. Congenital erythropoietic porphyria: advances in pathogenesis and treatment. *Br. J. Haematol.* **117,** 779–795 (2002).
16. Fortian, A. *et al.* Structural, thermodynamic, and mechanistical studies in uroporphyrinogen III synthase: molecular basis of congenital erythropoietic porphyria. *Adv. Protein Chem. Struct. Biol.* **83,** 43–74 (2011).
17. de Verneuil, H., Ged, C. & Moreau--Gaudry, F. in *The Porphyrin Handbook* (eds. Kadish, K. M, Smith, K. M. & Guilard, R.) 43–65 (Elsevier Science: San Diego, 2003).
18. Warner, C. A., Yoo, H. W., Roberts, A. G. & Desnick, R. J. Congenital erythropoietic porphyria: identification and expression of exonic mutations in the uroporphyrinogen III synthase gene. *J. Clin. Invest.* **89,** 693–700 (1992).
19. Fontanellas, A. *et al.* A systematic analysis of the mutations of the uroporphyrinogen III synthase gene in congenital erythropoietic porphyria. *Eur. J. Hum. Genet. EJHG* **4,** 274–282 (1996).
20. Desnick, R. J., Glass, I. A., Xu, W., Solis, C. & Astrin, K. H. Molecular genetics of congenital erythropoietic porphyria. *Semin. Liver Dis.* **18,** 77–84 (1998).
21. To-Figueras, J., Millet, O. & Herrero, C. Congenital Erythropoietic Porphyria. in *Handbook of Porphyrin Science (Volume 29)* **Volume 29,** 151–217 (World Scientific Publishing Company, 2012).
22. Griffiths, C., Barker, J., Bleiker, T., Chalmers, R. & Creamer, D. *Rook's Textbook of Dermatology*. (John Wiley & Sons, 2016).
23. Millot, S. *et al.* Hemolytic anemia repressed hepcidin level without hepatocyte iron overload: lesson from Günther disease model. *Haematologica* **102,** 260–270 (2017).
24. Sassa, S. Hematologic aspects of the porphyrias. *Int. J. Hematol.* **71,** 1–17 (2000).

25. Freesemann, A. G., Gross, U., Bensidhoum, M., de Verneuil, H. & Doss, M. O. Immunological, enzymatic and biochemical studies of uroporphyrinogen III-synthase deficiency in 20 patients with congenital erythropoietic porphyria. *Eur. J. Biochem.* **257,** 149–153 (1998).

26. Fritsch, C., Bolsen, K., Ruzicka, T. & Goerz, G. Congenital erythropoietic porphyria. *J. Am. Acad. Dermatol.* **36,** 594–610 (1997).

27. Wolff, K. *et al.* Fitzpatrick's Dermatology in General Medicine, 8th Edition. (2011).

28. Orkin, S. H. *et al. Nathan and Oski's Hematology of Infancy and Childhood E-Book*. (Elsevier Health Sciences, 2008).

29. Varadi, S. *Br J Haematol* **4,** 270–280

30. Pollack, S. S. & Rosenthal, M. S. Images in clinical medicine. Diaper diagnosis of porphyria. *N. Engl. J. Med.* **330,** 114 (1994).

31. Lim, C. K, Rideout, J. M. & Wright, D. J. *J Chromatogr* **282,** 629–641 (1983).

32. Tsai, S. F., Bishop, D. F. & Desnick, R. J. *J Biol Chem* **262,** 1268–1273 (1987).

33. Kaye, E. T., Levin, J. A., Blank, I. H., Arndt, K. A. & Anderson, R. R. Efficiency of opaque photoprotective agents in the visible light range. *Arch. Dermatol.* **127,** 351–355 (1991).

34. Seip, M., Thune, P. O. & Eriksen, L. *Acta Derm Venereol* **54,** 239–240 (1974).

35. Katugampola, R. P. *et al.* A management algorithm for congenital erythropoietic porphyria derived from a study of 29 cases. *Br. J. Dermatol.* **167,** 888–900 (2012).

36. Kauffman, L., Evans, D. I., Stevens, R. F. & Weinkove, C. Bone-marrow transplantation for congenital erythropoietic porphyria. *Lancet Lond. Engl.* **337,** 1510–1511 (1991).

37. Hogeling, M., Nakano, T., Dvorak, C. C., Maguiness, S. & Frieden, I. J. Severe neonatal congenital erythropoietic porphyria. *Pediatr. Dermatol.* **28,** 416–420 (2011).

38. Dupuis-Girod, S. *et al.* Successful match-unrelated donor bone marrow transplantation for congenital erythropoietic porphyria (Günther disease). *Eur. J. Pediatr.* **164,** 104–107 (2005).

39. Mazurier, F. *et al. H Mol Ther* **3,** 411–417 (2001).

40. Bedel, A. *et al.* Metabolic correction of congenital erythropoietic porphyria with iPSCs free of reprogramming factors. *Am. J. Hum. Genet.* **91,** 109–121 (2012).

41. Sachar, M., Anderson, K. E. & Ma, X. Protoporphyrin IX: the Good, the Bad, and the Ugly. *J. Pharmacol. Exp. Ther.* **356,** 267–275 (2016).

42. Petříček, M., Petříčková, K., Havlíček, L. & Felsberg, J. Occurrence of Two 5-Aminolevulinate Biosynthetic Pathways in Streptomyces nodosus subsp. asukaensis Is Linked with the Production of Asukamycin. *J. Bacteriol.* **188,** 5113–5123 (2006).

43. Jahn D & Heinz DW. in *Tetrapyrroles: birth, life and death.* (eds. Warren MJ, & Smith AG) 29–42 (Austin: Landes Bioscience, 2009).

44. Chiabrando, D., Mercurio, S. & Tolosano, E. Heme and erythropoieis: more than a structural role. *Haematologica* **99,** 973–983 (2014).

45. Ajioka, R. S., Phillips, J. D. & Kushner, J. P. Biosynthesis of heme in mammals. *Biochim. Biophys. Acta* **1763,** 723–736 (2006).

46. Guernsey, D. L. *et al.* Mutations in mitochondrial carrier family gene SLC25A38 cause nonsyndromic autosomal recessive congenital sideroblastic anemia. *Nat. Genet.* **41,** 651–653 (2009).

47. Bayeva, M. *et al.* ATP-binding cassette B10 regulates early steps of heme synthesis. *Circ. Res.* **113,** 279–287 (2013).

48. Jordan, P. M. & Berry, A. Preuroporphyrinogen, a universal intermediate in the biosynthesis of uroporphyrinogen III. *FEBS Lett.* **112,** 86–88 (1980).

49. Jordan, P. M., Thomas, S. D. & Warren, M. J. Purification, crystallization and properties of porphobilinogen deaminase from a recombinant strain of Escherichia coli K12. *Biochem. J.* **254,** 427–435 (1988).

50. Krishnamurthy, P. & Schuetz, J. D. The role of ABCG2 and ABCB6 in porphyrin metabolism and cell survival. *Curr. Pharm. Biotechnol.* **12,** 647–655 (2011).

51. Mathews, M. A. *et al.* Crystal structure of human uroporphyrinogen III synthase. *EMBO J.* **20,** 5832–5839 (2001).

52. Cunha, L. *et al.* Human uroporphyrinogen III synthase: NMR-based mapping of the active site. *Proteins* **71,** 855–873 (2008).

53. Moore, M. R. *et al.* The biosynthesis of haem in congenital (erythropoietic) porphyria. *Int. J. Biochem.* **9,** 933–938 (1978).

54. Aizencang, G., Solis, C., Bishop, D. F., Warner, C. & Desnick, R. J. Human uroporphyrinogen-III synthase: genomic organization, alternative promoters, and erythroid-specific expression. *Genomics* **70,** 223–231 (2000).

55. Blouin, J.-M. *et al.* Missense UROS mutations causing congenital erythropoietic porphyria reduce UROS homeostasis that can be rescued by proteasome inhibition. *Hum. Mol. Genet.* **26,** 1565–1576 (2017).

56. Frank, J. *et al.* C73R is a hotspot mutation in the uroporphyrinogen III synthase gene in congenital erythropoietic porphyria. *Ann. Hum. Genet.* **62,** 225–230 (1998).

57. Fortian, A. *et al.* Uroporphyrinogen III synthase mutations related to congenital erythropoietic porphyria identify a key helix for protein stability. *Biochemistry (Mosc.)* **48,** 454–461 (2009).

58. Baker, D. & Agard, D. A. Kinetics versus thermodynamics in protein folding. *Biochemistry (Mosc.)* **33,** 7505–7509 (1994).

59. Duy, C. & Fitter, J. Thermostability of irreversible unfolding alpha-amylases analyzed by unfolding kinetics. *J. Biol. Chem.* **280,** 37360–37365 (2005).

60. Shoolingin-Jordan, P. M. & Leadbeater, R. Coupled assay for uroporphyrinogen III synthase. in *Methods in Enzymology* **281,** 327–336 (Academic Press, 1997).

61. ben Bdira, F. *et al.* Tuning intracellular homeostasis of human uroporphyrinogen III synthase by enzyme engineering at a single hotspot of congenital erythropoietic porphyria. *Hum. Mol. Genet.* **23,** 5805–5813 (2014).

62. Fortian, A., González, E., Castaño, D., Falcon-Perez, J. M. & Millet, O. Intracellular rescue of the uroporphyrinogen III synthase activity in enzymes carrying the hotspot mutation C73R. *J. Biol. Chem.* **286,** 13127–13133 (2011).

63. Freesemann, A. G., Bhutani, L. K., Jacob, K. & Doss, M. O. Interdependence between degree of porphyrin excess and disease severity in congenital erythropoietic porphyria (Günther's disease). *Arch. Dermatol. Res.* **289,** 272–276 (1997).

64. Lim, C. K. & Peters, T. J. Urine and faecal porphyrin profiles by reversed-phase high-performance liquid chromatography in the porphyrias. *Clin. Chim. Acta Int. J. Clin. Chem.* **139,** 55–63 (1984).

65. Balch, W. E., Morimoto, R. I., Dillin, A. & Kelly, J. W. Adapting proteostasis for disease intervention. *Science* **319,** 916–919 (2008).

66. Dobson, C. M. Protein folding and misfolding. *Nature* **426,** 884–890 (2003).

67. Balchin, D., Hayer-Hartl, M. & Hartl, F. U. In vivo aspects of protein folding and quality control. *Science* **353,** aac4354 (2016).

68. Kim, Y. E., Hipp, M. S., Bracher, A., Hayer-Hartl, M. & Hartl, F. U. Molecular chaperone functions in protein folding and proteostasis. *Annu. Rev. Biochem.* **82,** 323–355 (2013).

69. Gershenson, A., Gierasch, L. M., Pastore, A. & Radford, S. E. Energy landscapes of functional proteins are inherently risky. *Nat. Chem. Biol.* **10,** 884–891 (2014).

70. Hartl, F. U., Bracher, A. & Hayer-Hartl, M. Molecular chaperones in protein folding and proteostasis. *Nature* **475,** 324–332 (2011).

71. Hartl, F. U. Protein Misfolding Diseases. *Annu. Rev. Biochem.* **86,** 21–26 (2017).

72. Anfinsen, C. B. The formation and stabilization of protein structure. *Biochem. J.* **128,** 737–749 (1972).

73. Sweeney, P. *et al.* Protein misfolding in neurodegenerative diseases: implications and strategies. *Transl. Neurodegener.* **6,** 6 (2017).

74. Hutt, D. M., Powers, E. T. & Balch, W. E. The Proteostasis Boundary in Misfolding Diseases of Membrane Traffic. *FEBS Lett.* **583,** 2639–2646 (2009).

75. Wong, M. Y. *et al.* Adapting Secretory Proteostasis and Function Through the Unfolded Protein Response. *Curr. Top. Microbiol. Immunol.* **414,** 1–25 (2018).

76. Valenzano, K. J. *et al.* Identification and characterization of pharmacological chaperones to correct enzyme deficiencies in lysosomal storage disorders. *Assay Drug Dev. Technol.* **9,** 213–235 (2011).

77. Kirstein-Miles, J. & Morimoto, R. I. Caenorhabditis elegans as a model system to study intercompartmental proteostasis: Interrelation of mitochondrial function, longevity, and neurodegenerative diseases. *Dev. Dyn. Off. Publ. Am. Assoc. Anat.* **239,** 1529–1538 (2010).

78. Kaushik, S. & Cuervo, A. M. Proteostasis and aging. *Nat. Med.* **21,** 1406–1415 (2015).

79. Douglas, P. M. & Dillin, A. Protein homeostasis and aging in neurodegeneration. *J. Cell Biol.* **190,** 719–729 (2010).

80. Hipp, M. S., Park, S.-H. & Hartl, F. U. Proteostasis impairment in protein-misfolding and -aggregation diseases. *Trends Cell Biol.* **24,** 506–514 (2014).

81. Labbadia, J. & Morimoto, R. I. The biology of proteostasis in aging and disease. *Annu. Rev. Biochem.* **84,** 435–464 (2015).

82. Soto, C. Protein misfolding and disease; protein refolding and therapy. *FEBS Lett.* **498,** 204–207 (2001).

83. Schmidt, M. & Finley, D. Regulation of proteasome activity in health and disease. *Biochim. Biophys. Acta* **1843,** 13–25 (2014).

84. Niforou, K., Cheimonidou, C. & Trougakos, I. P. Molecular chaperones and proteostasis regulation during redox imbalance. *Redox Biol.* **2,** 323–332 (2014).

85. Cohen, F. E. & Kelly, J. W. Therapeutic approaches to protein-misfolding diseases. *Nature* **426,** 905–909 (2003).

86. Chaudhuri, T. K. & Paul, S. Protein-misfolding diseases and chaperone-based therapeutic approaches. *FEBS J.* **273,** 1331–1349 (2006).

87. Welch, W. J. & Brown, C. R. Influence of molecular and chemical chaperones on protein folding. *Cell Stress Chaperones* **1,** 109–115 (1996).

88. Gekko, K. & Timasheff, S. N. Mechanism of protein stabilization by glycerol: preferential hydration in glycerol-water mixtures. *Biochemistry (Mosc.)* **20,** 4667–4676 (1981).

89. Raibekas, A. A. & Massey, V. Glycerol-assisted restorative adjustment of flavoenzyme conformation perturbed by site-directed mutagenesis. *J. Biol. Chem.* **272,** 22248–22252 (1997).

90. Cortez, L. & Sim, V. The therapeutic potential of chemical chaperones in protein folding diseases. *Prion* **8,** (2014).

91. Burrows, J. A., Willis, L. K. & Perlmutter, D. H. Chemical chaperones mediate increased secretion of mutant alpha 1-antitrypsin (alpha 1-AT) Z: A potential pharmacological strategy for prevention of liver injury and emphysema in alpha 1-AT deficiency. *Proc. Natl. Acad. Sci. U. S. A.* **97,** 1796–1801 (2000).

92. Galkin, O. & Vekilov, P. G. Mechanisms of homogeneous nucleation of polymers of sickle cell anemia hemoglobin in deoxy state. *J. Mol. Biol.* **336,** 43–59 (2004).

93. Tamarappoo, B. K. & Verkman, A. S. Defective aquaporin-2 trafficking in nephrogenic diabetes insipidus and correction by chemical chaperones. *J. Clin. Invest.* **101,** 2257–2267 (1998).

94. Loo, T. W. & Clarke, D. M. Correction of defective protein kinesis of human P-glycoprotein mutants by substrates and modulators. *J. Biol. Chem.* **272,** 709–712 (1997).

95. Sato, S., Ward, C. L., Krouse, M. E., Wine, J. J. & Kopito, R. R. Glycerol reverses the misfolding phenotype of the most common cystic fibrosis mutation. *J. Biol. Chem.* **271,** 635–638 (1996).

96. Tatzelt, J., Prusiner, S. B. & Welch, W. J. Chemical chaperones interfere with the formation of scrapie prion protein. *EMBO J.* **15,** 6363–6373 (1996).

97. Ringe, D. & Petsko, G. A. Q&A: What are pharmacological chaperones and why are they interesting? *J. Biol.* **8,** 80 (2009).

98. Papp, E. & Csermely, P. Chemical chaperones: mechanisms of action and potential use. *Handb. Exp. Pharmacol.* 405–416 (2006).

99. Leidenheimer, N. J. Pharmacological Chaperones: Beyond Conformational Disorders. *Handb. Exp. Pharmacol.* **245,** 135–153 (2018).

100. Hughes, D. A. *et al.* Oral pharmacological chaperone migalastat compared with enzyme replacement therapy in Fabry disease: 18-month results from the randomised phase III ATTRACT study. *J. Med. Genet.* **54,** 288–296 (2017).

101. Hatahet, F. & Ruddock, L. W. Modulating proteostasis: peptidomimetic inhibitors and activators of protein folding. *Curr. Pharm. Des.* **15,** 2488–2507 (2009).

102. Pratt, W. B., Gestwicki, J. E., Osawa, Y. & Lieberman, A. P. Targeting Hsp90/Hsp70-based protein quality control for treatment of adult onset neurodegenerative diseases. *Annu. Rev. Pharmacol. Toxicol.* **55,** 353–371 (2015).

103. Miyata, Y., Nakamoto, H. & Neckers, L. The therapeutic target Hsp90 and cancer hallmarks. *Curr. Pharm. Des.* **19,** 347–365 (2013).

104. Ezgu, F. Inborn Errors of Metabolism. *Adv. Clin. Chem.* **73,** 195–250 (2016).

105. Blouin, J.-M. *et al.* Therapeutic potential of proteasome inhibitors in congenital erythropoietic porphyria. *Proc. Natl. Acad. Sci. U. S. A.* **110,** 18238–18243 (2013).

106. Sterling, T. & Irwin, J. J. ZINC 15--Ligand Discovery for Everyone. *J. Chem. Inf. Model.* **55,** 2324–2337 (2015).

107. Balani, S. K., Miwa, G. T., Gan, L.-S., Wu, J.-T. & Lee, F. W. Strategy of utilizing in vitro and in vivo ADME tools for lead optimization and drug candidate selection. *Curr. Top. Med. Chem.* **5,** 1033–1038 (2005).

108. Congreve, M., Carr, R., Murray, C. & Jhoti, H. A 'rule of three' for fragment-based lead discovery? *Drug Discov. Today* **8,** 876–877 (2003).

109. Pellecchia, M., Sem, D. S. & Wüthrich, K. NMR in drug discovery. *Nat. Rev. Drug Discov.* **1,** 211–219 (2002).

110. Schanda, P., Kupce, E. & Brutscher, B. SOFAST-HMQC experiments for recording two-dimensional heteronuclear correlation spectra of proteins within a few seconds. *J. Biomol. NMR* **33,** 199–211 (2005).

111. Vranken, W. F. *et al.* The CCPN data model for NMR spectroscopy: Development of a software pipeline. *Proteins Struct. Funct. Bioinforma.* **59,** 687–696

112. Pagadala, N. S., Syed, K. & Tuszynski, J. Software for molecular docking: a review. *Biophys. Rev.* **9,** 91–102 (2017).

113. Trott, O. & Olson, A. J. AutoDock Vina: improving the speed and accuracy of docking with a new scoring function, efficient optimization and multithreading. *J. Comput. Chem.* **31,** 455–461 (2010).

114. Morris, G. M. *et al.* AutoDock4 and AutoDockTools4: Automated docking with selective receptor flexibility. *J. Comput. Chem.* **30,** 2785–2791 (2009).

115. Gill, S. C. & von Hippel, P. H. Calculation of protein extinction coefficients from amino acid sequence data. *Anal. Biochem.* **182,** 319–326 (1989).

116. Scianna, M., Merks, R. M. H., Preziosi, L. & Medico, E. Individual cell-based models of cell scatter of ARO and MLP-29 cells in response to hepatocyte growth factor. *J. Theor. Biol.* **260,** 151–160 (2009).

117. Graham, F. L., Smiley, J., Russell, W. C. & Nairn, R. Characteristics of a Human Cell Line Transformed by DNA from Human Adenovirus Type 5. *J. Gen. Virol.* **36,** 59–72 (1977).

118. Lozzio, C. B. & Lozzio, B. B. Human chronic myelogenous leukemia cell-line with positive Philadelphia chromosome. *Blood* **45,** 321–334 (1975).

119. Nakabayashi, H., Taketa, K., Miyano, K., Yamane, T. & Sato, J. Growth of human hepatoma cells lines with differentiated functions in chemically defined medium. *Cancer Res.* **42,** 3858–3863 (1982).

120. Riss, T. L. *et al. Cell Viability Assays.* (Eli Lilly & Company and the National Center for Advancing Translational Sciences, 2016).

121. Nevozhay, D. Cheburator Software for Automatically Calculating Drug Inhibitory Concentrations from In Vitro Screening Assays. *PLOS ONE* **9,** e106186 (2014).

122. Ged, C. *et al.* A knock-in mouse model of congenital erythropoietic porphyria. *Genomics* **87,** 84–92 (2006).

123. Kitchen, D. B., Decornez, H., Furr, J. R. & Bajorath, J. Docking and scoring in virtual screening for drug discovery: methods and applications. *Nat. Rev. Drug Discov.* **3,** 935–949 (2004).

124. McConkey, B. J., Sobolev, V. & Edelman, M. The performance of current methods in ligand–protein docking. *Curr. Sci.* **83,** 845–856 (2002).

125. Jorgensen, W. L. The Many Roles of Computation in Drug Discovery. *Science* **303,** 1813–1818 (2004).

126. Meng, X.-Y., Zhang, H.-X., Mezei, M. & Cui, M. Molecular docking: a powerful approach for structure-based drug discovery. *Curr. Comput. Aided Drug Des.* **7,** 146–157 (2011).

127. Cavasotto, C. N. & Orry, A. J. W. Ligand docking and structure-based virtual screening in drug discovery. *Curr. Top. Med. Chem.* **7,** 1006–1014 (2007).

128. Monod, J., Wyman, J. & Changeux, J.-P. On the nature of allosteric transitions: A plausible model. *J. Mol. Biol.* **12,** 88–118 (1965).

129. Lipinski, C. A., Lombardo, F., Dominy, B. W. & Feeney, P. J. Experimental and computational approaches to estimate solubility and permeability in drug discovery and development settings. *Adv. Drug Deliv. Rev.* **23,** 3–25 (1997).

130. Clark, null & Pickett, null. Computational methods for the prediction of 'drug-likeness'. *Drug Discov. Today* **5,** 49–58 (2000).

131. Veber, D. F. *et al.* Molecular properties that influence the oral bioavailability of drug candidates. *J. Med. Chem.* **45,** 2615–2623 (2002).

132. Carr, R. A. E., Congreve, M., Murray, C. W. & Rees, D. C. Fragment-based lead discovery: leads by design. *Drug Discov. Today* **10,** 987–992 (2005).

133. Becktel, W. J. & Schellman, J. A. Protein stability curves. *Biopolymers* **26,** 1859–1877 (1987).

134. Pey, A. L. *et al.* Identification of pharmacological chaperones as potential therapeutic agents to treat phenylketonuria. *J. Clin. Invest.* **118,** 2858–2867 (2008).

135. Pace, C. N. & Shaw, K. L. Linear extrapolation method of analyzing solvent denaturation curves. *Proteins* **Suppl 4,** 1–7 (2000).

136. Wurm, F. M. Production of recombinant protein therapeutics in cultivated mammalian cells. *Nat. Biotechnol.* **22,** 1393–1398 (2004).

137. Ponka, P. Tissue-Specific Regulation of Iron Metabolism and Heme Synthesis: Distinct Control Mechanisms in Erythroid Cells. *Blood* **89,** 1–25 (1997).

138. Tsien, R. Y. The green fluorescent protein. *Annu. Rev. Biochem.* **67,** 509–544 (1998).

139. Baba, A. I. & Câtoi, C. *TUMOR CELL MORPHOLOGY*. (The Publishing House of the Romanian Academy, 2007).

140. Palmer, A. G. NMR Characterization of the Dynamics of Biomacromolecules. *Chem. Rev.* **104,** 3623–3640 (2004).

141. Gerstein, M., Lesk, A. M. & Chothia, C. Structural Mechanisms for Domain Movements in Proteins. *Biochemistry (Mosc.)* **33,** 6739–6749 (1994).

142. Eisenmesser, E. Z. *et al*. Intrinsic dynamics of an enzyme underlies catalysis. *Nature* **438,** 117–121 (2005).

143. Sanchez-Ruiz, J. M. Protein kinetic stability. *Biophys. Chem.* **148,** 1–15 (2010).

144. Ding, Y., Li, H., Chen, L.-L. & Xie, K. Recent Advances in Genome Editing Using CRISPR/Cas9. *Front. Plant Sci.* **7,** (2016).

145. Chelikani, P., Reeves, P. J., Rajbhandary, U. L. & Khorana, H. G. The synthesis and high-level expression of a beta2-adrenergic receptor gene in a tetracycline-inducible stable mammalian cell line. *Protein Sci. Publ. Protein Soc.* **15,** 1433–1440 (2006).

146. Quiroz-Segoviano, R. I. Y. *et al*. On Tuning the Fluorescence Emission of Porphyrin Free Bases Bonded to the Pore Walls of Organo-Modified Silica. *Molecules* **19,** 2261–2285 (2014).

147. Oliver, F. J. *et al*. Importance of poly(ADP-ribose) polymerase and its cleavage in apoptosis. Lesson from an uncleavable mutant. *J. Biol. Chem.* **273,** 33533–33539 (1998).

148. Taylor, C., Duffy, L. K., Plumley, F. G. & Bowyer, R. T. Comparison of spectrofluorometric and HPLC methods for the characterization of fecal porphyrins in river otters. *Environ. Res.* **84,** 56–63 (2000).

149. Zarember, K. A., Cruz, A. R., Huang, C.-Y. & Gallin, J. I. Antifungal activities of natural and synthetic iron chelators alone and in combination with azole and polyene antibiotics against Aspergillus fumigatus. *Antimicrob. Agents Chemother.* **53,** 2654–2656 (2009).

150. Vasconcelos, P., Luz-Rodrigues, H., Santos, C. & Filipe, P. Desferrioxamine treatment of porphyria cutanea tarda in a patient with HIV and chronic renal failure. *Dermatol. Ther.* **27,** 16–18 (2014).

151. Heli, H., Mirtorabi, S. & Karimian, K. Advances in iron chelation: an update. *Expert Opin. Ther. Pat.* **21,** 819–856 (2011).

152. Shen, T. *et al*. Ciclopirox inhibits cancer cell proliferation by suppression of Cdc25A. *Genes Cancer* **8,** 505–516 (2017).

153. Neubert, R. H. H., Gensbügel, C., Jäckel, A. & Wartewig, S. Different physicochemical properties of antimycotic agents are relevant for penetration into and through human nails. *Pharm.* **61,** 604–607 (2006).

154. Kellner, H. M. *et al.* [Pharmacokinetics and biotransformation of the antimycotic drug ciclopiroxolamine in animals and man after topical and systemic administration]. *Arzneimittelforschung.* **31,** 1337–1353 (1981).

155. Lukášová, I. *et al.* Pharmacokinetics of Ciclopirox Olamine after Buccal Administration in Rabbits. *Curr. Drug Deliv.* **14,** 99–108 (2017).

156. Minden, M. D. *et al.* Oral ciclopirox olamine displays biological activity in a phase I study in patients with advanced hematologic malignancies. *Am. J. Hematol.* **89,** 363–368

157. Parenti, G., Andria, G. & Valenzano, K. J. Pharmacological Chaperone Therapy: Preclinical Development, Clinical Translation, and Prospects for the Treatment of Lysosomal Storage Disorders. *Mol. Ther. J. Am. Soc. Gene Ther.* **23,** 1138–1148 (2015).

158. Biffi, A. Genetically-modified hematopoietic stem cells and their progeny for widespread and efficient protein delivery to diseased sites: the case of lysosomal storage disorders. *Curr. Gene Ther.* **12,** 381–388 (2012).

159. Loo, T. W. & Clarke, D. M. Chemical and pharmacological chaperones as new therapeutic agents. *Expert Rev. Mol. Med.* **9,** 1–18 (2007).

160. Citro, V. *et al.* Identification of an Allosteric Binding Site on Human Lysosomal Alpha-Galactosidase Opens the Way to New Pharmacological Chaperones for Fabry Disease. *PLOS ONE* **11,** e0165463 (2016).

161. Harms, J. H., Lautenschlager, S., Minder, C. E. & Minder, E. I. Mitigating photosensitivity of erythropoietic protoporphyria patients by an agonistic analog of alpha-melanocyte stimulating hormone. *Photochem. Photobiol.* **85,** 1434–1439 (2009).

162. Subissi, A., Monti, D., Togni, G. & Mailland, F. Ciclopirox: recent nonclinical and clinical data relevant to its use as a topical antimycotic agent. *Drugs* **70,** 2133–2152 (2010).

163. Eberhard, Y. *et al.* Chelation of intracellular iron with the antifungal agent ciclopirox olamine induces cell death in leukemia and myeloma cells. *Blood* **114,** 3064–3073 (2009).

164. Zhou, H. *et al.* The antitumor activity of the fungicide ciclopirox. *Int. J. Cancer* **127,** 2467–2477 (2010).

165. Clement, P. M. J., Hanauske-Abel, H. M., Wolff, E. C., Kleinman, H. K. & Park, M. H. The antifungal drug ciclopirox inhibits deoxyhypusine and proline hydroxylation, endothelial cell growth and angiogenesis in vitro. *Int. J. Cancer* **100,** 491–498 (2002).

166. Luo, Y. *et al.* The fungicide ciclopirox inhibits lymphatic endothelial cell tube formation by suppressing VEGFR-3-mediated ERK signaling pathway. *Oncogene* **30,** 2098–2107 (2011).

167. Rosen, T., Schell, B. J. & Orengo, I. Anti-inflammatory activity of antifungal preparations. *Int. J. Dermatol.* **36,** 788–792 (1997).

168. Lassus, A., Nolting, K. S. & Savopoulos, C. Comparison of ciclopirox olamine 1% cream with ciclopirox 1%-hydrocortisone acetate 1% cream in the treatment of inflamed superficial mycoses. *Clin. Ther.* **10,** 594–599 (1988).

169. Sato, E., Kohno, M., Nakashima, T. & Niwano, Y. Ciclopirox olamine directly scavenges hydroxyl radical. *Int. J. Dermatol.* **47,** 15–18 (2008).

170. Nakashima, T. *et al.* Inhibitory or scavenging action of ketoconazole and ciclopiroxolamine against reactive oxygen species released by primed inflammatory cells. *Br. J. Dermatol.* **156,** 720–727 (2007).

171. Mihailidou, C., Chatzistamou, I., Papavassiliou, A. G. & Kiaris, H. Ciclopirox enhances pancreatic islet health by modulating the unfolded protein response in diabetes. *Pflugers Arch.* **468,** 1957–1968 (2016).

172. Jue, S. G., Dawson, G. W. & Brogden, R. N. Ciclopirox olamine 1% cream. A preliminary review of its antimicrobial activity and therapeutic use. *Drugs* **29,** 330–341 (1985).

173. Korting, H. C. & Grundmann-Kollmann, M. The hydroxypyridones: a class of antimycotics of its own. *Mycoses* **40,** 243–247 (1997).

174. Gupta, A. K. & Skinner, A. R. Ciclopirox for the treatment of superficial fungal infections: a review. *Int. J. Dermatol.* **42 Suppl 1,** 3–9 (2003).

175. Bissell, D. M. & Wang, B. Acute Hepatic Porphyria. *J. Clin. Transl. Hepatol.* **3,** 17–26 (2015).

ABBREVIATIONS

aa	Amino acids
ABC	ATP-binding cassette
ABCB	ATP-binding cassette subfamily B member membrane transporter
AD	Alzheimer disease
ADME	Absorption, Distribution, Metabolism and Excretion
ADT	Android Development Tools
ALA	δ-aminolevulinic acid
ALAD	δ-aminolevulinic acid dehydratase
ALAS	δ-aminolevulinate synthase
ALAS1	δ-aminolevulinate synthase 1
ALAS2	δ-aminolevulinate synthase 2
Amp	Ampicillin
ANOVA	Analysis of variance
ATP	Adenosine triphosphate
BiP	Binding immunoglobulin protein
BSA	Bovine serum album
Cas9	CRISPR-associated protein 9
CCPNMR	Collaborative Computing Project for the NMR community
CD	Circular dichroism
cDNA	Copy Deoxyribonucleic acid
CEP	Congenital erythropoietic porphyria
CFTR	Cystic fibrosis transmembrane regulator
CG	Chemical group
cLogP	Calculated Log P
CO_2	Carbon dioxide
COPRO I	Coproporphyrin I
COPRO III	Coproporphyrin III
COPROgen I	Coproporphyrinogen I
COPROgen III	Coproporphyrinogen III
CPOX	Coproporphyrinogen oxidase
CPX	Ciclopirox
CPXglu	Ciclopirox beta-D-Glucuronide
CPXol	Ciclopirox olamine
CRISPR	Clustered Regularly Interspaced Short Palindromic Repeats
CSP	Chemical shift perturbation
CYP	Cytochrome P450
D_2O	Deuterated water
Da	Dalton
DAPI	4',6-diamidino-2-phenylindole
DMEM	Dulbecco's modified Eagle's medium
DMSO	Dimethyl sulfoxide
DMSO-6d	Deuterated dimethyl sulfoxide
DNA	Deoxyribonucleic acid

DSS	4,4-dimethyl-4-silapentane-1-sulfonic acid
EBV	Epstein - Barr virus
ECL	Enhanced chemiluminescence
EDTA	Ethylenediaminetetraacetic acid
Eea1	Early endosomal antigen 1
EPP	Erythropoietic protoporphyria
ER	Endoplasmic reticulum
ERAD	Endoplasmic-reticulum-associated protein degradation
FBS	Fetal Bovine Serum
FC	Fluorescence cells
FDA	Food and Drug Administration
FECH	Ferrochelatase
FF	Fraction of folded
GFP	Green fluorescent protein
GluTR	Glutamyl-tRNA reductase
GPCR	G protein-coupled receptor
GSAM	Glutamate-1-semialdehyde-2,1-aminomutase
HBA	Hydrogens-bond acceptors
HCl	Chlorhydric acid
HCP	Hereditary coproporphyria
HD	Huntington disease
HDR	Homology directed repair
HE	Hematoxylin-eosin staining
HEK 293	Human embryonic kidney 293
HEP	Hepatoerythropoietic porphyria
Hepta I	Heptaporphyrin I
Hepta III	Heptaporphyrin III
Heptagen I	Heptaporphyrinogen I
Heptagen III	Heptaporphyrinogen III
Hexa I	Hexaporphyrin I
Hexa III	Hexaporphyrin III
Hexagen I	Hexaporphyrinogen I
Hexagen III	Hexaporphyrinogen III
His-Tag	Histidine-Tagged
HMB	Hydroxymethylbilane
HMQC	Heteronuclear Multiple-Quantum Correlation
HPLC	High-performance liquid chromatography
HRP	Horseradish-peroxidase
HSCT	Stem cell transplantation
Hsp	Heat shock protein
Hsp70	Heat shock protein 70
Hsp90	Heat shock protein 90
HSQC	Heteronuclear Single-Quantum Correlation
HSR	Heat shock response
hν	Planck's energy–frequency relation

I_2	Iodine
iPSCs	Induced pluripotent stem cells
IPTG	Isopropyl-β-D-Thiogalactopyranoside
Kan	Kanamycin
KCl	Potassium chloride
kDa	Kilodalton
KI	Potassium iodide
Lamp1	Lysosome-associated membrane glycoprotein 1
LB	Lysogeny Broth
LCL	Lymphoblastoid cell line
L-CPL	Left-handed circularly polarised light
MED	Minimum effective dose
MLP29	Mouse liver progenitor 29
mRNA	Messenger Ribonucleic acid
MTD	Maximum tolerated dose
MTT	3-(4,5-dimethylthiazol-2-yl)-2,5-diphenyltetrazolium bromide
MW	Molecular weight
N_2	Nitrogen
NaCl	Sodium Chloride
NFC	Number fluorescent cells
NH	Amine group
NH_4Cl	Ammonium chloride
NH_4Cl	Ammonium chloride
NMR	Nuclear magnetic resonance
NO	Nitric Oxide
NROT	Rotatable bonds
NTC	Total cell number
O_2	Oxygen
OH	Hydroxyl group
PAM	Protospacer adjacent motif
PARP	PAR-Polymerase
PBA	Sodium 4-phenylbutyrate
PBG	Porphobilinogen
PBGD	Porphobilinogen deaminase
PBS	Phosphate buffered saline
PCR	Polymerase chain reaction
PCT	Porphyria cutanea tarda
PD	Parkinson disease
PDB	Protein Data Bank
PE	Erythroid promoter region.
Penta I	Pentaporphyrin I
Penta III	Pentaporphyrin III
Pentagen I	Pentaporphyrinogen I
Pentagen III	Pentaporphyrinogen III
PH	Housekeeping promoter region

PIC	Protease Inhibitor Cocktail
PLP	Pyridoxal 5'-phosphate
PN	Proteostasis network
PPIX	Protoporphyrin IX
PPOX	Protoporphyrinogen oxidase
PROTOgen IX	Protoporphyrinogen IX
PS	Perls Prussian Blue Staining
PSA	Polar surface area
PTS	Protein Thermal Shift Assay
qPCR	Quantitative polymerase chain reaction
RBC	Reb Blood Cells
R-CPL	Right-handed circularly polarised light
RNA	Ribonucleic acid
Ro3	Rule of 3
Ro5	Rule of 5
ROS	Reactive Oxygen Species
RPMI	Roswell Park Memorial Institute medium
RQC	Ribosome quality control machinery
rRNA	Ribosomal Ribonucleic acid
RT-PCR	Real-time polymerase chain reaction
sgRNA	Single guide RNA
SLC	Solute carrier
SLC25A38	Solute carrier family 25-member 38 membrane transporter
SOFAST	Sensitive fast-pulsing spectroscopy
SR	Sirius Red Stain
ssODN	Single-stranded oligonucleotide donor
Tg	Transgenic
Tris	Tris(hidroximetil)aminometano
tRNA	Transfer Ribonucleic acid
TROSY	Transverse relaxation optimized spectroscopy
TS	Transition state
UPR	Unfolded protein response
UPS	Ubiquitin proteasome system
UQ	Ubiquitin
URO I	Uroporphyrin I
URO III	Uroporphyrin III
UROD	Uroporphyrinogen decarboxylase
UROgen I	Uroporphyrinogen I
UROgen III	Uroporphyringen III
UROIIIS	Uroporphyringen III synthase
UV	Long-wave ultraviolet
VP	Variegate porphyria
WT	Wild Type
α-MSH	α-melanocyte stimulating hormone

LIST OF FIGURES

LIST OF TABLES


CIC
bioGUNE
Biozientzietako Ikerkuntza Kooperatiboko Zentroa
Centro de Investigación Cooperativa en Biociencias
EXCELENCIA
SEVERO
OCHOA